Engineering Journal

American Institute of Steel Construction

Fourth Quarter 2008 olume 45, No. 4

www.aisc.org

ENGINEERING JOURNAL

AMERICAN INSTITUTE OF STEEL CONSTRUCTION

Dedicated to the development and improvement of steel construction, through the interchange of ideas, experiences and data.

ENGINEERING JOURNAL (ISSN 0013-8029) is published quarterly. Subscriptions: Members: one subscription, $20 per year, included in dues; Additional Member Subscriptions: $15 per year. Non-Members U.S., Canada, and Mexico: $40 per year, $110 for three years, single copy $15. International Members and Non-Members: $90 per year; $250 for three years; single copy $25. Published by the American Institute of Steel Construction at One East Wacker Drive, Suite 700, Chicago, IL 60601.

Periodicals postage paid at Chicago, IL and additional mailing offices. **Postmaster:** Send address changes to ENGINEERING JOURNAL in care of the American Institute of Steel Construction, One East Wacker Drive, Suite 700, Chicago, IL 60601.

The Best
Engineering Journal
Article of 2008

Visit the AISC web site **(www.aisc.org/ejsurvey)** to cast your vote for the best *Engineering Journal* Article of 2008.

The award will be presented to the winning author at the 2009 North American Steel Construction Conference (NASCC: The Steel Conference) to be held in Phoenix, Arizona, April 1–4. The winning author will receive free registration and travel expenses to attend the 2009 NASCC.

Cast your vote today! Votes will not be accepted after February 8, 2009.

Subscribe to *Engineering Journal* by visiting our web site **www.aisc.org** or by calling 312.670.5444.

Copies of current and past *Engineering Journal* articles are available free to members online at **www.aisc.org/epubs.**

Non-members may purchase *Engineering Journal* article downloads at the AISC Bookstore at **www.aisc.org/bookstore** for $10 each. Starting with the First Quarter 2008, complete issue downloads of *Engineering Journal* are available for $15 each at **www.aisc.org/bookstore.**

An archival CD-ROM of past issues of *Engineering Journal* is available by calling 800.644.2400.

Cyclic Behavior and Seismic Design of Bolted Flange Plate Steel Moment Connections

ATSUSHI SATO, JAMES D. NEWELL and CHIA-MING UANG

Steel moment connections in high seismic regions typically use welded beam flange-to-column flange joints. Field welding of these connections has significant economic impact on the overall cost of the building. A moment connection that could eliminate field welding in favor of field bolting and shop welding could result in a more economical seismic moment frame connection.

One type of bolted moment frame connection consists of plates that are shop welded to the column flange and field bolted to the beam flange and is known as the bolted flange plate (BFP) moment connection. As a part of the SAC Joint Venture Phase II Connection Performance Program, eight full-scale BFP moment connection specimens were tested (Schneider and Teeraparbwong, 2000). Tested connections exhibited predictable, ductile behavior and met established acceptance criteria. However, beam sizes were limited to W24×68 and W30×99.

The AISC Connection Prequalification Review Panel (CPRP) is currently reviewing the bolted flange plate moment connection for inclusion in the next edition of the AISC *Prequalified Connections for Special and Intermediate Steel Moment Frames for Seismic Applications* (AISC 2005a). To expand the experimental database for prequalifying the BFP moment connection for special moment frames, cyclic testing of three full-scale BFP steel moment connection specimens has been conducted. Beam sizes for these specimens (W30×108, W30×148, and W36×50) were larger than previously tested to extend the range of available experimental results.

Atsushi Sato is assistant professor, department of architecture and architectural engineering, Kyoto University, Kyoto, Japan, and formerly visiting scholar, department of structural engineering, University of California, San Diego, La Jolla, CA.

James D. Newell is graduate student researcher, department of structural engineering, University of California, San Diego, La Jolla, CA.

Chia-Ming Uang is professor, department of structural engineering, University of California, San Diego, La Jolla, CA.

EXPERIMENTAL PROGRAM

Connection Details and Test Setup

Three full-scale, one-sided moment connection specimens, without a concrete slab were fabricated and tested in accordance with Appendix S of the AISC *Seismic Provisions for Structural Steel Buildings*, hereafter referred to as the AISC *Seismic Provisions* (AISC, 2005b). Specimens were designed in accordance with the design procedure developed by the BFP Committee of AISC's CPRP. The design procedure (see Appendix I) assumes the beam plastic hinge is located at the center of the outermost (farthest from the column face) row of bolts. Tables 1a and 1b list the member sizes and connection details for the specimens. Beam-to-column connection details are shown in Figure 1. As indicated in Table 1, Specimens BFP-1 and BFP-2 had 1 in. continuity plates and Specimen BFP-3 did not have continuity plates. Specimen BFP-1 did not have a panel zone doubler plate while Specimens BFP-2 and BFP-3 included a ¾-in. doubler plate.

Bolt holes in the beam shear tab were short-slotted with the slot length oriented parallel to the beam span and bolt holes in the beam web were standard holes. Bolt holes in the flange plate were oversized holes (1¼-in. diameter for 1-in. diameter bolts) and bolt holes in the beam flange were standard holes (1$\frac{1}{16}$-in. diameter for 1-in. diameter bolts). The short-slotted holes in the shear tab and oversized holes in the flange plate were provided to accommodate erection tolerances.

The distance between the two bolted flange plates was detailed to be ⅜ in. larger than the nominal beam depth. This tolerance accommodates typical variations in actual beam depth and any gaps between the beam flange and flange plate larger than ⅛ in. are filled with finger shims. For all specimens, two ⅛-in. finger shim plates (total ¼ in.) were installed between the top flange plate and beam top flange. No shims were used between the bottom flange plate and beam bottom flange.

The clear-bay-width to beam-depth ratio of previously tested BFP moment connection specimens varied from approximately 9 to 12 (Schneider and Teeraparbwong, 2000). For Specimens BFP-1, BFP-2 and BFP-3 the beam length varied in order to maintain a target clear-bay-width to beam-depth ratio of 12. The overall specimen geometry and test setup is shown in Figure 2. Simulated pins were provided at the ends of the column, and actuator attachment point at the

Table 1a. Member Sizes				
Specimen Designation	Column	Beam	L_c (in.)	L_c/d_b[a]
BFP-1	W14×233	W30×108	355¾	11.94
BFP-2	W14×233	W30×148	367½	11.97
BFP-3	W14×311	W36×150	426⅞	11.89
[a] Clear bay width-to-beam depth ratio, L_c/d_b (target ratio = 12)				

Table1b. Connection Details					
Specimen Designation	Flange Plates (in.)	Flange Plate Welding	Row of Bolts	Panel Zone Doubler Plate (in.)	Continuity Plates (in.)
BFP-1	1½	ESW	7	NA	1
BFP-2	1¾	ESW	11	¾	1
BFP-3	1¾	FCAW	10	¾	NA

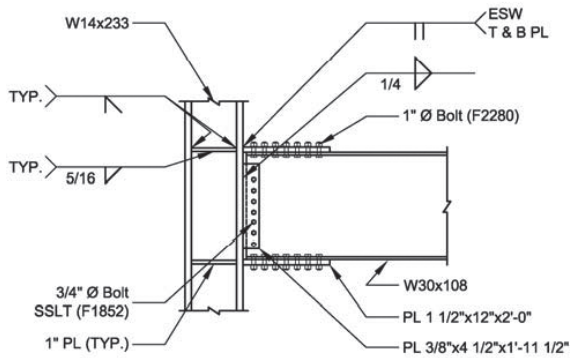

(a) Specimen BFP-1

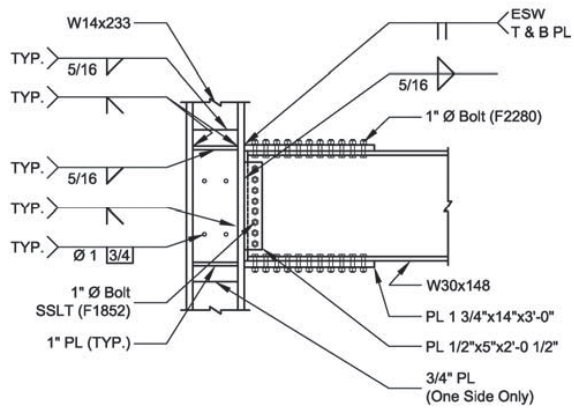

(b) Specimen BFP-2

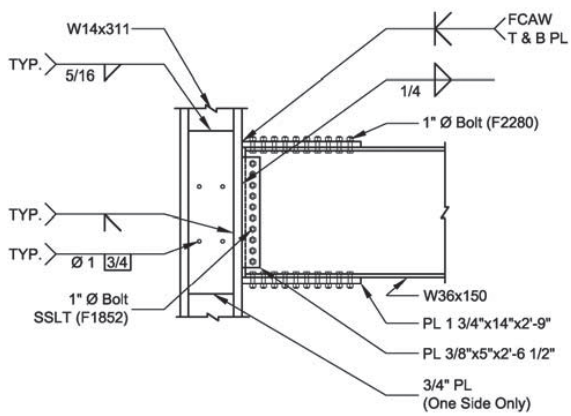

(c) Specimen BFP-3

Fig. 1. Moment connection details.

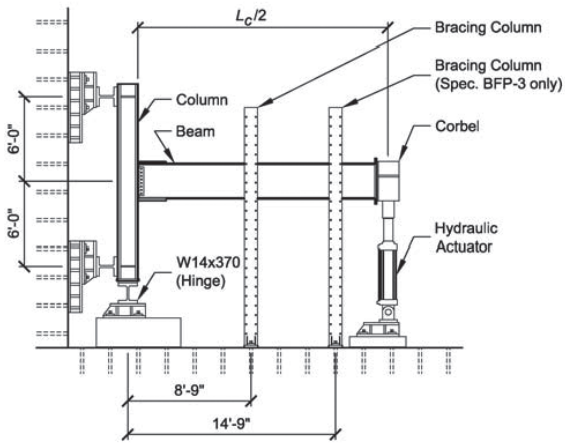

(a) Schematic

(b) Specimens BFP-1 and BFP-2

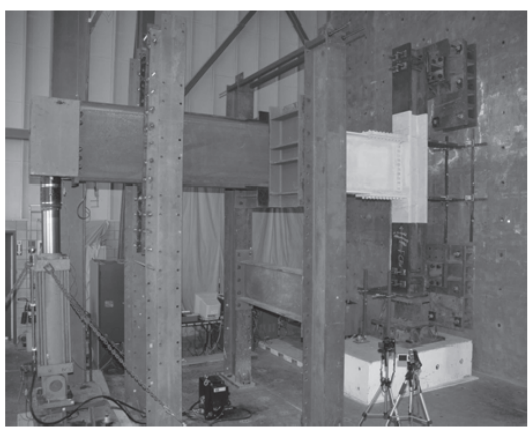

(c) Specimen BFP-3

Fig. 2. Test setup.

end of the beam to simulate inflection points in the actual building. A load transfer corbel was bolted to the end of the beam and attached to a servo-controlled hydraulic actuator.

The maximum lateral bracing spacing permitted by the AISC *Seismic Provisions* for Specimens BFP-1, BFP-2 and BFP-3 was 107, 113 and 123 in., respectively. For Specimens BFP-1 and BFP-2 lateral bracing of the beam was provided approximately 105 in. from the centerline of the column. The same lateral bracing at a distance of 105 in. from the column was also used for Specimen BFP-3. But since testing of both Specimens BFP-1 and BFP-2 showed significant beam lateral-torsional buckling and column twisting, it was decided to add additional lateral bracing at 177 in. from the column centerline (see Figure 2).

Fabrication and Erection

Two different welding processes were used for the flange-plate to column-flange complete joint penetration groove welds. Flange plates were welded to the column using the electroslag welding (ESW) process for Specimens BFP-1 and BFP-2 and using the flux-cored arc welding (FCAW) process for Specimen BFP-3.

For the ESW flange-plate to column-flange welds the sides of the weld were formed by water-cooled copper shoes. Two Arcmatic 105-VMC 3/32 in. diameter electrodes were placed inside a consumable guide tube. Flux (FES72) was added by hand per the fabricator's standard procedure. It took approximately 15 minutes to completely weld each flange plate. The electrode used has a specified minimum Charpy-V notch (CVN) toughness of 15 ft-lb at –20 °F. [AISC *Seismic Provisions* specifies a minimum CVN toughness of 20 ft-lb at –20 °F and 40 ft-lb at 70 °F for demand critical welds. On the other hand, American Welding Society (AWS) *Structural Welding Code–Seismic Supplement*, AWS D1.8 (AWS, 2005) specifies a minimum CVN toughness of 20 ft-lb at 0 °F and 40 ft-lb at 70 °F for demand critical welds.]

FCAW of the flange plates to the column flange was done with an E70T-1 gas-shielded flux-cored electrode (Hobart Brothers TM-11, 3⁄32-in. diameter) and 100% CO_2 shielding gas. This electrode has a specified minimum CVN toughness of 20 ft-lb at 0 °F.

Welding of continuity plates and panel zone doubler plates for all specimens used the FCAW process. Welding was done with an E70T-1/E70T-9 gas-shielded flux-cored electrode (Lincoln Outershield 70, 3⁄32-in. diameter) and 100% CO_2 shielding gas. This electrode has a specified minimum CVN Toughness of 20 ft-lb at –20 °F.

Specimens were erected at University of California, San Diego, by laboratory staff. The column was first placed in position in the test setup, followed by installation of the beam to simulate the field erection process. Beam web to shear tab bolts were ASTM F1852 (A325TC) tension control bolts. Flange plate to beam flange bolts were

Table 2. Steel Mechanical Properties					
Member	**Size**	**Steel Grade**	**Yield Strength[a] (ksi)**	**Tensile Strength[a] (ksi)**	**Elongation[a,b] (%)**
Column	W14×233	A992	51.5	76.5	28
	W14×311		55.0	78.0	27
Beam	W30×108		52.0	77.5	30
	W30×148		58.5	80.0	27
	W36×150		63.5	81.0	31
Bolted Flange Plate	1½-in. PL	A572 Gr. 50	60.5	87.5	25
	1¾-in. PL		54.5	81.5	27
Doubler Plate	¾ in. PL		(57.0)	(78.0)	(20)
Continuity Plate	1 in. PL		(56.7)	(80.3)	(20)

[a] Values in parentheses are based on Certified Mill Test Reports.
[b] Certified Mill Test Report elongation in parentheses based on 8-in. gage length, others based on 2-in. gage length.

ASTM F2280 (A490TC) tension control bolts. Bolts were initially brought to the snug-tight condition with connected plies in firm contact followed by systematic tensioning of the bolts. For the beam web to shear tab connection the middle bolt was tensioned first and then bolts were tensioned outward from the middle progressing in an alternating up and down pattern. Flange plate to beam flange bolts were tensioned, starting with the most rigid portion of the connection near the face of the column and then working progressively outward.

Material Properties

ASTM A992 steel was specified for all beam and column members. ASTM A572 Gr. 50 steel was specified for all plate material. Material properties determined from tension coupon testing are shown in Table 2 and additional information may be found in Sato, Newell and Wang (2008).

Loading Protocol and Instrumentation

The loading sequence for beam-to-column moment connections as defined in the 2005 AISC *Seismic Provisions* was used for testing (see Figure 3). Displacement was applied at the beam tip and was controlled by the interstory drift angle. Specimens were instrumented with a combination of displacement transducers, strain gage rosettes, and uniaxial strain gages to measure global and local responses. Figure 4 shows the location of displacement transducers. Displacement transducer δ_{total} measured the overall vertical displacement of the beam tip. δ_1 and δ_2 measured column movement. δ_3 and δ_4 measured the average shear deformation of the column panel zone. δ_5 and δ_6 measured the slippage between flange plates and beam flanges. For additional instrumentation information see Sato et al. (2008). The data reduction procedure was a modified version of one formulated by Uang and Bondad (1996). The procedure (see Appendix II) was used to compute the components of beam tip displacement, δ_{total}, that are contributed by deformation of the beam, column, panel zone and slip-bearing between the flange plates and beam flanges.

EXPERIMENTAL RESULTS

Several observations were made during testing that were similar for all three specimens. Bolt slip, which produced very loud noises, occurred during early cycles (at 0.375% or 0.5% drift) and on all subsequent cycles. Yielding in the connection region, as evidenced by flaking of the whitewash, was observed to initiate at 2% drift. Beam flange and web local buckling initiated at 4% drift, and lateral-torsional buckling (LTB) of the beam together with twisting of the column was observed at 5% drift.

Testing of Specimen BFP-2 was stopped after one complete cycle at 6% drift due to safety concerns resulting from the observed column twisting [see Figure 5(a)]. For Specimen BFP-3 significant beam LTB and column twisting, as shown in Figure 5(b), were observed at 6% drift. For this specimen, which did not require continuity plates, the unusual yielding pattern of the column, shown in Figure 6, might have been caused by column flange local bending, web local yielding, and column twisting (i.e., warping stress).

Specimen BFP-1 experienced net section fracture of the beam bottom flange at the outermost bolt row on the second excursion to 6% drift. Specimen BFP-3 failed in the same

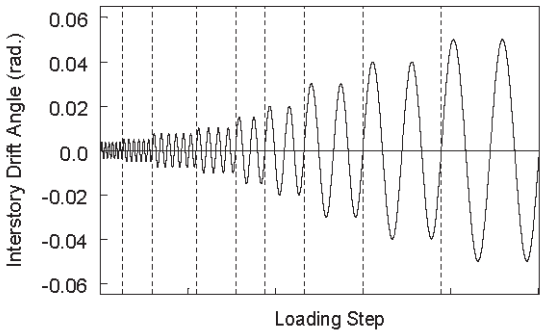

Fig. 3. AISC loading sequence.

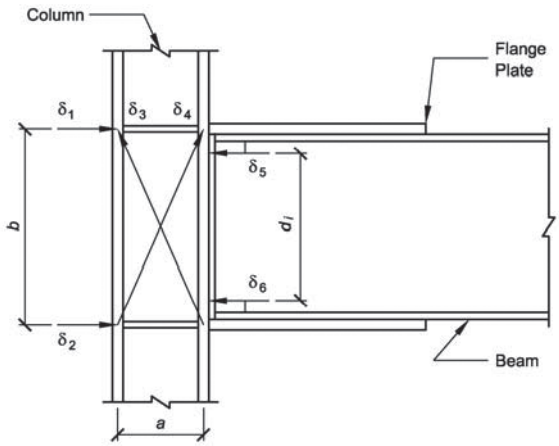

Fig. 4. Instrumentation plan.

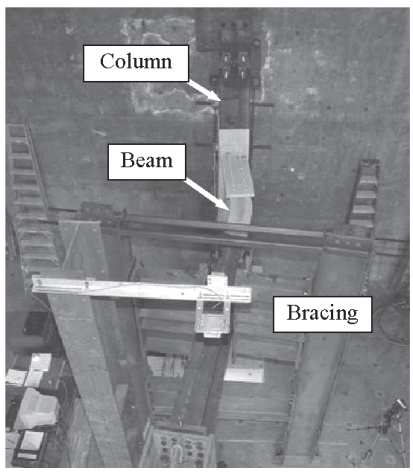

(a) Specimen BFP-2

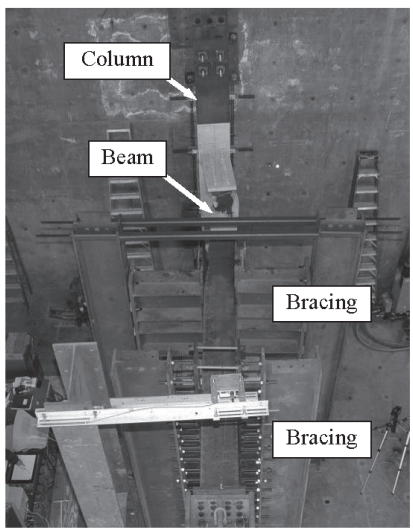

(b) Specimen BFP-3

Fig. 5. Beam lateral-torsional buckling and column twisting at 6% drift.

(a) Overall (west side)

(b) West side detail

(c) East side detail

Fig. 6. Specimen BFP-3: yielding in column.

manner on the first excursion to 7% drift. Figure 7 shows the location and a close-up view of the fracture. For both specimens LTB of the beam increased the tensile strain demand on the edge of the flange net section (i.e., between the flange edge and bolt hole) where failure was observed. Maintaining an adequate edge distance is, therefore, important for the design of BFP connections. Fracture was preceded by the occurrence of necking at the net section. It is likely that Specimen BFP-2 would have experienced net section fracture had testing not been stopped due to safety concerns.

A plot of the moment (at column face) versus beam tip displacement relationship is shown in Figure 8 for the three specimens. To meet the acceptance criteria of the AISC *Seismic Provisions*, specimens shall satisfy the following requirements: (1) the connection must be capable of sustaining an interstory drift angle of at least 0.04 rad, and (2) the required flexural strength of the connections, determined at the column face, must equal at least 80% of the nominal plastic moment (M_{pn}) of the connected beam at an interstory drift angle of 0.04 rad. The vertical dashed lines shown in Figure 8 are at 4% drift and the horizontal dashed lines are at 80% of the nominal plastic moment. Specimens exceeded the requirements of the AISC acceptance criteria and achieved an interstory drift angle of at least 0.06 rad. The pinching observed in the hysteresis loops is mainly attributed to the slip-bearing behavior of the bolted connection. After some amount of initial slippage, hardening behavior can be observed due to bearing between the bolt, flange plate and beam flange.

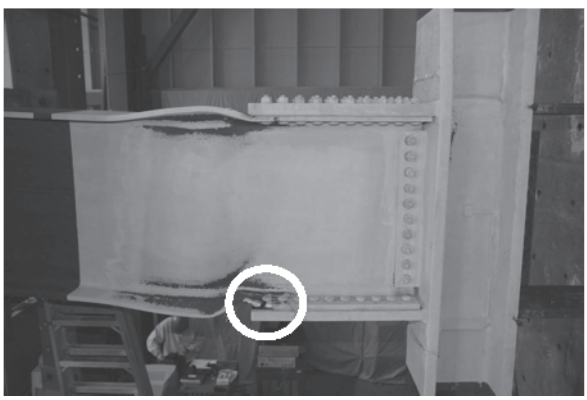

(a) Fracture Location

(b) Close-up

Fig. 7. Specimen BFP-3: beam flange net section fracture.

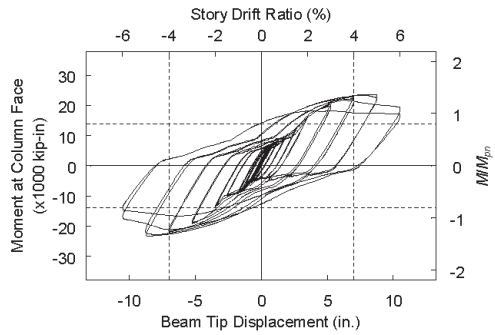

(a) Specimen BFP-1

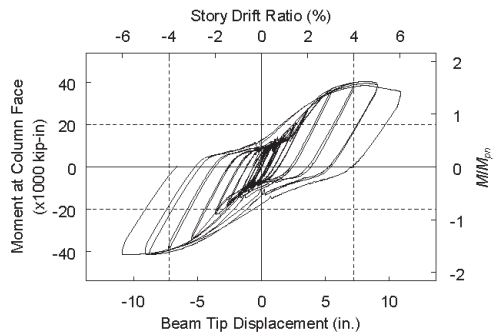

(b) Specimen BFP-2

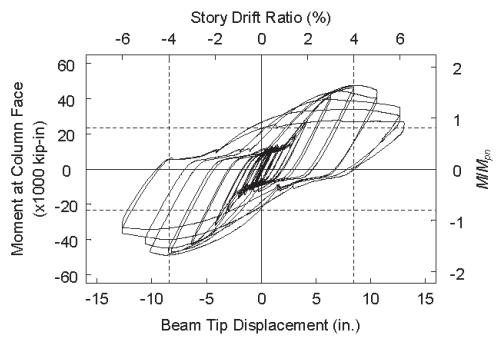

(c) Specimen BFP-3

Fig. 8. Moment versus beam tip displacement relationships.

Figure 9 shows the relative contribution of the column, beam, panel zone, and slip-bearing deformation to the overall beam tip displacement at different drift levels. [For Specimen BFP-2, components at 5% and 6% drift are not shown in Figure 9(b) because column twisting affected the measurements.] Shear deformation in the panel zone and slippage between the flange plate and beam flange made significant contributions to the total beam tip displacement of Specimens BFP-1 and BFP-2. Deformation in the panel zone of Specimen BFP-3 was limited because of the strong panel zone (demand-capacity ratio of 0.73). But slippage and bearing between the flange plate and beam flange made a significant contribution to the total beam tip displacement.

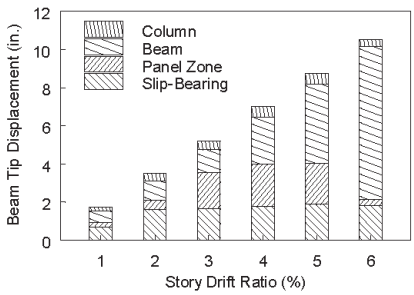

(a) Specimen BFP-1

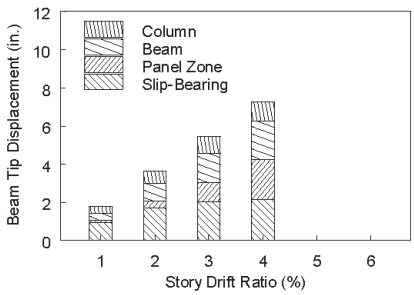

(b) Specimen BFP-2

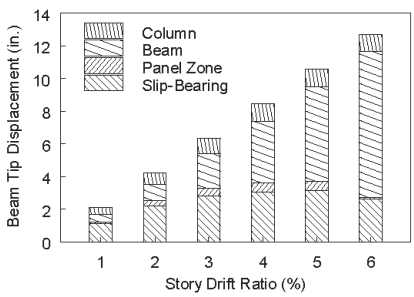

(c) Specimen BFP-3

Fig. 9. Components of beam tip displacement.

COMPARISON OF RESULTS

The overstrength factor, α, resulting from cyclic strain hardening, for each specimen as computed from Equation 1 is shown in Figure 10.

$$\alpha = \frac{M_u}{M_{pa}} \tag{1}$$

Ultimate moment, M_u, was calculated from test data at the assumed plastic hinge location and M_{pa} was the plastic moment of the beam based on measured flange yield strength. Specimen overstrength values were similar to the value of 1.15 [= $(F_y + F_u)/2F_y$] given by AISC *Prequalified Connections for Special and Intermediate Steel Moment Frames for Seismic Applications* (AISC, 2005a).

Significant LTB of the beam and twisting of the column were observed in all specimens. Figure 11(b) shows one column flange strain gauge, near the flange tip, plotted versus the gauge near the opposite flange tip [see Figure 11(a)] for Specimen BFP-2. Deviation from the one-to-one (dashed) line provides an indication of column twisting (i.e., warping stress). Similar evidence of column twisting was observed for the other specimens. The specimens did not include a concrete structural slab, which would have provided lateral bracing to the beam top flange and torsional restraint to the column. Column twisting has been observed in testing of RBS moment connection specimens with deep columns and without a concrete structural slab (Chi and Uang, 2002), but not in testing with W14 columns. Additional deep column moment connection testing has indicated that the presence of a concrete structural slab mitigates column twisting issues associated with deep columns (Zhang and Ricles, 2006). However, the column twisting observed in this testing is a phenomenon that has not been previously observed in testing of moment connections with W14 columns with or without a concrete structural slab.

Potential contributing factors to the observed column twisting include (1) the geometry of the flange plate connection, which pushes the plastic hinge location further away from the column face, and (2) the oversized holes in

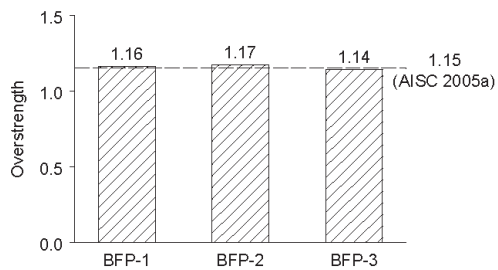

Fig. 10. Beam cyclic overstrength ratio.

the flange plates allowing transverse movement of the beam. The gap between oversized bolt holes and the bolt shank allows for transverse movement of the beam; the second-order effect resulting from such eccentricity in the beam compression flange, although small initially, promotes LTB of the beam. With the plastic hinge located farther away from the column face than for typical (e.g., reduced beam sections) welded moment connections, the effect of out-of-plane forces is magnified (Chi and Uang, 2002).

It is expected based on the design of the bolted connection that slip will occur. However, slip occurred at approximately one-half the expected slip capacity considering the total resistance of all bolts in the connection. As shown in Figure 9, deformation from slip-bearing made a significant contribution to the total deformation. For all specimens at 4% drift slip-bearing deformation contributed approximately 30% of the total deformation. The level of slip-bearing deformation was observed to be consistent for different loading amplitudes (i.e., 2, 3, 4%, drift).

The contribution of slip-bearing deformation to the total deformation is dependent on the oversize of the bolt holes in the flange plate and beam flange. During testing, bolt slip was observed to occur on early cycles and significantly contributed to the overall beam tip displacement on these cycles. As a result, beam flange yielding for the BFP specimens was not observed to occur until 2% drift, whereas for a typical welded moment connection, flange yielding would be expected at about 1% drift. Also, the observed level of beam flange and web local buckling was less severe than observed in previous testing of welded moment connections (Uang, Yu, Noel and Gross, 2000). Bolt slippage and bearing deformation in the BFP connection accommodated deformation that would have induced both local and lateral-torsional buckling in a welded connection.

Specimens BFP-1 and BFP-3 eventually failed by net section fracture of the beam flange at the outermost row of bolts. Testing of Specimen BFP-2 was stopped before fracture, but necking at the outermost row of bolts was observed and it is likely that fracture on the net section would have occurred if testing was continued. Demand on the net section was exacerbated by LTB of the beam. Figure 12 shows strain profiles across the Specimen BFP-3 beam bottom flange for different drift levels. The skew of the strain profiles at higher drift levels resulted from beam LTB.

SUMMARY AND CONCLUSIONS

Three full-scale, one-sided, bolted flange plate steel moment-frame connection specimens consisting of W14 columns and W30 to W36 beams were subjected to increasing amplitude cyclic testing to support prequalification of the bolted flange plate connection for special moment resisting frames. All three specimens performed well and met the acceptance criteria of the AISC *Seismic Provisions*.

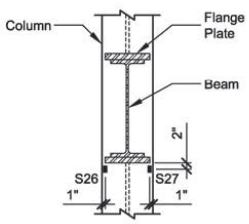

(a) Strain gauge locations

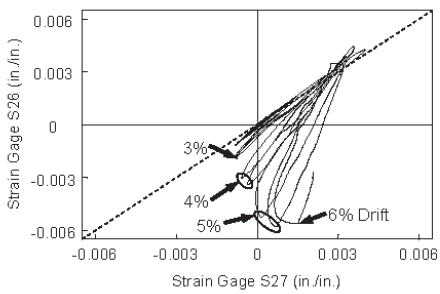

(b) Comparison of strain gauges S26 and S27

Fig. 11. Specimen BFP-2: column flange strains.

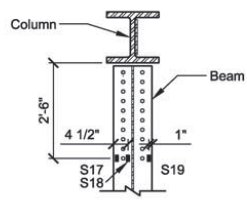

(a) Strain gauge locations

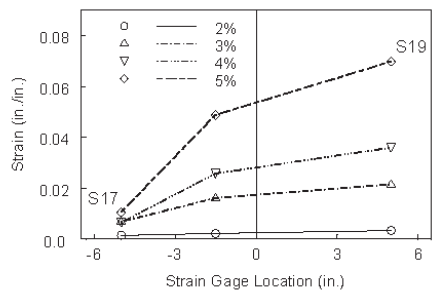

(a) Strain profile (S17, S18, S19)

Fig. 12. Specimen BFP-3: strain profiles across beam bottom flange.

Specimens achieved an interstory drift angle of 0.06 rad before failure. Specimens BFP-1 and BFP-3 failed by beam flange net section fracture and for Specimen BFP-2 necking at the outermost row of bolts was observed. The tensile demand on the net section where fracture occurred was further increased by LTB of the beam.

On large drift cycles (5% and 6%) column twisting was observed in addition to beam LTB. The specimens did not include a concrete structural slab, which would limit LTB and column twisting. However, column twisting has not previously been observed in testing of moment connection specimens with W14 columns without a concrete structural slab.

Bolt-slip occurred early during testing of all three specimens. The BFP connection differs from welded moment connections in that the additional component of bolt slip-bearing contributes to overall inelastic deformation of the connection. Slip-bearing deformation contributed a significant amount to the total deformation (approximately 30% of the total deformation at 4% drift).

ACKNOWLEDGMENTS

Funding for this project was provided by the American Institute of Steel Construction; Mr. Tom Schlafly was the project manager. Design of the test specimens was provided by Professor Linda Hanagan of Pennsylvania State University. Materials and fabrication were donated by Schuff Steel Company and Nucor Fastener.

APPENDIX I: DESIGN PROCEDURE

The draft design procedure outlined below has been developed by AISC's CPRP BFP Committee for inclusion in Supplement Number 1 to *Prequalified Connections for Special and Intermediate Steel Moment Frames for Seismic Applications,* hereafter referred to as AISC *Prequalified Connections* (ANSI/AISC 358-05). The design procedure assumes the beam plastic hinge is located at the center of the outermost (furthest from the column face) row of bolts. The required number of bolts is determined from the force in the flange plates due to the expected moment demand at the face of the column. Controlling shear strength per bolt is determined considering the limit states of bolt shear strength and bearing strength on the beam flange and flange plate. Tensile rupture of the flange plate and block shear of the beam flange are checked. Continuity plate and column panel zone requirements are similar to typical special moment frame requirements.

1. Compute the probable maximum moment at the beam hinge using the requirements of AISC *Prequalified Connections* Section 2.4.3.

$$M_{pr} = C_{pr} R_y F_y Z_x \tag{A-1}$$

2. Compute the maximum bolt diameter preventing beam flange tensile rupture. For standard holes with two bolts per row:

$$d_b \le \frac{b_f}{2}\left(1 - \frac{R_y F_y}{R_t F_u}\right) - \frac{1}{8}\text{ in.} \tag{A-2}$$

3. Considering bolt shear and bolt bearing, determine the controlling nominal shear strength per bolt.

$$r_n = \min\begin{Bmatrix} 1.1 A_b F_{nv} \\ 2.4 d_b t_f F_{ub} \\ 2.4 d_b t_p F_{up} \end{Bmatrix} \tag{A-3}$$

4. Select a trial number of bolts. The following equation may be a useful way of estimating the trial number of bolts.

$$n \ge \frac{1.25 M_{pr}}{\phi_n r_n (d + t_p)} \tag{A-4}$$

5. Determine the beam plastic hinge location, as dimensioned from the face of the column.

$$S_h = S_1 + s\left(\frac{n}{2} - 1\right) \tag{A-5}$$

The bolt spacing between rows, s, and the edge distance shall be large enough to ensure that L_c, as defined in AISC *Specification* (AISC, 2005c) Section J3.10, is greater than or equal to $2d_b$.

6. Compute the shear force at the beam plastic hinge location at each end of the beam. The shear force at the hinge location, V_h, shall be determined by a free body diagram of the portion of the beam between the hinge locations. This calculation shall assume the moment at the hinge location is M_{pr} and shall include gravity loads acting on the beam based on the load combination, $1.2D + f_1 L + 0.2S$.

7. Calculate the moment expected at the face of the column flange.

$$M_f = M_{pr} + V_h S_h \tag{A-6}$$

8. Compute the force in the flange plate due to M_f.

$$F_{pr} = \frac{M_f}{\left(d + t_p\right)} \tag{A-7}$$

9. Confirm that the number of bolts selected in Step 4 is adequate.

$$n \geq \frac{F_{pr}}{\phi_n r_n} \quad \text{(A-8)}$$

10. Determine the required thickness of the flange plate.

$$t_p \geq \frac{F_{pr}}{\phi_d F_y b_{fp}} \quad \text{(A-9)}$$

11. Check the flange plate for tensile rupture.

$$F_{pr} \leq \phi_n R_n \quad \text{(A-10)}$$

where R_n is defined in AISC *Specification* Section J4.1.

12. Check the beam flange for block shear.

$$F_{pr} \leq \phi_n R_n \quad \text{(A-11)}$$

where R_n is defined in AISC *Specification* Section J4.3.

13. Check the flange plate for compression buckling.

$$F_{pr} \leq \phi_n R_n \quad \text{(A-12)}$$

where R_n is defined in AISC *Specification* Section J4.4. When checking compression buckling of the flange plate, the effective length, KL, may be taken as $0.65S_1$.

14. Determine the required shear strength, V_u, of beam and beam web-to-column connection from:

$$V_u = \frac{2M_{pr}}{L'} + V_{gravity} \quad \text{(A-13)}$$

Check design shear strength of beam according to Chapter G of the AISC *Specification*.

15. Design a single plate shear connection for the required strength, V_u, calculated in Step 14 and located at the face of the column, meeting the limit state requirements of the AISC *Specification*.

16. Check the continuity plate requirements according to Chapter 2 of AISC *Prequalified Connections*.

17. Check the column panel zone according to Section 9.3 or 10.3 of the AISC *Seismic Provisions*, as appropriate. The required shear strength of the panel zone shall be determined from the summation of the moments at the column faces as determined by projecting moments equal to $R_y F_y Z_x$ at the plastic hinge points to the column faces. Add twice the thickness of the flange plate to the beam depth for determining the value of d.

18. Check the column-beam moment ratio according to Section 9.6 or 10.6 of the AISC *Seismic Provisions*, as appropriate.

APPENDIX II: DATA REDUCTION PROCEDURE

1. Panel Zone Component: Use Equation A-14 to compute the average panel zone shear strain, $\overline{\gamma}$, and Equation A-15 to compute the panel zone deformation contribution, δ_{pz}, to total beam tip displacement, δ_{total}.

$$\overline{\gamma} = \frac{\sqrt{a^2 + b^2}}{2ab}\left(\delta_3 - \delta_4\right) \quad \text{(A-14)}$$

$$\delta_{pz} = \overline{\gamma} L_b \quad \text{(A-15)}$$

2. Column Component: The column rotation, θ_c, can be computed from Equation A-16 and the column deformation contribution, δ_c to δ_{total}, from Equation A-17.

$$\theta_c = \frac{\left(\delta_2 - \delta_1\right)_{total}}{d_b} - \overline{\gamma}\left(1 - \frac{d_b}{H}\right) \quad \text{(A-16)}$$

$$\delta_c = \theta_c\left(L_b + \frac{d_c}{2}\right) \quad \text{(A-17)}$$

3. Slip-Bearing Component: The slip-bearing rotation, θ_{SB}, and slip-bearing beam tip displacement component, δ_{SB}, can be computed from Equations A-18 and A-19, respectively.

$$\theta_{SB} = \frac{\left(\delta_5 - \delta_6\right)}{d_i} \quad \text{(A-18)}$$

$$\delta_{SB} = \theta_{SB} L \quad \text{(A-19)}$$

4. Beam Component: The beam component, δ_b of δ_{total}, can be computed from Equation A-20.

$$\delta_b = \delta_{total} - \delta_{pz} + \frac{\overline{\gamma} d_b}{H}\left(L_b + \frac{d_c}{2}\right) - \delta_c - \delta_{SB} \quad \text{(A-20)}$$

NOTATION

A_b Nominal unthreaded body area of bolt

C_{pr} Factor to account for peak connection strength, including strain hardening, local restraint, additional reinforcement, and other connection conditions

D Nominal dead load

F_{nv} Nominal shear stress from AISC *Specification* Table J3.2

F_{pr} Probable maximum flange plate force

F_u Specified minimum tensile strength

F_y Specified minimum yield stress

F_{ub} Specified minimum tensile strength of beam material

F_{up} Specified minimum tensile strength of plate material

H Column height

L Nominal live load

L' Distance between hinge locations

L_b Beam clear length

L_c Clear bay width

L_c Clear distance, in the direction of the force, between the edge of the hole and the edge of the adjacent hole or edge of the material

M_f Expected moment at the face of the column flange

M_{pa} Actual plastic moment of the beam

M_{pn} Nominal plastic moment of the beam

M_{pr} Probable maximum moment at plastic hinge

M_u Ultimate moment of the beam achieved at assumed plastic hinge location (outermost row of bolts)

R_n Nominal strength

R_t Ratio of the expected tensile strength to the specified minimum tensile strength F_u

R_y Ratio of the expected yield stress to the specified minimum yield stress F_y

S Snow load

S_1 Distance from face of column to the first row of bolts

S_h Distance from face of column to the plastic hinge location

$V_{gravity}$ Beam shear force resulting from $1.2D + f_1L + 0.2S$

V_h Larger of the two values of shear force at the beam hinge location at each end of the beam

V_u Required shear strength of beam and beam web to column connection

Z_x Plastic section modulus of a member

a Panel zone width

b Panel zone depth

b_f Width of beam flange

b_{fp} Width of flange plate

d Beam depth

d_b Beam depth

d_b Nominal bolt diameter

d_c Column depth

d_i Distance between displacement transducers δ_5 and δ_6

f_1 Load factor determined by the applicable building code for live loads, but not less than 0.5

n Number of bolts

r_n Nominal strength

s Bolt spacing between rows

t_f Beam flange thickness

t_p Flange plate thickness

α Overstrength factor accounting for cyclic strain hardening

δ_1, δ_2 Column displacement transducer (see Figure 4)

δ_3, δ_4 Panel zone displacement transducer (see Figure 4)

δ_5, δ_6 Slip-bearing displacement transducer (see Figure 4)

δ_b Beam component of δ_{total}

δ_c Column component of δ_{total}

δ_{pz} Panel zone component of δ_{total}

δ_{SB} Slip-bearing component of δ_{total}

δ_{total} Total beam tip displacement

θ_c Column rotation

θ_{SB} Slip-bearing rotation

ϕ_d Resistance factor for ductile limit states

ϕ_n Resistance factor for non-ductile limit states

$\bar{\gamma}$ Average panel zone shear strain

REFERENCES

AISC (2005a), ANSI/AISC 358-05, *Prequalified Connections for Special and Intermediate Steel Moment Frames for Seismic Applications*, American Institute of Steel Construction, Chicago, IL.

AISC (2005b), ANSI/AISC 341-05, *Seismic Provisions for Structural Steel Buildings,* American Institute of Steel Construction, Chicago, IL.

AISC (2005c), ANSI/AISC 360-05, *Specification for Structural Steel Buildings,* American Institute of Steel Construction, Chicago, IL.

AWS (2005), *Structural Welding Code—Seismic Supplement*, AWS D1.8, American Welding Society, Miami, FL.

Chi, B. and Uang, C.M. (2002), "Cyclic Response and Design Recommendations of Reduced Beam Section Moment Connections with Deep Columns," *Journal of Structural Engineering*, ASCE, Vol. 128, Issue 4, pp. 464–473.

Schneider, S. and Teeraparbwong, I. (2000), *Bolted Flange Plate Connections*, *Report No. SAC/BD-00/05*, SAC Joint Venture, Sacramento, CA.

Sato, A., Newell, J. and Uang, C.M. (2008), *Cyclic Testing of Bolted Flange Plate Steel Moment Connections for Special Moment Frames, Report No. SSRP-07/10*, Department of Structural Engineering, University of California, San Diego, La Jolla, CA.

Uang, C.M. and Bondad, D. (1996), *Static Cyclic Testing of Pre-Northridge and Haunch Repaired Steel Moment Connections, Report No. SSRP-96/02*, Division of Structural Engineering, University of California, San Diego, La Jolla, CA.

Uang, C.M., Yu, Q.S., Noel, S. and Gross, J. (2000), "Cyclic Testing of Steel Moment Connection Rehabilitated with RBS or Welded Haunch," *Journal of Structural Engineering*, ASCE, Vol. 126, Issue 1, pp. 57–68.

Zhang, X. and Ricles, J. (2006), "Experimental Evaluation of Reduced Beam Section Connections to Deep Columns," *Journal of Structural Engineering*, ASCE, Vol. 132, Issue 3, pp. 346–357.

Simplified LRFD Design of Steel Members for Fire

TAI-KUANG LEE, AUSTIN D.E. PAN and KEN HWA

When a steel structure is exposed to fire, the steel temperatures increase and the strength and stiffness of the steel are reduced, leading to possible deformation and failure, depending on the applied loads and the support conditions. The increase in steel temperatures depends on the severity of the fire, the area of steel exposed to the fire, the amount of applied fire protection, the orientation and geometry of members, compartments, and properties/types of steel.

The control of structural behavior under fire conditions has historically been based on highly prescriptive building code requirements that specify hourly fire resistance ratings. A popular misconception concerning fire resistance ratings for walls, columns, floors and other building components is that the ratings imply the length of time that a building component will remain in place when exposed to an actual fire (FEMA, 2002). However, the traditional approach, based on standard testing methodologies such as ASTM E119 (ASTM, 2000), is often overly conservative and may not be realistic, since a number of factors, such as continuity, member interaction, restraint conditions and load intensity, are not accounted for. Furthermore, the characteristics and location of the structural member, as well as the actual nature of the fire scenario also influence the behavior and eventual failure of the structure and are often not accounted for, especially in the standard furnace test.

Modern structural steel design codes use an ultimate strength design format in which internal actions resulting from the maximum likely values of load are compared with the expected member strength using the short-term strength of the materials under ambient temperature. This design format is referred to as load and resistance factor design (LRFD) in North America (AISC, 2005a and 2005b), and limit states design in Europe (ECS, 1992).

Eurocode 3 provides design guidelines to follow when designing structural members to fire standards (ECS, 1995). These methods involve determining the fire loads imposed on a structure and analyzing the strength of each member at elevated temperatures. The structural design for fire in the Eurocode is conceptually similar to structural design for normal temperature conditions, but with reduction factors accounting for the strength loss at elevated temperatures. The methodologies for the calculation of the temperature of unprotected and protected steel members are given in lumped mass, time-step form, with the increase in temperature being based on energy transferred to the member.

Fire design has been recently stipulated in the AISC *Specification for Structural Steel Buildings,* hereafter referred to as the AISC *Specification* (2005). The new design stipulations, and fire design in general, remain relatively unfamiliar to most structural engineers. This paper proposes a simplified design methodology based on the AISC *Specification*. Design examples are presented and results are compared with experimental data.

LITERATURE REVIEW

A comprehensive overview of the fire resistance of building structures is described in *Structural Design for Fire Safety* (Buchanan, 2001). According to Buchanan, structural steel design for fire is conceptually similar to normal design. The three main differences are (1) the applied live loads are generally lower, (2) internal forces may be induced by thermal expansion and (3) steel strengths are reduced by elevated temperatures. Bailey and Moore (2000a) have developed a design method for calculating the performance of steel-framed structures subjected to fire, with composite flooring systems. Their companion paper (Bailey and Moore, 2000b) shows how the proposed design method can be applied to practical buildings. Usmani, Rotter, Lamont, Sanad and Gillie (2001) present theoretical descriptions of the key phenomena that govern the behavior of composite framed structures in fires. They discuss both thermal expansion and thermal bowing. Simplified fire design based on LRFD remain absent in the literature.

Tai-Kuang Lee is associate researcher, architecture and building research institute, Ministry of the Interior, Sindian, Taipei, Taiwan.

Austin D.E. Pan is senior project engineer, T.Y. Lin International, San Francisco, CA.

Ken Hwa is associate professor, department of architecture, Nanya Institute of Technology, Chungli, Taoyuan, Taiwan.

LRFD DESIGN FOR FIRE

For LRFD, the AISC *Specification* requires that the design strength of each structural component, ϕR_n, equals or exceeds the required strength, R_u, determined on the basis of LRFD load combinations,

$$\phi R_n \geq R_u \tag{1}$$

where

R_u = required strength
R_n = nominal strength
ϕ = resistance factor corresponding to R_n
ϕR_n = design strength

The deterioration in strength and stiffness of structural members, components and systems shall be taken into account in accordance with Appendix 4 of the AISC *Specification*, Structural Design for Fire Conditions. For the purpose of design, the reduction factors k_E, k_y and k_u are defined as the ratio of, respectively, the elastic modulus, yield strength and tensile strength of steel, at elevated temperature to normal temperature. Normal or ambient temperature is assumed to be 20 °C (68 °F).

Tension Members

The design strength of tension members, $\phi_t P_n$, is the lower value obtained according to the limit states of yielding in the gross section and fracture in the net section (Chapter D of the AISC *Specification*). The design strength of a tension member for fire conditions (AISC Appendix 4.2.4.3b) assumes a uniform temperature over the cross section using the temperature equal to the maximum steel temperature.

(a) For yielding in the gross section

$$P_n = k_{y,max} F_y A_g \tag{2}$$

(b) For fracture in the net section

$$P_n = k_{u,max} F_u A_e \tag{3}$$

where

$k_{y,max}$ = reduction factor for the yield strength of steel at the maximum steel temperature
F_y = specified minimum yield strength
A_g = gross area of member
$k_{u,max}$ = reduction factor for the tensile strength of steel at the maximum steel temperature
F_u = specified minimum tensile strength
A_e = effective net area

Compression Members

The design strength of compression members whose elements have width-thickness ratios less than λ_y (compact and non-compact sections) is $\phi_c P_n$ (AISC *Specification* Chapter E). The nominal design strength of a compression member for fire conditions is

For $\dfrac{KL_{ub}}{r} \leq 4.71\sqrt{\dfrac{E}{F_y}} \times \sqrt{\dfrac{k_{E,max}}{k_{y,max}}}$

$$F_{cr} = \left[0.658^{\frac{k_{y,max}F_y}{k_{E,max}F_e}}\right] k_{y,max} F_y \tag{4}$$

For $\dfrac{KL_{ub}}{r} > 4.71\sqrt{\dfrac{E}{F_y}} \times \sqrt{\dfrac{k_{E,max}}{k_{y,max}}}$

$$F_{cr} = 0.877 k_{E,max} F_e \tag{5}$$

where

K = effective length factor
L_{ub} = laterally unbraced length of the member
r = governing radius of gyration about the axis of buckling
E = modulus of elasticity
$k_{E,max}$ = reduction factor for the elastic modulus of steel at the maximum steel temperature

$$F_e = \frac{\pi^2 E}{\left(\dfrac{KL_{ub}}{r}\right)^2} = \text{elastic buckling stress}$$

Flexural Members

The flexural design strength of doubly-symmetric compact I-shaped members bent about their major axis is $\phi_b M_n$ (AISC *Specification* Chapter F). Under fire, the design strength of a flexural member is determined assuming that the bottom flange temperature is constant over the depth of the member.

Case (i)

$$L_b \leq L_p \sqrt{\frac{k_{E,max}}{k_{y,max}}}$$

$$M_n = k_{y,max} F_y Z_x \tag{6}$$

Case (ii)

$$L_p \sqrt{\frac{k_{E,max}}{k_{y,max}}} < L_b \leq L_r \sqrt{\frac{k_{E,max}}{k_{y,max}}}$$

$$M_n = C_b \left[k_{y,max} F_y Z_x - (k_{y,max} F_y Z_x - 0.7 k_{y,max} F_y S_x) \right. \quad (7)$$

$$\left. \times \left(\frac{L_b - L_p \sqrt{\frac{k_{E,max}}{k_{y,max}}}}{L_r \sqrt{\frac{k_{E,max}}{k_{y,max}}} - L_p \sqrt{\frac{k_{E,max}}{k_{y,max}}}} \right) \right] \leq k_{y,max} F_y Z_x$$

Case (iii)

$$L_b > L_p \sqrt{\frac{k_{E,max}}{k_{y,max}}}$$

$$M_n = \frac{C_b \pi^2 k_{E,max} E S_x}{\left(\frac{L_b}{r_{ts}} \right)^2} \leq k_{y,max} F_y Z_x \quad (8)$$

where

L_b = length between points which are either braced against lateral displacement of compression flange or braced against twist of the cross section

$L_p = 1.76 r_y \sqrt{\frac{E}{F_y}}$

Z_x = plastic section modulus about the major axis

$L_r = \pi r_{ts} \sqrt{\frac{E}{0.7F_y}}$

C_b = lateral-torsional buckling modification factor for nonuniform moment diagrams when both ends of the unsupported segment are braced and is permitted to be conservatively taken as 1.0 for all cases

S_x = elastic section modulus about the major axis

$r_{ts} = \sqrt{\frac{I_y h_o}{2S_x}}$

I_y = moment of inertia about the minor axis

h_o = distance between the flange centroids

PROPOSED SIMPLIFIED DESIGN METHOD FOR STEEL MEMBERS UNDER FIRE

As seen in the previous discussion, structural design for fire is conceptually similar to structural design for normal temperature conditions. Design of members is the same as normal temperature design but with degradation factors accounting for the strength and stiffness loss at elevated temperatures. This paper proposes a design methodology, suitable for preliminary design that correlates the design strength of the member at normal temperature. Reduction factors for design strengths under fire for tension, compression and flexural are presented in the following. The reduction factor is defined as the ratio of the design strength at elevated temperature to the design strength at normal temperature:

1. Tension members: The reduction factors, $k_{y,max}$ or $k_{u,max}$, in Equations 2 and 3, are plotted in Figure 1 against temperature.

2. Compression members: The reduction factors due to $k_{E,max}$ and $k_{y,max}$ in Equaitons 4 and 5 are plotted in Figure 2 with respect to

$$R = \frac{KL_{ub}/r}{\sqrt{E/F_y}}$$

R is a nondimensional stability factor. R = 4.71 is the transition point between elastic and inelastic buckling.

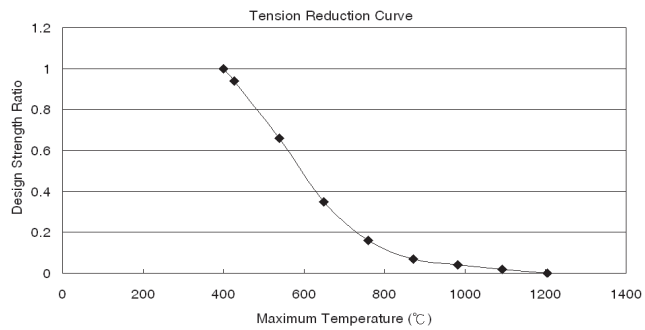

Fig. 1. Strength reduction curve of tension members.

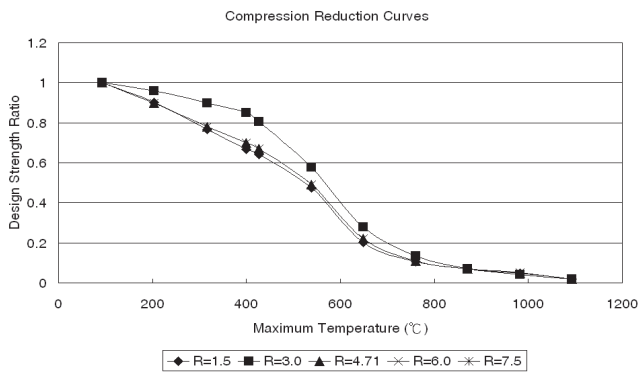

Fig. 2. Strength reduction curves of compression members.

3. Flexural members: The reduction factors due to $k_{E,max}$ and $k_{y,max}$, in Equations 6 through 8, are plotted in Figure 3 with respect to $RL = L_b/L_p$. It is assumed the area of the web is half the flange area, $A_w = 0.5A_f$. RL is a non-dimensional length factor. $RL = 1$ and $RL = L_y/L_p$ are transition points for the different design cases. The following additional simplifying and conservative assumptions are taken for determining the reduction factors and L_r/L_p.

$$S_x = Z_x = b_f t_f h_o$$

$$C_b = 1.0$$

$$r_{ts} = \sqrt{\frac{I_y h_o}{2S_x}} = \sqrt{\frac{I_y}{2b_f t_f}} = \sqrt{\frac{I_y}{2A_f}}$$

$$r_y = \sqrt{\frac{I_y}{A}} = \sqrt{\frac{I_y}{2A_f + A_w}}$$

$$L_p = 1.76 r_y \sqrt{\frac{E}{F_y}} = 1.76 \sqrt{\frac{I_y}{2A_f + A_w}} \sqrt{\frac{E}{F_y}}$$

$$L_r = \pi r_{ts} \sqrt{\frac{E}{0.7F_y}} = \frac{\pi}{\sqrt{0.7}} \sqrt{\frac{I_y}{2A_f}} \sqrt{\frac{E}{F_y}}$$

Therefore,

$$\frac{L_r}{L_p} = \frac{\frac{\pi}{\sqrt{0.7}} \sqrt{\frac{I_y}{2A_f}} \sqrt{\frac{E}{F_y}}}{1.76 \sqrt{\frac{I_y}{2A_f + A_w}} \sqrt{\frac{E}{F_y}}} = \frac{\pi}{1.76 \times \sqrt{0.7}} \sqrt{\frac{2 + (A_w/A_f)}{2}}$$

where

A_w = $(h_o - t_f)\, t_w$ = web area
t_w = web thickness
A_f = $b_f t_f$ = flange area

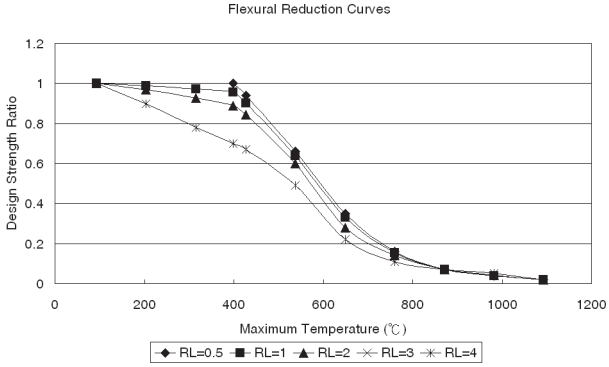

Fig. 3. Strength reduction curves of flexural members ($A_w = 0.5A_f$).

b_f = flange width
t_f = flange thickness

Load Combination

For checking the capacity of a structure or structural element to withstand the effect of an extraordinary event such as fire, the load combination from ASCE 7-02 (ASCE, 2002) is adopted:

$$1.2D + A_k + 0.5L \tag{9}$$

where

D = dead load
L = live load
A_k = load or load effect resulting from an extraordinary event

According to Section C2.5 of ASCE 7-02, extraordinary events arise from extraordinary service or environmental conditions that traditionally are not considered explicitly in design of ordinary buildings and structures. Such events are characterized by a low probability of occurrence and usually a short duration. Specific design provisions to control the effect of extraordinary loads and risk of progressive failure can be developed with a probabilistic basis. But often is the case that data available are limited to define the frequency distribution of the load. A_k must be specified by the authority having jurisdiction. Moreover, as discussed by Usmani et al. (2001), members may experience thermally induced axial force and moment due to thermal expansion and thermal bowing.

Derivation of the Required Design Strength Ratio under Fire

For fire conditions, the structural design follows the basic requirement,

$$\phi R_{nf} \geq R_{uf} \tag{10}$$

where

R_{uf} = required strength under fire
R_{nf} = nominal strength under fire
ϕR_{nf} = design strength under fire

Equation 10 may be rewritten as

$$\frac{\phi R_{nf}}{\phi R_n} \geq \frac{R_{uf}}{\phi R_n} \times \frac{R_u}{R_u} \tag{11}$$

or

$$\frac{\phi R_{nf}}{\phi R_n} \geq \frac{R_{uf}}{R_u} \times \frac{R_u}{\phi R_n} \tag{12}$$

The left side of Equation 12 can be referred to as the required design strength ratio. The required design strength ratio can be expressed as two independent factors,

$$\frac{\phi R_{nf}}{\phi R_n} \geq F_R \times F_{os} \tag{13}$$

where

$F_R = \dfrac{R_{uf}}{R_u}$ = required strength factor; ratio of strength under fire conditions over the strength under normal temperature conditions

$F_{os} = \dfrac{R_u}{\phi R_n}$ = overstrength factor of load demand over the provided capacity (less than 1.0)

Based on the preceding derivation, the required design strength ratio is defined as the product of F_R and F_{os}. The design criterion for fire is thus simplified to one that correlates the required design strength ratio with the reduction factors for fire conditions (see Figures 1, 2 and 3). The overstrength factor, F_o, is obtained from normal temperature design. The required strength factor, F_R, is discussed further.

Required Strength Factor, F_R

In most structural designs, the structure is analyzed elastically and the support and restraint conditions are assumed to remain unchanged. For the purpose of simplification, uniform thermal expansion and unrestrained boundary conditions are assumed in this paper. Because member internal forces are proportional to the applied loading combination, the required strength factor can be simplified as follows:

$$F_R = \frac{1.2D + 0.5L}{1.2D + 1.6L} \tag{14}$$

Equation 14 could be rewritten as

$$F_R = \frac{1.2 + 0.5\left(\dfrac{L}{D}\right)}{1.2 + 1.6\left(\dfrac{L}{D}\right)} \tag{15}$$

CRITICAL TEMPERATURE

Fire design, based on member strength, can be carried out using Equation 13 and Figures 1 through 3. But sometimes, instead of strength, member design based on the critical temperature is a more convenient indicator of structural performance under fire. Regression formulas are derived for the critical temperatures for different types of members.

Tension Members

For the design strength ratio, $\phi R_{nf}/\phi R_n$, given in Figure 1, the regression equation is plotted in Figure 4 (for T ≥ 400 °C).

$$\frac{\phi R_{nf}}{\phi R_n} \approx C_3 T^3 + C_2 T^2 + C_1 T + C_0 \tag{16}$$

where

$C_3 = -1.1497 \times 10^{-9}$

$C_2 = 5.0871 \times 10^{-6}$

$C_1 = -7.0096 \times 10^{-3}$

$C_0 = 3.0862$

Combining Equations 13, 15 and 16, the critical temperature can be obtained by solving the following equation:

$$C_3 T_{cr}^3 + C_2 T_{cr}^2 + C_1 T_{cr} + C_0 = \frac{1.2 + 0.5\left(\dfrac{L}{D}\right)}{1.2 + 1.6\left(\dfrac{L}{D}\right)} \times F_{os} \tag{17}$$

The critical temperatures under different live load and overstrength conditions are shown in Figure 5. Equation 17 may

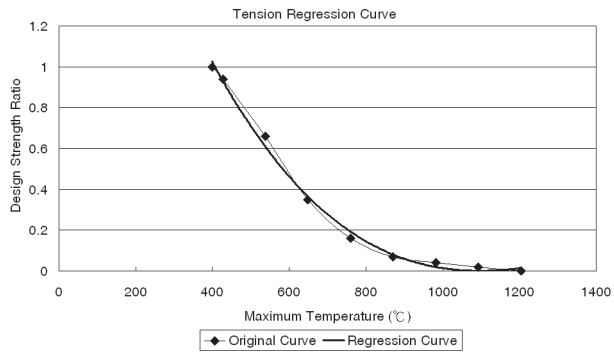

Fig. 4. Strength reduction regression curves of tension members.

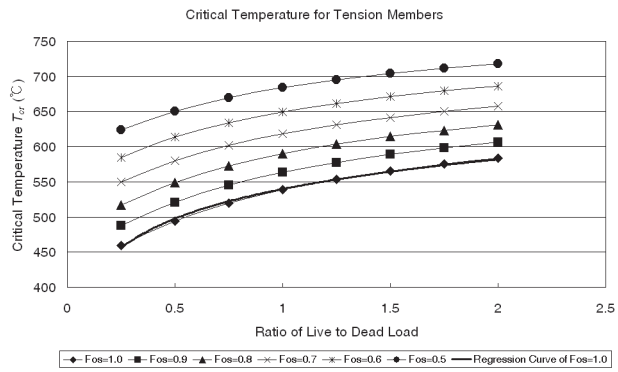

Fig. 5. Critical temperatures of tension members.

Table 1. Regression Coefficients for Critical Temperature of Tension Members (°C)		
F_{os}	$T_{cr} = A \times \ln\left(\frac{L}{D}\right) + B$	
	A	**B**
1.0	60.705	539.82
0.9	58.276	564.52
0.8	55.660	590.97
0.7	52.822	619.51
0.6	49.700	650.63
0.5	46.218	685.07

be expressed in the following simpler form for the critical temperatures of tension members (°C):

$$T_{cr} = A \times \ln\left(\frac{L}{D}\right) + B \tag{18}$$

where coefficients of A and B are listed in Table 1.

Alternatively, A and B may be approximated by these equations:

$$A = 29F_{os} + 32 \tag{19}$$

$$B = 826 - 290F_{os} \tag{20}$$

Compression Members

Referring to Figure 2, the design strength ratio, $\phi R_{nf}/\phi R_n$, does not vary greatly with the stability ratio R. To obtain a simplified formula, use R = 1.5 as the mean value, and a regression curve is obtained as shown in Figure 6 ($T \geq 93$ °C):

$$\frac{\phi R_{nf}}{\phi R_n} \approx C_6T^6 + C_5T^5 + C_4T^4 + C_3T^3 + C_2T^2 + C_1T + C_0 \tag{21}$$

where

$C_6 = -1.2137 \times 10^{-18}$

$C_5 = -1.1832 \times 10^{-14}$

$C_4 = 3.9768 \times 10^{-11}$

$C_3 = -4.0404 \times 10^{-8}$

$C_2 = 1.6093 \times 10^{-5}$

$C_1 = -3.5752 \times 10^{-3}$

$C_0 = 1.2256$

Combining Equations 13, 15 and 21, the critical temperature can be obtained by solving the following equation:

$$C_6T_{cr}^6 + C_5T_{cr}^5 + C_4T_{cr}^4 + C_3T_{cr}^3 + C_2T_{cr}^2 + C_1T_{cr} + C_0 = \frac{1.2 + 0.5\left(\frac{L}{D}\right)}{1.2 + 1.6\left(\frac{L}{D}\right)} \times F_{os} \tag{22}$$

The critical temperatures under different dead and live load ratios are shown in Figure 7. Equation 22 may be expressed in the following simpler form for the critical temperatures of compression members (°C):

$$T_{cr} = C \times \ln\left(\frac{L}{D}\right) + F \tag{23}$$

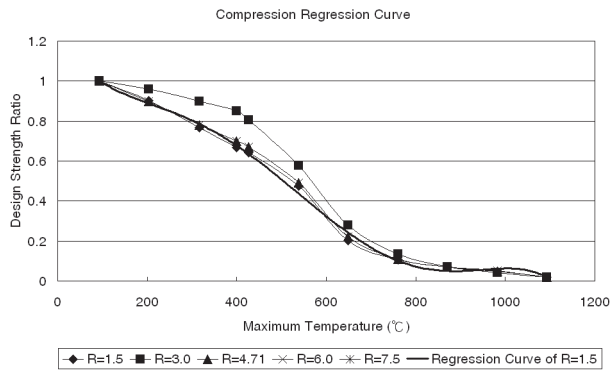

Fig. 6. Strength reduction regression curves of compression members.

Table 2. Regression Coefficients for Critical Temperature of Compression Members (°C)		
F_{os}	$T_{cr} = C \times \ln\left(\frac{L}{D}\right) + F$	
	C	F
1.0	109.94	436.79
0.9	87.342	475.14
0.8	72.330	510.27
0.7	61.308	543.98
0.6	52.604	577.47
0.5	45.371	611.82

Table 3. Regression Coefficients for Flexural Members Under Fire				
$RL = 0.5$	C_6	C_5	C_4	C_3
	8.5426×10^{-17}	-3.5679×10^{-13}	5.8637×10^{-10}	-4.7694×10^{-7}
	C_2	C_1	C_0	
	1.9915×10^{-4}	-4.1899×10^{-2}	4.7078	
$RL = 4$	C_6	C_5	C_4	C_3
	2.8344×10^{-18}	-2.8605×10^{-14}	6.7037×10^{-11}	-6.2053×10^{-8}
	C_2	C_1	C_0	
	2.4495×10^{-5}	-4.9401×10^{-3}	1.2953	

where coefficients of C and F are listed in Table 2.

Alternatively, C and F may be approximated by these equations:

$$C = 182F_{os}^2 - 148F_{os} + 75 \tag{24}$$

$$F = 787 - 347F_{os} \tag{25}$$

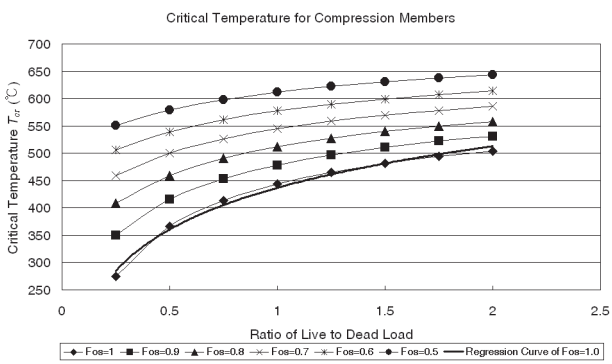

*Fig. 7. Critical temperatures of compression members (*R *=1.5).*

Flexural Members

Referring to Figure 8, the design strength ratios, $\phi R_{nf}/\phi R_n$, are plotted together with regression equations for the two extreme cases of braced length condition, RL = 0.5 and RL = 4.

$$\frac{\phi R_{nf}}{\phi R_n} \approx C_6T^6 + C_5T^5 + C_4T^4 + C_3T^3 + C_2T^2 + C_1T + C_0 \tag{26}$$

The coefficients of regression curves of flexural members are listed in Table 3. Combining Equations 13, 15 and 26, the critical temperature can be obtained by solving the following equation:

$$C_6T_{cr}^6 + C_5T_{cr}^5 + C_4T_{cr}^4 + C_3T_{cr}^3 + C_2T_{cr}^2 + C_1T_{cr} + C_0 = \frac{1.2 + 0.5\left(\frac{L}{D}\right)}{1.2 + 1.6\left(\frac{L}{D}\right)} \times F_{os} \tag{27}$$

Table 4. Regression Coefficients for Critical Temperature of Flexural Members (°C)				
F_{os}	$T_{cr} = G \times \ln\left(\frac{L}{D}\right) + H$ (°C) (RL = 0.5)		$T_{cr} = G \times \ln\left(\frac{L}{D}\right) + H$ (°C) (RL = 4)	
	G	H	G	H
1.0	56.954	553.74	109.03	451.55
0.9	51.019	575.52	84.463	489.23
0.8	46.157	597.59	69.618	523.15
0.7	42.042	620.46	59.048	555.65
0.6	38.490	644.71	50.807	587.99
0.5	35.406	671.20	44.005	621.28

The critical temperatures under different dead and live load ratios are shown in Figures 9 and 10. Equation 27 may be expressed in the following simpler form for the critical temperatures of flexural members (°C):

$$T_{cr} = G \times \ln\left(\frac{L}{D}\right) + H \quad (°C) \tag{28}$$

where coefficients of G and H are listed in Table 4.

Alternatively, G and H may be approximated by these equations:

For $RL = 0.5$

$$G = 35F_{os}^2 - 10F_{os} + 32 \tag{29}$$

$$H = 786 - 234F_{os} \tag{30}$$

For $RL = 4$

$$G = 206F_{os}^2 - 184F_{os} + 86 \tag{31}$$

$$H = 791 - 336F_{os} \tag{32}$$

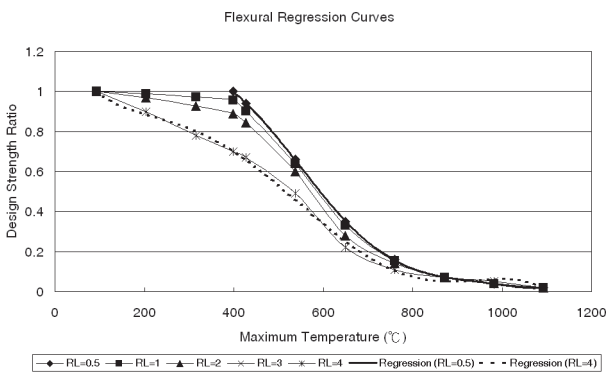

Fig. 8. Strength reduction regression curves of flexural members ($A_w = 0.5A_f$).

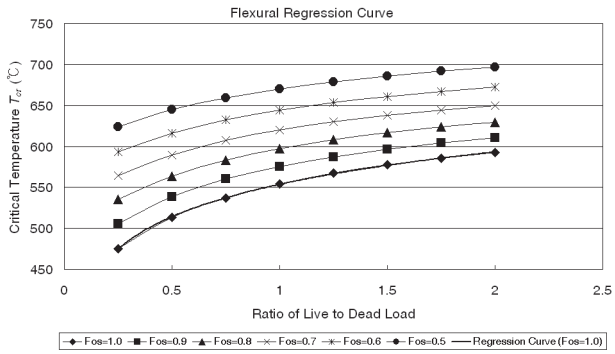

*Fig. 9. Critical temperatures of flexural members (*RL = *0.5).*

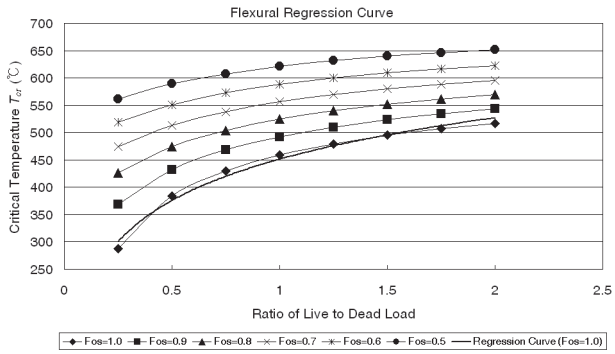

*Fig. 10. Critical temperatures of flexural members (*RL = *4).*

ILLUSTRATIVE EXAMPLE

The following example illustrates how the proposed methodology is applied for a simply supported steel beam with the given design data:

Dead load = 4 kN/m^2; Design live load = 2 kN/m^2
Span length (l) = 9000 mm; Width of the slab = 3000 mm
Adequate lateral restraint is assumed, i.e., $L_b < L_p$
Design mean temperature = 500 °C
Steel material is ASTM A36 (F_y = 250 MPa), modulus of elasticity (E) = 200000 MPa
Start out with a trial steel beam section W18×40

Normal temperature design

1. Check the local buckling of flange and web:

   Flange: $\dfrac{b_f}{2t_f} = \dfrac{152.8}{2\times 13.3} = 5.74 < \lambda_p$

   where

   $$\lambda_p = 0.38\sqrt{\frac{E}{F_y}} = 0.38\times\sqrt{\frac{200000}{250}}$$
   $$= 10.75 \quad \textbf{o.k.}$$

   Web: $\dfrac{h}{t_w} = \dfrac{402.7}{8} = 50.34 < \lambda_p$

   where

   $$\lambda_p = 3.76\sqrt{\frac{E}{F_y}} = 3.76\times\sqrt{\frac{200000}{250}}$$
   $$= 106.35 \quad \textbf{o.k.}$$

   This beam section is a compact one and the proposed methodology is applicable (doubly-symmetric compact I-shaped members bent about their major axis).

2. Calculate the moment capacity of the steel beam:

   For W18 × 40, Z_x = 1293 cm^3

   $$M_n = F_y Z_x = \frac{250\times 1293}{1000} = 323.25 \text{ kN-m}$$

3. Combine factored dead and live loads and moments:

   $w_u = 1.2w_D + 1.6w_L = 1.2\times 4 + 1.6\times 2 = 8$ kN/m^2

   $$M_u = \frac{1}{8} w_u l^2 = \frac{1}{8}\times 8\times 3\times (9)^2 = 243 \text{ kN-m}$$

4. Compare the moment capacity against demand:

   $\phi_b M_n = 0.9\times 323.25 = 290.93$ kN-m $> M_u$ **o.k.**

Simplified LRFD fire design based on critical temperature

Calculate the moment overstrength ratio,

$$F_{os} = \frac{243}{290.93} = 0.835$$

Assume a braced length factor, RL = 0.5, since adequate lateral restraint is provided. Then, using Equations 28, 29 and 30, determine the critical temperature and compare with the design temperature of 500 °C.

$$T_{cr} = [35(0.835)^2 - 10(0.835) + 32]\times \ln\left(\frac{2}{4}\right)$$
$$+ [786 - 234(0.835)]$$

T_{cr} = 557 °C > 500 °C **o.k.**

Simplified LRFD fire design procedures based on member strength

1. Calculate the moment capacity of the steel beam:

   Determine $k_{y,max}$ from linear interpolation. See Table 5.

   $$k_{y,max} = 0.66 + (0.94 - 0.66)\left[\frac{(538-500)}{(538-427)}\right] = 0.76$$

   The nominal moment capacity at 500 °C is

   $M_{nf} = k_{y,max} F_y Z_x = 0.76\times 323.25 = 246$ kN-m

2. The combined dead and live load moment for fire design:

   $w_{uf} = 1.2w_D + 0.5w_L = (1.2\times 4) + (0.5\times 2) = 5.8$ kN/m^2

   $$M_{uf} = \frac{1}{8} w_{uf} l^2 = \frac{1}{8}(5.8)(3)(9)^2 = 176 \text{ kN-m}$$

3. Compare with the moment capacity of the steel beam:

   $\phi_b M_{nf} = 0.9(245.67) = 221$ kN-m $> M_{uf}$ **o.k.**

Cross-check critical temperature with the design strength

1. Determine, by linear interpolation, $k_{y,max}$ for the critical temperature = 557 °C. See Table 5.

   $$k_{y,max} = 0.35 + (0.66 - 0.35)\left[\frac{(649-557)}{(649-538)}\right] = 0.6$$

   Calculate the nominal moment strength,

   $M_{nf} = k_{y,max} F_y Z_x = 0.6\times 323.25 = 194$ kN-m

2. Compare the moment capacity with the combined dead and live load moment:

   $\phi_b M_{nf} = 0.9(194) = 175$ kN-m

   M_{uf} =176 kN-m

   The two moment values are very close.

Table 5. Reduction Factor of Steel at Elevated Temperatures [from AISC *Specification* (AISC, 2005)]			
Steel Temperature	$k_E = E_m/E$	$k_y = F_{ym}/F_y$	$k_u = F_{um}/F_u$
20 °C	*	*	*
93 °C	1.00	*	*
204 °C	0.90	*	*
316 °C	0.78	*	*
399 °C	0.70	1.00	1.00
427 °C	0.67	0.94	0.94
538 °C	0.49	0.66	0.66
649 °C	0.22	0.35	0.35
760 °C	0.11	0.16	0.16
871 °C	0.07	0.07	0.07
982 °C	0.05	0.04	0.04
1093 °C	0.02	0.02	0.02
1204 °C	0.00	0.00	0.00
*Use ambient properties			

The main advantage of the proposed LRFD design methodology is that fire design is greatly simplified. The critical design temperature is obtained from one equation, e.g., Equation 28. At the preliminary design stage, structural designers can readily estimate the critical temperatures of steel members from two design parameters: the ratio of live to dead load and the overstrength factor, F_{os}.

EXPERIMENTAL VALIDATION

The simplified LRFD fire calculations are now compared with experimental results reported by Rubert and Schaumann (1986). Shown in Figure 11 are the simply supported I-section beams tested by Rubert and Schaumann. The beams were subjected to a constant load at mid-span and heated along the entire length. These beams were subject to various load ratios F_c/F_u ranging from 0.20 to 0.85, in which F_c and F_u are, respectively, the applied and ultimate concentrated loads. The experimental results are summarized in Table 6 and compared the simplified fire calculations. The self-weight of steel beams and applied concentrated load are dead loads; no live loads are included. Unrestrained boundary conditions are assumed. The predicted temperatures are calculated by Equation 27, assuming $RL = 0.5$ (span length is 1140 mm) and $F_R = 1.0$. It can be seen in Table 6 that the predicted critical temperatures, T_P, by the simplified fire calculations are in reasonable agreement with the critical temperatures reported experimentally, T_E. The predicted or calculated critical temperatures are lower than the experimental failure temperatures, thus, they are conservative.

CONCLUSIONS

This paper proposes a simplified LRFD design methodology for steel members under fire. By extending LRFD design under normal temperatures, the fire design criterion is derived that compares the required design strength ratio with the design strength reduction ratio. Design strength ratios are derived from the required strength factor and the overstrength factor. Simplified formulas for member strength at elevated temperatures, as well as their corresponding critical temperatures, are derived for steel members under tension, compression, and flexure (doubly-symmetric compact I-shaped members bent about their major axis). Sections may be compact or noncompact, but boundary conditions

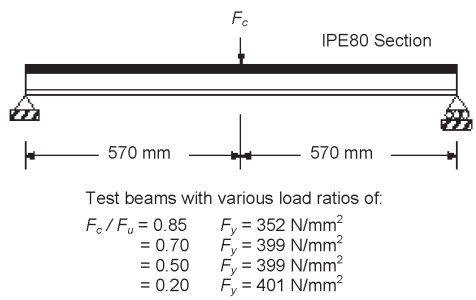

Fig. 11. Simply supported beam tested under fire (Rubert and Schaumann, 1986).

Table 6. Comparison of Calculated Results with Experimental Data from Rubert and Schaumann (1986)				
Specimen	**1**	**2**	**3**	**4**
F_y (N/mm^2)	352	399	399	401
F_c/F_u	0.85	0.70	0.50	0.20
1.2 M_D (kN-mm)	8338.63	7785.86	5564.61	2243.87
ϕM_n (kN-mm)	7356.10	8338.30	8338.30	8380.10
Normal Temperature Design	NG	OK	OK	OK
F_R	–	1.0	1.0	1.0
F_{os}	–	0.9337	0.6674	0.2678
Required $\frac{\phi_b M_{nf}}{\phi_b M_n}$	–	0.9337	0.6674	0.2678
Predicted T_P (°C)	–	431	533	688
Experimental T_E (°C)	520	540	600	730
T_P/T_E	–	0.80	0.89	0.94

are assumed to be unrestrained. Engineers and architects using the proposed methodology should be aware of the limitations of the member sections and boundary conditions. One set of experimental data was taken for comparison, and the calculated results predicted by the proposed simplified formulas compare reasonably well. However, the proposed methodology is best suited for preliminary design purposes, individual users should verify their specific design situation and final design should be carried out in conjunction with the AISC *Specification*.

NOTATION

A = regression coefficient

A_e = effective net area, mm^2

A_f = $b_f t_f$ = flange area, mm^2

A_g = gross area of member, mm^2

A_k = value of the load or load effect resulting from an extraordinary event

A_w = $(h_o - t_f)\, t_w$ = web area, mm^2

B = regression coefficient

b_f = width of flange, mm

C = regression coefficient

C_b = lateral-torsional buckling modification factor for nonuniform moment diagrams when both ends of the unsupported segment are braced and is permitted to be conservatively taken as 1.0 for all cases

C_i = regression coefficients, where i = 0, 1, 2, 3, 4, 5, 6

D = dead load

E = modulus of elasticity, MPa

F = regression coefficient

F_c = applied concentrated load

F_{cr} = critical stress, MPa

F_e = elastic buckling stress, MPa

F_{os} = $\frac{R_u}{\phi R_n}$ = overstrength factor

F_R = $\frac{R_{uf}}{R_u}$ = required strength factor

F_u = specified minimum tensile strength or ultimate concentrated load

F_y = specified minimum yield stress, MPa

G = regression coefficient

H = regression coefficient

h = clear distance between flanges less the fillet or corner radius at each flange, mm

h_o = distance between the flange centroids, mm

I_y = moment of inertia about the minor axis, mm^4

K = effective length factor

k_E = reduction factor for the elastic modulus of steel at the steel temperature

$k_{E,max}$ = reduction factor for the elastic modulus of steel at the maximum steel temperature

k_u = reduction factor for the tensile strength of steel at the steel temperature

$k_{u,max}$ = reduction factor for the tensile strength of steel at the maximum steel temperature

k_y = reduction factor for the yield strength of steel at the steel temperature

$k_{y,max}$ = reduction factor for the yield strength of steel at the maximum steel temperature

L = live load

L_b = distance between points braced against lateral displacement of the compression flange, or between points braced to prevent twist of the cross section

L_p = $1.76 r_y \sqrt{\frac{E}{F_{yf}}}$ for I-shaped members including hybrid sections and channels, mm

L_r = $\pi r_{ts} \sqrt{\frac{E}{0.7F_y}}$, mm

L_{ub} = laterally unbraced length of the member

l = span of a simply supported steel beam, mm

M_n = nominal flexural strength

M_{nf} = nominal flexural strength for fire design

M_u = required flexural strength

M_{uf} = required flexural strength for fire design

P_n = nominal compressive or tension strength

R = $\frac{KL_{ub}/r}{\sqrt{E/F_y}}$

RL = $\frac{L_b}{L_p}$

R_n = nominal strength

R_{nf} = nominal strength under fire

R_u = required strength

R_{uf} = required strength under fire

r = governing radius of gyration about the axis of buckling, mm

r_{ts} = $\sqrt{\frac{I_y h_o}{2S_x}}$, mm

r_y = radius of gyration about y-axis, mm

S_x = elastic section modulus about the major axis, mm^3

T_{cr} = critical temperature, °C

T_E = critical temperature reported experimentally, °C

T_P = predicted critical temperature by the simplified fire calculations, °C

t_f = thickness of flange, mm

t_w = thickness of web, mm

w_D = design dead load, kN/m^2

w_L = design live load, kN/m^2

w_u = design required load, kN/m^2

w_{uf} = design required load for fire design, kN/m^2

x = subscript relating symbol to strong axis bending

y = subscript relating symbol to weak axis bending

Z_x = plastic section modulus about the major axis

ϕ = resistance factor corresponding to R_n

ϕ_b = resistance factor for flexure = 0.90

ϕ_c = resistance factor for compression = 0.90

ϕ_t = resistance factor for tension = 0.90 or 0.75

λ_p = limiting slenderness parameter for compact element

λ_y = limiting slenderness parameter for noncompact element

REFERENCES

AISC (2005), *Specification for Structural Steel Buildings*, American Institute of Steel Construction, Inc., Chicago, IL.

ASTM (2000), *Standard Test Methods for Fire Tests of Building Construction and Materials*, ASTM E119-00a, American Society for Testing and Materials.

ASCE (2002), *Minimum Design Loads for Buildings and Other Structures*, SEI/ASCE 7-02, American Society of Civil Engineers.

Bailey, C.G. and Moore, D.B. (2000a), "The Structural Behaviour of Steel Frames with Composite Floor Slabs Subject to Fire: Part 1: Theory," *The Structural Engineer*, Vol. 78, No. 11, pp. 19–27.

Bailey, C.G. and Moore, D.B. (2000b), "The Structural Behaviour of Steel Frames with Composite Floor Slabs Subject to Fire: Part 2: Design," *The Structural Engineer*, Vol. 78, No. 11, pp. 28–33.

Buchanan, A.H. (2001), *Structural Design for Fire Safety*, John Wiley & Sons.

ECS (1992), *Eurocode 3: Design of Steel Structures—Part 1.1: General Rules and Rules for Buildings,* European Committee for Standardization.

ECS (1995), *Eurocode 3: Design of Steel Structures—Part 1.2: General Rules—Structural Fire Design*, European Committee for Standardization.

FEMA (2002), *World Trade Center Building Performance Study: Data Collection, Preliminary Observations, and Recommendations*, FEMA 403, Federal Emergency Management Agency.

Rubert, A. and Schaumann, P. (1986), "Structural Steel and Plane Frame Assemblies under Fire Action," *Fire Safety Journal*, Vol. 10, pp. 173–184.

Usmani, A.S., Rotter, J.M., Lamont, S., Sanad, A.M. and Gillie, M. (2001), "Fundamental Principles of Structural Behaviour under Thermal Effects," *Fire Safety Journal*, Vol. 36, pp. 721–744.

Quantifying and Enhancing the Robustness in Steel Structures: Part 1—Moment-Resisting Frames

CHRISTOPHER M. FOLEY, CARL SCHNEEMAN and KRISTINE BARNES

Unusual or abnormal are the adjectives most often used to describe loading imparted to a structural system through events of such low probability of occurrence that they can be omitted in design of the structural system. When a structural system is subjected to an abnormal loading event, there is the probability that a component or components will be compromised and their load-carrying capacity reduced or rendered entirely ineffective. Progressive (disproportionate) collapse describes a scenario whereby localized damage to the structural system propagates into a failure that is much greater than the instigating event. Experience with natural disasters (e.g., earthquakes) and performance of structures in the World Trade Center complex (NIST, 2005) provides evidence that buildings can withstand significant damage and localized component failure without total collapse in the absence of specialized structural engineering consideration for these severe damage states during the original design.

The need to prevent progressive collapse during the design phase and examples of structural systems suffering damage without progressive collapse presents a conundrum to the structural engineering profession. Does the profession stay the previous course under the assumption that nothing needs to be changed? Does it develop load and resistance factor design procedures that include target reliabilities against progressive collapse for all structural systems? Does it recommend that all buildings be designed using such procedures? It is interesting to note that this conundrum is nothing new as the Institution of Structural Engineers faced it in the aftermath of the Ronan Point collapse (ISE, 1969, 1971, 1972a, 1972b).

Christopher M. Foley is associate professor, department of civil and environmental engineering, Marquette University, Milwaukee, WI.

Carl Schneeman is a structural engineer, Walker Parking Consultants, Minneapolis, MN.

Kristine Barnes is a structural engineer, AREVA NP, Inc., Naperville, IL.

The two most commonly referenced United States design guidelines to evaluate progressive collapse resistance in structural systems are published by the General Services Administration (GSA, 2003) and the Department of Defense (DOD, 2005). These guidelines and criteria exercise indirect and direct design procedures (Leyendecker and Ellingwood, 1977). An indirect design approach would be to require that all structural systems have vertical and horizontal ties of minimum specified capacities to facilitate the activation of alternate load paths in the event of an abnormal loading scenario. A direct design approach would be to require the structural engineer to explicitly create alternative load paths in the structural system by considering element removal scenarios and designing members and connections to accommodate the secondary load paths that result. The Unified Facilities Criteria (DOD, 2005) contains a process whereby the structural engineer can align his/her desired protection levels against progressive collapse with a suitable design and analysis procedure. The engineer will implement an indirect or direct design approach based upon the protection level sought. The GSA guidelines (GSA, 2003) essentially guide the structural engineer into a direct design process.

By ensuring orthogonal tying mechanisms are present and/or carrying out element removal with subsequent structural analysis, the structural engineer can enhance a system's ability to resist disproportionate collapse. However, tying a structural system together (e.g., external cabling) may establish conditions whereupon portions of a structural system that is collapsing pull down adjacent portions of the structure (Magnusson, 2004; Loizeaux and Osborn, 2006). These issues add another layer to the conundrum facing the structural engineer. For example, is there a single tying force magnitude that can be used for typical structures? When and where should the ties in the system be broken to facilitate compartmentalization of damage?

ACI 318 (ACI, 2005) has had minimal general structural integrity provisions for decades. Furthermore, other North American specifications for steel design (CISC, 2004) explicitly state that "the requirements of this Standard generally provide a satisfactory level of structural integrity for steel structures." Although one could argue the efficacy of general structural integrity provisions in providing definitive mitigation of disproportionate collapse, and debate the evidentiary support for broad-based statements regarding the levels of structural integrity provided by typical design specifications,

there is no denying that provisions and statements such as these give structural engineers and the general public confidence that if a design is undertaken using these codes and specifications, disproportionate collapse is unlikely. General structural integrity provisions and/or general statements regarding the effectiveness of designs carried out using specifications in resisting disproportionate collapse are highly desirable.

The objective of this two-part article is to provide information that can lead to (1) better understanding of disproportionate collapse in structural steel framing systems; (2) improved understanding of secondary load paths that form within structural steel framing systems in the event of a localized failure; (3) development of minimum general structural integrity provisions for structural steel framing systems analogous to those present in ACI 318; (4) recommendations for minimum tie forces that can be used as the basis of indirect design methodologies for structural steel framing systems; (5) an understanding of the distribution of tensile forces within typical steel floor framing systems to facilitate compartmentalization damage or collapse; and (6) identification of simple and economical means with which to enhance the robustness in the typical structural steel framing system.

LITERATURE REVIEW AND SYNTHESIS

Length constraints preclude a detailed literature review. However, there are three sources that the reader can review to gain a complete understanding of the body of literature related to progressive collapse. The first is the annotated bibliography of Leyendecker, Breen, Somes and Swatta (1976). This document covers the body of knowledge accumulated during the time frame 1948 to 1976. Foley, Martin and Schneeman (2007) provide a thorough literature review covering the years 1976 through 2005, and Mohamed (2006) provides a targeted review of state-of-the-art design provisions and several relatively recent research efforts.

The Ronan Point collapse in the United Kingdom was the structural engineering profession's first real-life example of progressive collapse after an abnormal loading event (Griffiths, Pugsley and Saunders, 1968). The report describing the cause of the collapse event and design recommendations to mitigate progressive collapse drew considerable discussion (ISE, 1969, 1971, 1972a, 1972b). The U.K. experience very quickly evolved into building regulations that have been updated and modified through the years (ODPM, 2005).

Following Ronan Point, considerable attention was paid to developing requirements for reinforcement continuity and tie arrangements within concrete structural systems (Popoff, 1975; Speyer, 1976; Breen and Siess, 1979; Fintel and Schultz, 1979). Reinforcement continuity recommendations for slab systems were also developed to mitigate the tendency for disproportionate collapse in the event of a punching shear failure in a two-way slab system (Hawkins and Mitchell, 1979; Mitchell and Cook, 1984). These research efforts serve as the basis for minimum general structural integrity provisions in the current concrete code (ACI, 2005).

Studies quantifying the incidence of abnormal loading events have been undertaken (Leyendecker and Burnett, 1976) and serve as the foundation for probability models for failure (Ellingwood, Leyendecker and Yao, 1983). These efforts eventually migrated into design strategies for mitigating progressive collapse after abnormal loading events (Leyendecker and Ellingwood, 1977; Ellingwood and Leyendecker, 1978; Ellingwood, 2002, 2005; Ellingwood and Dusenberry, 2005; Ellingwood, 2006).

Objective evaluation of codes and design guidelines for progressive collapse mitigative design have been completed (Marchand and Alfawakhiri, 2004; Liu, Davison and Tyas, 2005; Abruzzo, Matta and Panariello, 2006; Ettouney, Smilowitz, Tang and Hapij, 2006; Majanishvili and Agnew, 2006; Ruth, Marchand and Williamson, 2006). There have also been thorough reviews of the progressive collapse mechanism and abnormal loading events with subsequent practical recommendations for mitigating the tendency for disproportionate collapse (Iwankiw and Griffis, 2004; Nair, 2004; Shipe and Carter, 2004; Nair, 2006). Design strategies that can be used to generate structural engineering solutions with low architectural impact have also been proposed (Hamburger and Whittaker, 2004) and the suitability of seismic detailing practice in mitigating progressive collapse in concrete structures has been evaluated (Corley, 2002).

A main focus area of past research efforts has been simulating response of structural systems to abnormal loading events and simulating the progressive collapse mechanism. Girhammar (1980c) examined the role of catenary action in a two-span continuous beam system after loss of interior support and the dynamic loading sensitivity of a small structural system has been evaluated (Christiansson, 1982). McNamara (2003) evaluated the response of a 39-story steel building using static pushdown analysis and an energy-based methodology for evaluating the tendency for progressive collapse following a compromising event has been proposed (Dusenberry and Hamburger, 2005, 2006). Recommendations regarding the use of energy-based procedures for non-single-degree-of-freedom (SDOF) systems and case studies outlining sudden column removal in building systems have been made (Powell, 2005). Rahamian and Moazami (2003) considered a 35-story steel building and several compromising scenarios that involve column removal. Khandelwal and El-Tawil (2005) discuss the results of detailed finite element analysis of large-scale building systems and the tendency for collapsing portions of a structural system to generate large

out-of-plane forces on perimeter framing systems. Grierson, Safi, Xu and Liu (2005a) and Grierson, Xu and Liu (2005b) outline several methodologies intended to be used for progressive collapse analysis that include the capability to consider debris loading. General evaluation of two-dimensional steel building systems with partially restrained connections subjected to compromising events has recently been undertaken (Lim and Krauthammer, 2006).

In comparison to analytical work, there have been relatively few experimental efforts undertaken to understand the impact of abnormal loading scenarios on members and connections within a structural steel system. Owens and Moore (1992) evaluated the ability of double angle web cleat and flush end plate connections (considered flexible in the United States) to support tie forces found in British Standards (BSI, 2003). Munoz-Garcia, Davison and Tyas (2005) conducted experimental testing and finite element analysis of these connections to help support and extend this earlier effort through use of high-strain-rate loading protocols. Dynamic testing of a two-span continuous flush end plate connected steel beam with instantaneous loss of interior support was completed (Girhammar, 1980b). Similar testing with extended end plate connections have also occurred (Girhammar, 1980a). Relatively recent testing on simple beam connections (Guravich and Dawe, 2006) provide information on the likely capacities for simple framing connections when subjected to combined shear and tension loading.

A synthesis of the literature leads to the foundation for the present effort. First of all, there are very few studies that provide detailed evaluation of member and connection demands suitable for the development of general structural integrity provisions for steel structural systems. Furthermore, there has been limited study of the impact of framing system topology on the response of steel framing systems to abnormal loading events, and there have been very few efforts undertaken that consider the response of three-dimensional (3D) systems to compromising scenarios. To achieve the objectives listed earlier and address gaps in the body of knowledge revealed through the literature review and synthesis, this two-part article outlines and implements a series of transient and static analyses to quantify demands placed on members, connections, and the floor diaphragm within structural steel moment-resisting framing systems with various topologies when a compromising event occurs. Secondary load paths likely to be activated in the event a structural member is compromised are identified, and attempts to quantify their participation in resisting applied loading are included in a series of three-dimensional inelastic structural analyses. This first paper focuses on moment-resisting frames within the overall building and a companion manuscript; the second paper (Foley, Barnes and Schneeman, 2008) focuses on the typical structural steel floor framing system.

MOMENT-RESISTING FRAMES CONSIDERED

Evaluating the robustness and structural integrity inherent with the steel structural framing system is a relatively daunting task given the fact that there are limitless combinations of shapes, connections and framing configurations. The SAC-FEMA suite of buildings (Gupta and Krawinkler, 1999) were selected as base topologies for the research effort. Pre-Northridge configurations located in Boston were chosen. The framing configurations considered do not satisfy strong-column-weak-beam criteria at all beam-to-column connection locations within the framework. Steel wide-flange shapes with 50-ksi lower-bound yield stress typical of ASTM A992 were used. Framing plans and column schedules for the frames considered are given in Figures 1 through 6. Interior beams and girders were assumed to be connected using *flexible* connections (solid circles at the beam ends). Moment-resisting (fully restrained) connections at the ends of the beams are indicated with solid triangles. A penthouse was located at the roof level and its location is indicated in the plans. Column splice locations are indicated in the column schedules, but these splices were not simulated in the analysis.

The bases of all columns were assumed to be pinned. This is a modification to the three-story SAC-Boston frame. The 10-story building contains one subterranean level and the 20-story frame considers two subterranean levels. Nodes in the analytical model immediately adjacent to the vertical ground edge were assumed to have horizontal movement restrained, but were free to move vertically. The pinned connections at the ends of the infill beams and any girders were considered fully restrained with regard to bending about the member's minor and longitudinal axes (torsion) to reflect the presence of a concrete floor slab. The floor-to-floor heights shown in the column schedules are assumed to be taken from centerline of beam/girder to centerline of beam/girder. No rigid offsets or flexible panel zones were considered. Centerline-to-centerline horizontal dimensions were considered throughout. It should be noted that the structural analysis model included two elements per column member and four elements per beam member. In order to attain a better distribution of mass through the framing system (Powell, 2005), all in-fill beams were divided into two elements.

A relatively simplistic loading scenario was used. The floors were assumed to support a superimposed dead loading of 83 psf, which included concrete-steel composite slab, steel decking, ceilings/flooring/fireproofing, mechanical/electrical/plumbing systems, and partitions (20 psf). The live loading applied to the floors was assumed to be typical office occupancy with a magnitude of 50 psf. The region of the roof in the penthouse area was assumed to have a superimposed dead loading of 96 psf applied. The live loading in this area was taken to be 50 psf. The roof in regions outside of the penthouse area was assumed to support a superimposed

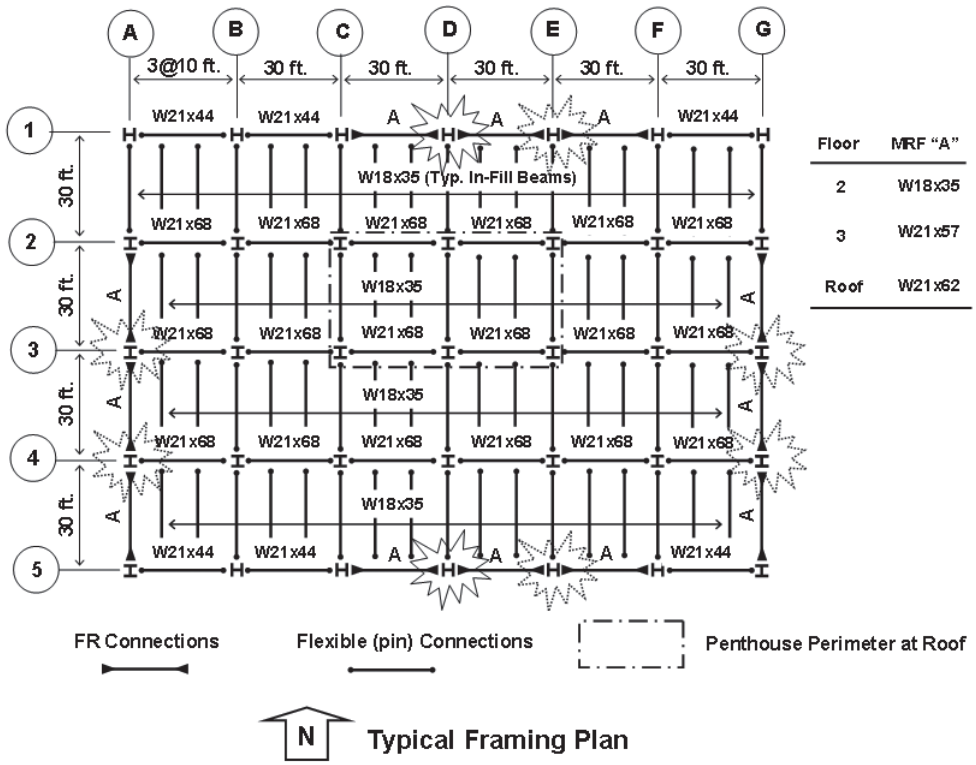

Fig. 1. Framing plan used for the 3-story building frame.

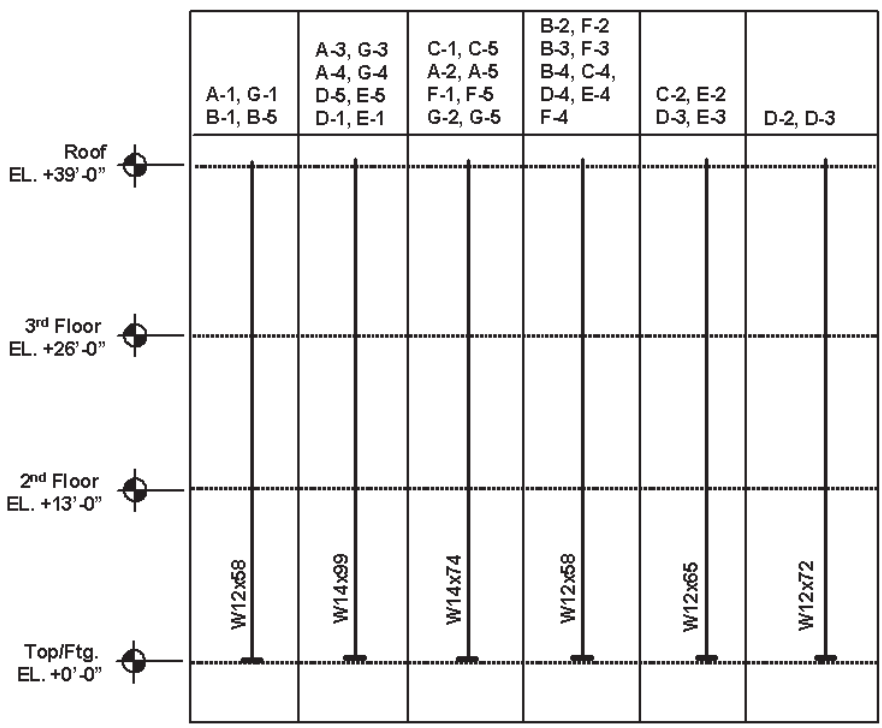

Fig. 2. Column schedule for the 3-story building frame.

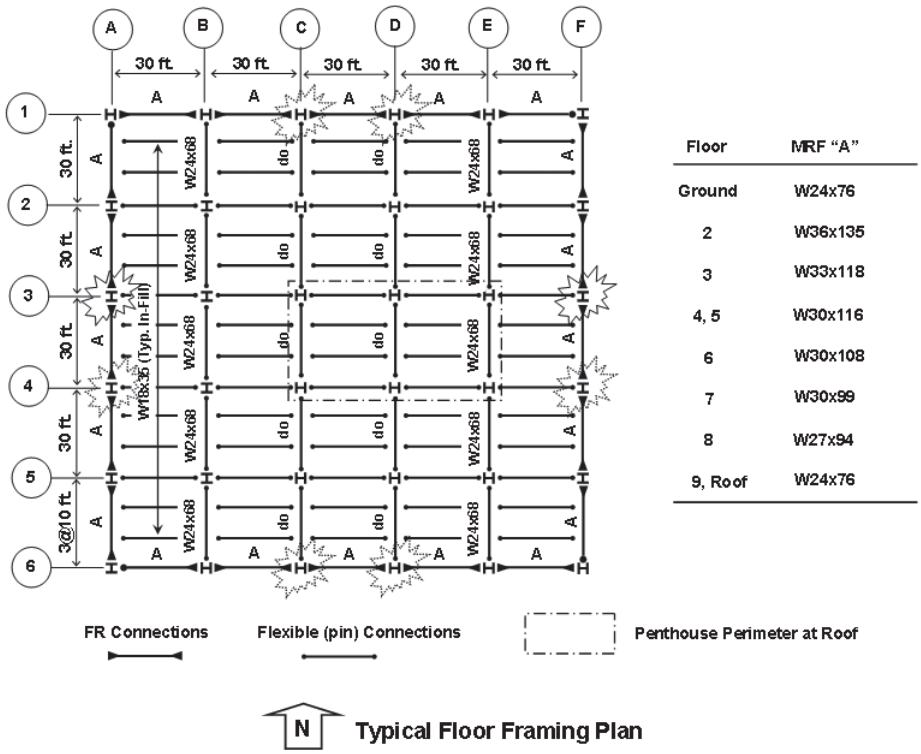

Floor	MRF "A"
Ground	W24x76
2	W36x135
3	W33x118
4, 5	W30x116
6	W30x108
7	W30x99
8	W27x94
9, Roof	W24x76

Fig. 3. Framing plan used for the 10-story building frame.

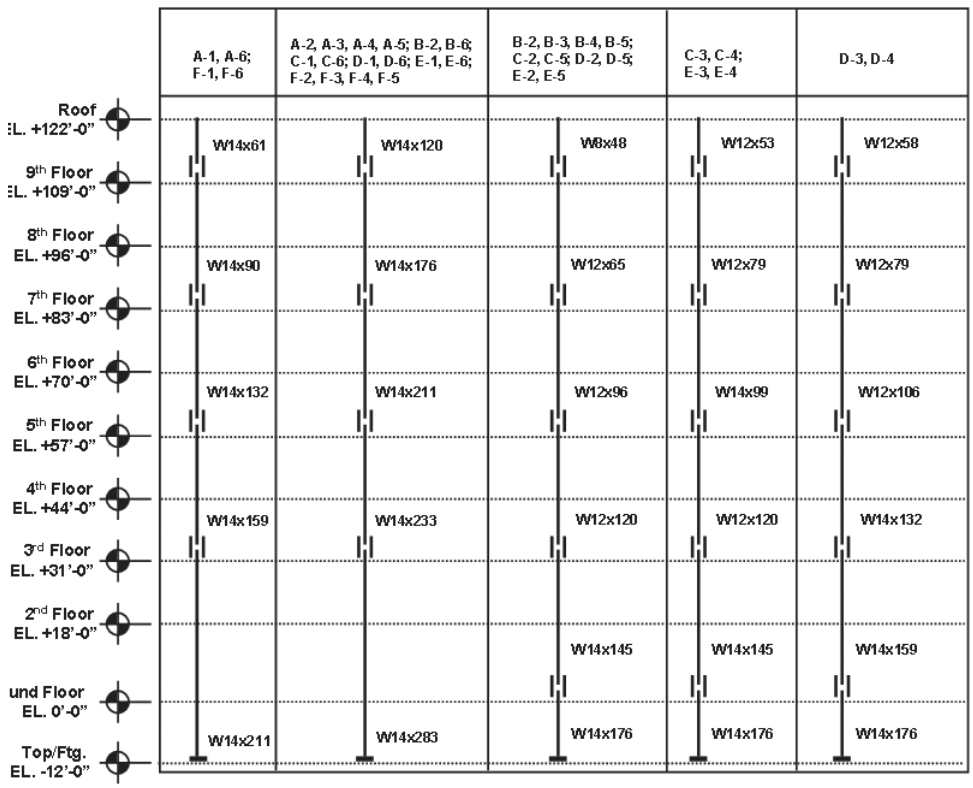

Fig. 4. Column schedule for the 10-story building frame.

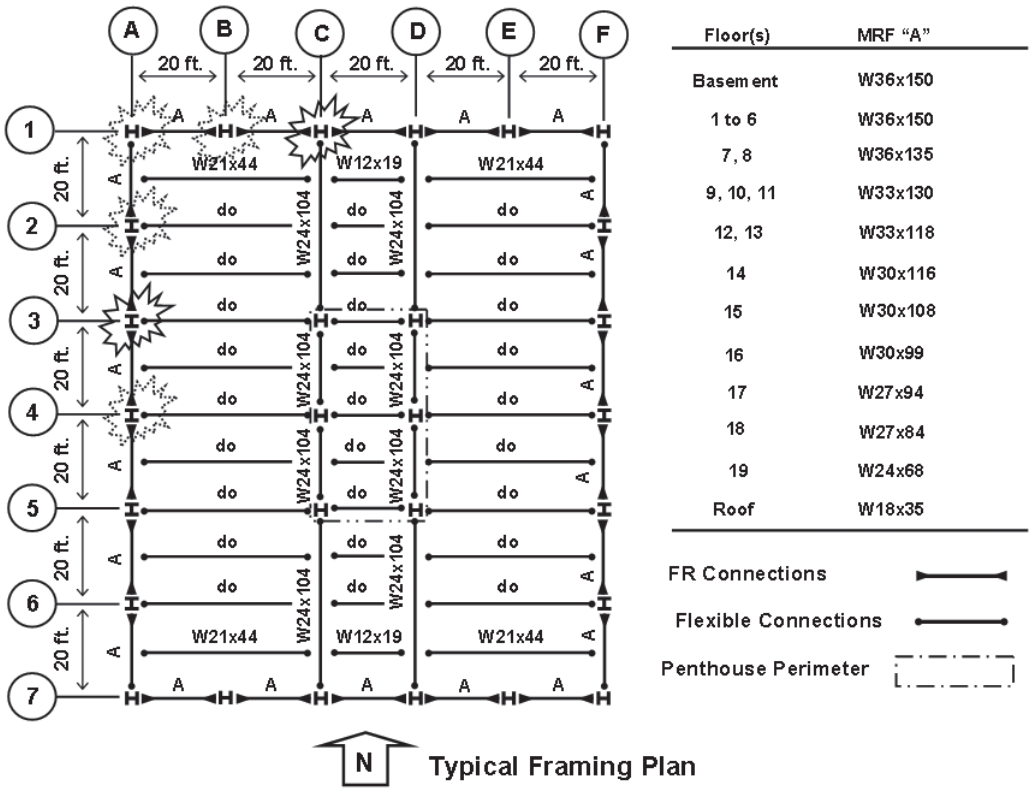

Fig. 5. Framing plan used for the 20-story building frame.

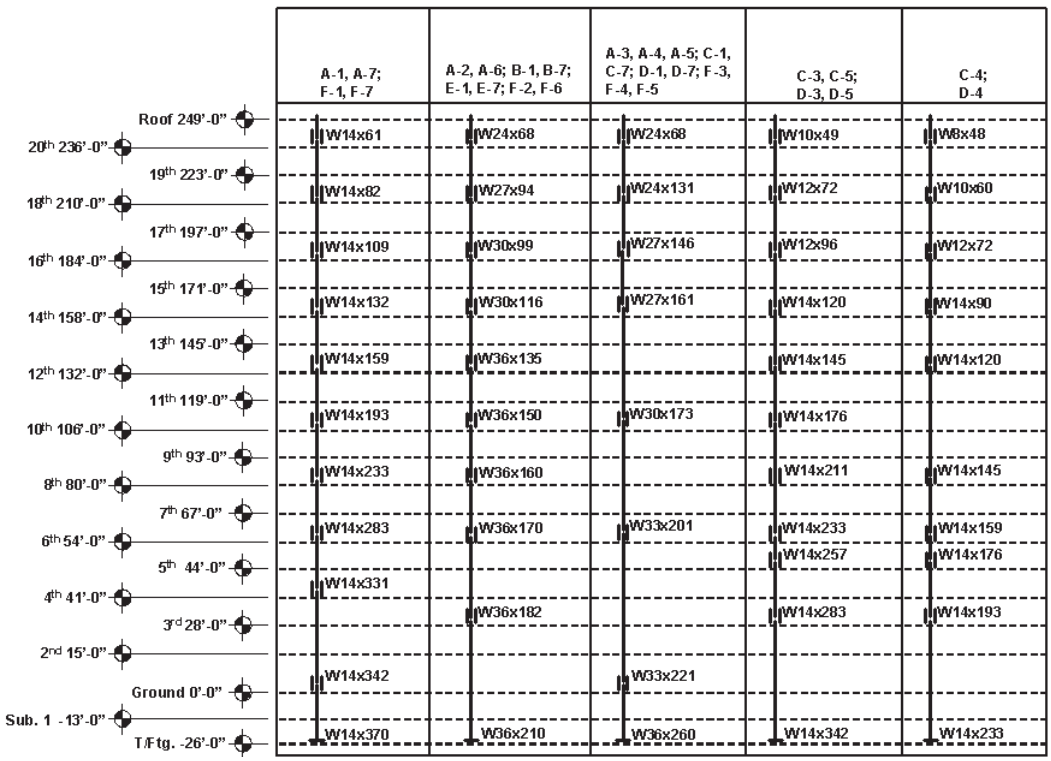

Fig. 6. Column schedule for the 20-story building frame.

dead loading of 63 psf and a live loading of 50 psf (one could argue for a 30-psf snow load). Exterior cladding was assumed around the perimeter of the building. This cladding was assumed to weigh 25 psf over the wall area, including a 3.5-ft-high parapet at the roof level. The self-weight of the structural steel framing members was computed automatically by the computer software.

There are several recommended procedures that can be used to evaluate the tendency for disproportionate collapse (GSA, 2003; DOD, 2005). These procedures were reviewed and the transient analysis approach is used in the present effort. The loading combination applied to the frame at the time of the compromising events is

$$1.0D + 0.25L \quad (1)$$

The live loading used is intended to simulate the live loading present at the time of the compromising event. The live load models used as the basis for U.S. structural engineering involve two components: (1) sustained loading and (2) extraordinary loading. The sustained portion is assumed to be continuously present (with varying magnitude), and it represents ordinary office furniture, bookcases, desks, safes, their contents, and normal personnel (McGuire and Cornell, 1974). Variation in the sustained loading magnitude would likely be generated by tenant occupancy changes. The extraordinary portion of the live loading is intended to simulate those instances where people group during office parties, or cases where office furniture is temporarily stacked during remodeling (McGuire and Cornell, 1974).

The present study assumes that the live loading present when the structural system is compromised is the expected arbitrary point-in-time sustained live loading (Ellingwood and Culver, 1977). Extraordinary live loading components are not considered. Surveys and analysis of office live loading (Culver, 1976; Ellingwood and Culver, 1977) indicate that the expected arbitrary point-in-time sustained live loading is on the order of 11 psf. The present study assumes the live loading present at the time of the compromising event is 12.5 psf. It should be noted that no live load reduction is utilized.

THREE-STORY BUILDING

A three-dimensional structural model was developed for the three-story building using SAP2000 (CSI, 2004). A systematic series of analyses with increasing complexity was conducted. Further details of the modeling and analyses undertaken and results can be found elsewhere (Foley et al., 2007). An initial critical load analysis conducted without diaphragm stiffness modeling resulted in very low elastic critical load factors arising from the lack of a "rigid" diaphragm in the system, and the buckling modes were not consistent with reality. As a result, modeling diaphragm action in the framing system was included. The models implemented in the analysis assumed that the concrete floor slab does not act compositely with the steel skeleton. The slab system deformation that is likely to arise subsequent to a column member within the framing system becoming ineffective is schematically shown in Figure 7. Massless X-bracing members were used to simulate the presence of a composite-steel concrete deck diaphragm at the floor and roof levels through the assumption that the lines of principal tension and compression can be replaced with discrete members with an equivalent shear racking stiffness to that of the concrete portion of the deck system. This concept is very similar to that used by Mahendran and Moor (1999) in the analysis of three-dimensional metal buildings. The present analysis assumed a W14×159 diagonal member with zero material density and eigenvalue analysis of the 3D framework with diaphragm members in place indicated buckling mode shapes that were in line with engineering intuition.

An examination of the framing plan shown in Figure 1 indicates the simply-supported interior framing likely leads to limited ability of the system to overcome an interior or corner column becoming ineffective without activating load resisting mechanisms that are exceedingly difficult to include in the SAP2000 models utilized (e.g., two-way catenary/membrane action in the floor slab). As a result, interior and corner columns becoming ineffective were not considered in this frame analysis. It should be noted that conclusions regarding interior and corner column removal should not be made until two-way catenary action in the floor system,

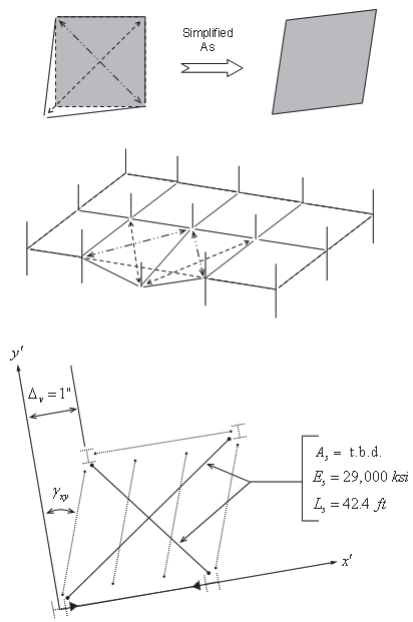

Fig. 7. Conceptualization of diaphragm behavior with a compromised building and diagonal bracing members used to model diaphragm shear deformations.

3D response, and connection characteristics are considered in the analysis. It was decided to examine a scenario whereby an exterior (perimeter) column at the first floor level in the building was rendered entirely ineffective. The ineffective column is located immediately below the second floor level. It should also be noted that only one column at a time is considered to be ineffective. The moment-resisting frame layout in the building considered suggested several compromised column events (highlighted in Figure 1) could be handled with a single analysis. Although the manner in which the gravity load is delivered through the framing system to columns D1, E1, D5 and E5, and A3, A4, G4 and G3 differ, the magnitude of the gravity loading that arrives at each of these columns is the same and a plastic mechanism analysis would illustrate that one group or the other can be considered in the analysis. Therefore, the present analysis considered columns D1, E1, D5 and E5 being compromised.

An elastic buckling analysis was conducted to gain an engineering feel for the system in the compromised state. The first two critical elastic buckling modes were translational sway modes. Higher torsional buckling modes were also present. The magnitudes of the loads at elastic instability were significantly greater than the magnitudes implied in Equation 1 with applied load ratios at instability exceeding 2.0. The elastic critical load analysis was used simply as another check point along the way to detailed nonlinear (geometry and material) transient analysis of the frame.

Elastic dynamic analysis was conducted to evaluate the effect of column loss rates and geometric nonlinearity on the response. The process by which a column in the framework becomes ineffective is modeled using time-history analysis.

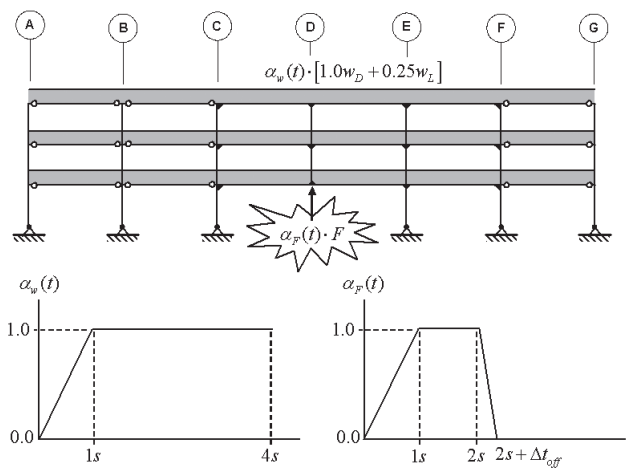

Fig. 8. Conceptualization of column loss scenario implemented in the time-history analysis of the compromised framework.

Both the gravity loading and a concentrated vertical force simulating the loading in the column are applied as time-history functions (Figure 8). The entire analysis duration (4 seconds in this case) was determined via trial and error. The gravity loading and column force are applied over a 1-second interval with an additional 1-second interval with constant magnitude that allows the frame to settle in place with the gravity loads applied. The column's resisting axial load is then turned off over a time interval, Δt_{off}, and the frame is allowed to dynamically respond to this event. One can argue that damping levels during an event whereby beams and/or columns in the framing system become ineffective will be higher than levels during seismic events (i.e., significant deformations, cracking, etc., will occur). However, the present structural analysis assumes damping at a level equal to 5% of critical. Default magnitudes of material-level damping in SAP2000 were also used (CSI, 2004).

The impact of turn-off rate and geometric nonlinearity on the response was examined. Figure 9 illustrates very little difference in peak displacement and the period of the response exists with turn-off rates equal to Δt_{off} = 0.05 s. The response seen with inclusion of geometric nonlinearity is nearly identical to the linear geometric response. This is expected since the applied gravity loading is very small relative to the factored load levels used in design, the axial load in the columns is very small relative to the Euler critical load, and there is minimal translation of column ends relative to one another.

The SAC-FEMA study of moment-resisting connections (FEMA, 2000a, 2000c) pointed out the importance of strain rate. To this end, the elastic strain rates for axial loading, shear loading, and bending moment were computed (Foley et al., 2007). Linear geometric response, 5% damping, elastic material response, and a turn-off rate of 0.01 second were utilized. Local connection effects causing stress concentrations were not considered. The strain rates resulting from axial loading in the columns and beams range from a low of 1,875 με/s (0.0019 in./in./s) and a high of 6,250 με/s (0.0062 in./in./s). The strain rates resulting from transverse shear were significantly higher in all members. Peak shear strain rates occur in the columns of the framework at the top of the third story columns. These rates were on the order of 28,000 με/s (0.028 in./in./s). Strain rates resulting from bending moment for most members in the frame were comparable to the axial and shear rates. An exception is element 1,143, which is a third story column at column line C (see Figure 9). The bending moment normal strain rate for this member is relatively rapid with a peak equal to 50,000 με/s (0.05 in./in./s).

The fracture toughness of steel materials can be reduced as the loading rate increases from that used in determining the fracture toughness according to ASTM E399 (ASTM, 1997; Barsom and Rolfe, 1999). Dynamic and intermediate

loading rates are often taken to be on the order of 1.0×10^7 με/s (10 ε/s) and 1,000 με/s (0.001 ε/s), respectively (Barsom and Rolfe, 1999). The time to maximum bending moment or maximum shear was on the order of 0.15 second. If it is assumed that the event rendering the column ineffective occurs when the steel's temperature is near room temperature, the loading rates found in the elastic time-history analysis give no indication that fracture toughness of the constituent materials will be significantly diminished. It is understood that local strain concentrations resulting from connection details and flaws that may be generated through welding have been ignored. These issues need further evaluation.

The SAP2000 program has the capability of defining a variety of hinge types in addition to interaction surfaces. Shakedown analysis on benchmark problems led to concerns that the version of SAP2000 (CSI, 2004) being implemented was unable to properly follow axial load moment interaction surfaces; therefore, hinges used in nonlinear material analysis for the present study were limited to moment only, with subsequent checks validating this modeling assumption.

The interaction surface assumed in the present study utilizes nominal moment capacities that include limit states of lateral-torsional buckling and yielding. In those cases where the nominal moment capacity is less than the plastic moment capacity of the cross-section, the moment hinge incorporates a yield moment that is less than the plastic moment capacity. Figure 10 illustrates the moment hinges defined for the inelastic analysis of the three-dimensional framework and their locations within the analytical model. As indicated in the figure, the moment capacities of the W14×74 and W14×99 cross-sections are limited by flange local buckling. The moment hinges were defined using the expected yield stress of the material. Points B, C and D are defined with a small amount of hardening to aid in convergence during the nonlinear solution.

Inelastic time-history analysis was carried out by starting with a model that was a modification of the elastic analysis model. Major-axis plastic-moment hinge behavior was modeled at the locations indicated in Figure 10, and the time-step increments used during the Newmark solution algorithm were reduced to 0.001 second. The analytical hinges indicated in the figure were friction-free pins inserted in the model to conservatively simulate flexible connection behavior at the indicated locations. The convergence tolerance was relaxed slightly from the default values, and the event tolerance parameter was set to 0.01. The same time-history functions and column upward axial load magnitudes were used in the inelastic analysis. Because the elastic time-history analysis demonstrated that nonlinear geometric effects were negligible, a first-order materially nonlinear analysis was executed here. The system deformations seen in the inelastic analysis support this assumption.

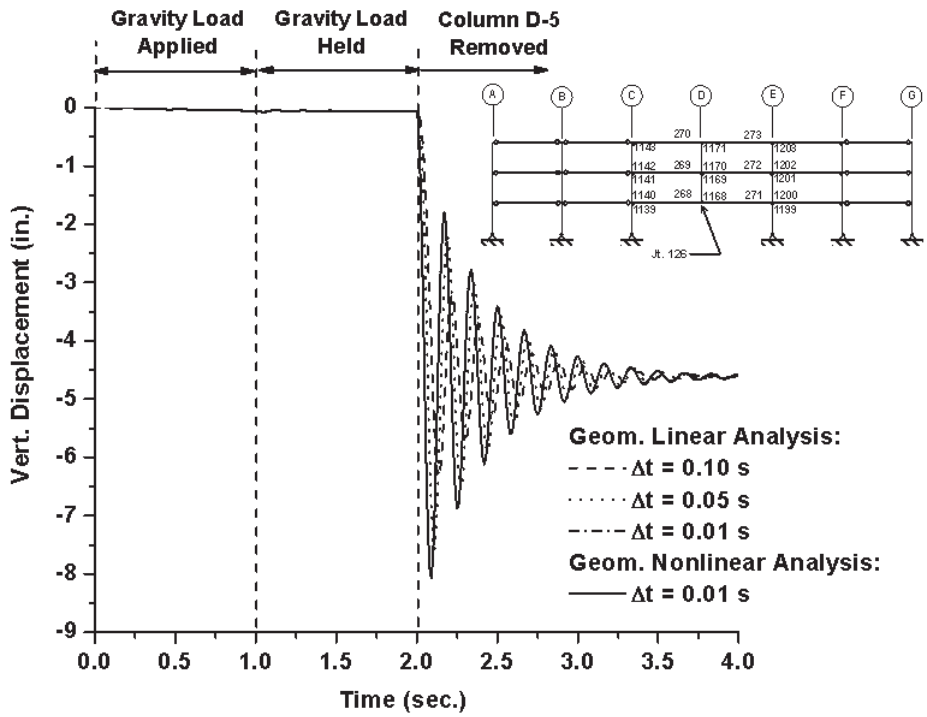

Fig. 9. Impact of column turn-off rates (Δt) on elastic linear and nonlinear geometric response of the 3-story framework.

Figure 11 illustrates the peak inelastic displacement is 50% greater than the elastic displacement. This 12.5-in. peak displacement is essentially 1.7% of the 60-ft span length in the compromised system. A flexural hinge collapse mechanism did not form in the framework at this imposed demand, and the use of geometrically linear analysis is justified (a later figure illustrates the hinge mechanism). Furthermore, assumptions regarding catenary action as a primary load transfer mechanism preventing progressive collapse should be carefully evaluated. This confirms earlier recommendations (Powell, 2005). Catenary forces can become substantial if elastic flexural behavior is demanded. The structural engineer should seek balance between primary flexural resistance and secondary catenary action. The frame's configuration after the event resulted in 11 in. of permanent deformation. Plastic hinging is present in this configuration, but a flexural collapse mechanism has not formed. Loading combinations used for static analysis recommended often include a 2.0 multiplier to simulate dynamic loading effects (GSA, 2003). The results for the elastic and inelastic analysis in Figure 11 appear to indicate that this is conservative as suggested by others (Marchand and Alfawakhiri, 2004).

The X-bracing diaphragm simulation used in the analysis affords an opportunity to examine the activation of the floor slab system as a column is compromised. Figure 12 shows the three floors in the framing system and the axial forces present at the instant the peak vertical displacement is reached in the time-history analysis. The diaphragm system is activated from front to back of the structural system, and the floor slab should not be ignored when assessing general structural integrity. Bending stiffness in the floor slab system is ignored in the present analysis, and it is likely that this is important at the vertical deformation magnitudes seen in the analysis. It is also important to note that the axial forces in the girders on either side of column line D are preserved. Rigid diaphragm modeling would result in these axial forces being zero. The axial tension magnitudes present in the diagonal members at the second and third floors indicates that the system may be amendable to damage compartmentalization within the influence area of the column line containing the ineffective column at these levels. The roof level contains significant compression forces.

The bending moment response history for three members coming together at the second floor at column line C is shown in Figure 13. At shortly after 2 seconds, a plastic hinge forms in beam 268 (refer to Figure 9 for element indexing). This hinge serves to cap the bending moment at the corresponding beam-to-column joint. As a result, the

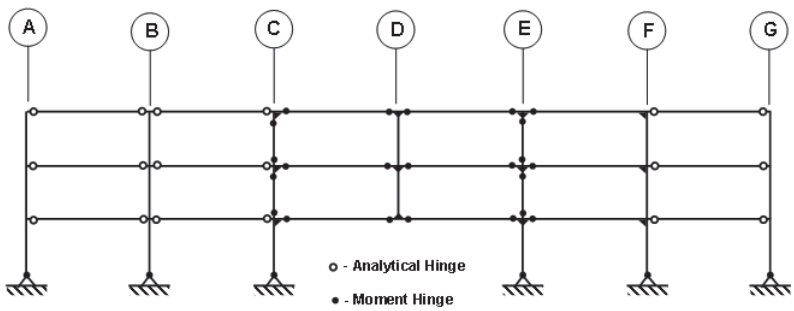

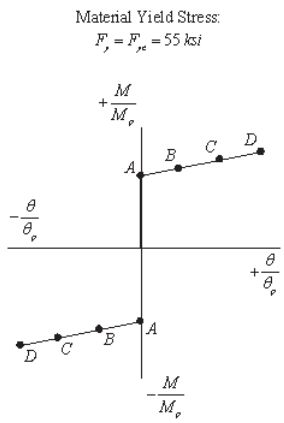

Section	Point	$\frac{M}{M_p}$	$\frac{\theta}{\theta_p}$
W18 W21	A	1.00	0
	B	1.05	8
	C	1.10	16
	D	1.15	24
W14×74	A	0.88	0
	B	0.94	8
	C	0.99	16
	D	1.04	24
W14×99	A	0.99	0
	B	1.04	8
	C	1.09	16
	D	1.14	24

Fig. 10. Moment hinge locations and modeling parameters used.

bending moments in adjacent columns are capped as well. Thus, the hinging in beam 268 serves to protect the columns framing into the common joint. Bending moment response histories for members 270 and 1,143 are shown in Figure 14. In this case, the column forms the plastic hinge first, and the demand in the adjacent beam is immediately capped at that moment magnitude. It is interesting to note that the elastic and inelastic response dampen out to the same static bending moment capacity as required by equilibrium and yielding is temporary. The bending moment response histories at each end of element 268 given in Figure 15 illustrate complete reversal of bending moment as the column is rendered ineffective. The hinge formations that occurred during the structural analysis are graphically depicted in Figure 16.

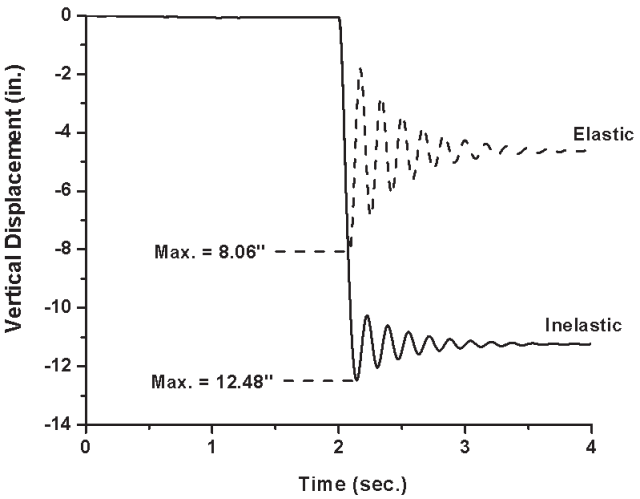

Fig. 11. Response comparison at joint 126 for three-story frame with ineffective column at first floor and location D-5.

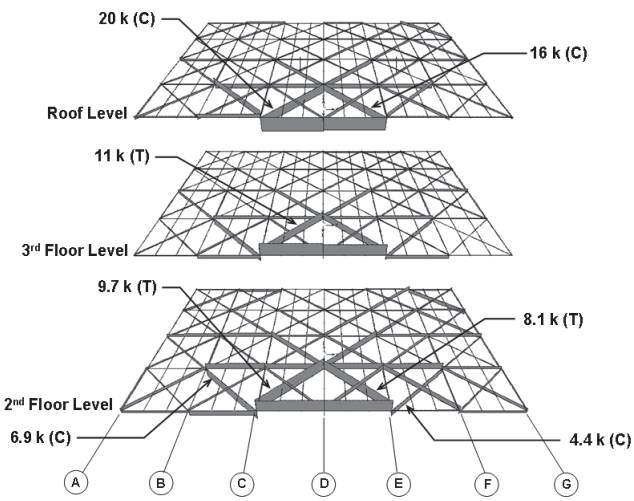

Fig. 12. Axial forces present in floor framing system with bracing elements simulating diaphragm.

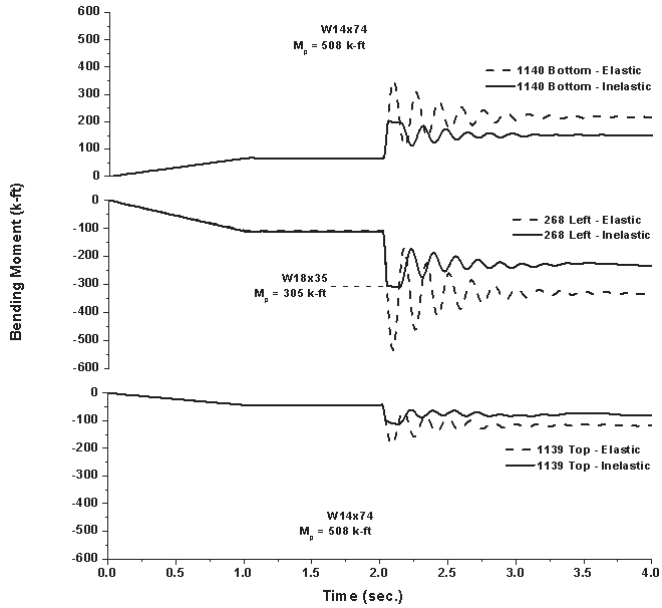

Fig. 13. Bending moment time-history response for members framing together at the second floor beam-to-column connection at column line C.

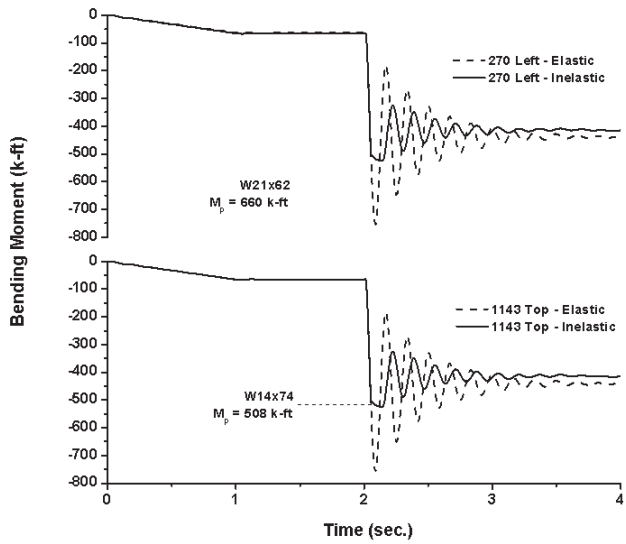

Fig. 14. Bending moment time-history response for members framing together at the roof beam-to-column connection at column line C.

In general, the peak transient bending moments seen in the members are much lower when inelastic behavior is included (refer to Figures 13 through 15). The response seen also stresses the importance of designing moment-resisting connections for full reversal of moment and robustness in the structural steel framing system can be enhanced by designing moment-resisting connections for equal moment magnitudes in positive and negative bending.

Because the moment hinges utilized in the structural analysis did not consider axial-load bending-moment interaction, a demand-to-capacity ratio was utilized to help quantify the extent to which the cross-section yield surface may or may not be violated. The demand-to-capacity ratio (DCR) is defined as follows,

$$\text{DCR} = \frac{P}{P_n} + \frac{M}{M_n} + \left(\frac{V}{V_n}\right)^2 \qquad (2)$$

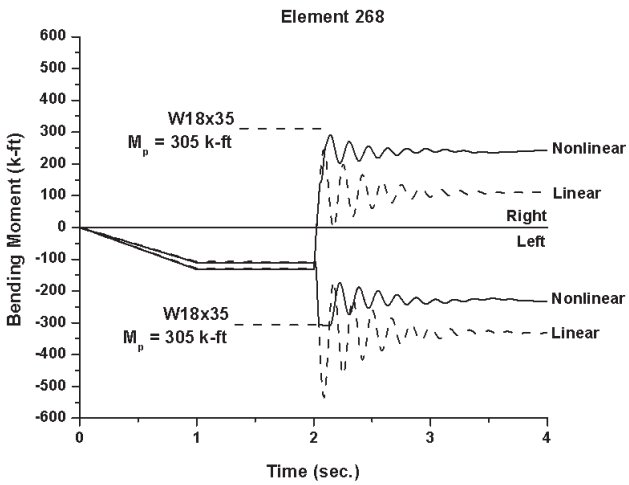

Fig. 15. Bending moment time-history response for second floor beam (element 268) spanning from column line C to D (nonlinear indicates material nonlinearity considered).

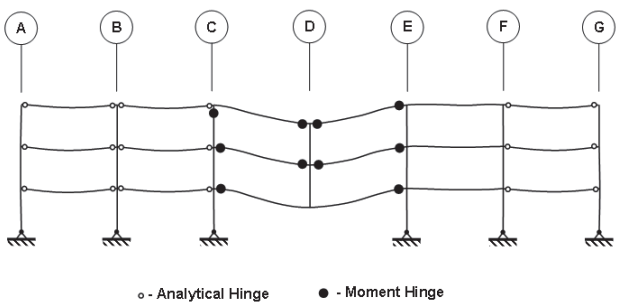

Fig. 16. Moment hinge formation computed during response of frame to ineffective column at the first floor at location D-5.

It should be noted that the DCR defined in this manner is different than that used in seismic specifications (FEMA, 2000b) and progressive collapse mitigative design guidelines (GSA, 2003).

The demand-to-capacity ratio expressed in Equation 2 is conservative with regard to the interaction of bending moment and axial loading. Traditional interaction equations for wide-flange shapes (AISC, 2005) do not involve the quadratic term accounting for the influence of shear. However, the interaction equations for HSS do involve a quadratic shear contribution (AISC, 2005). Quadratic (circular) models for the interaction of transverse shear and bending moment have a long history (Hodge, 1959). Rectangular yield surfaces (no influence of transverse shear on the plastic moment capacity) for modeling the interaction of shear and bending have also been utilized in eccentrically braced frame (EBF) research (Ricles and Popov, 1994).

The AISC *Specification for Structural Steel Buildings* (AISC, 2005), hereafter referred to as the AISC *Specification*, is utilized to determine the nominal axial capacities, shear capacities, and bending moment capacities for the members. The nominal axial capacities of the vertical elements in the framework are defined using an effective length factor for both axes of flexural buckling equal to 1.0 and a C_m factor of 1.0. Moment amplification for P-δ and P-Δ effects were ignored because the axial loading in the members is much less than the Euler critical load and translation of the column ends relative to one another was negligible. The unbraced length of the member was taken to be the story height (13 ft). Horizontal element (i.e., beams) axial strengths were taken to be full yield strengths using expected yield stress with the assumption that connections are adequate. In compression, the concrete slab is likely to take a significant amount of compression force, thus limiting axial compression carried by the beam. The bending moment capacity for the vertical elements in the system are defined using pure-bending modifiers of C_b = 1.0, which is conservative. Horizontal element bending capacity is determined assuming the fully braced condition. Local buckling was considered in the definition of bending capacity for all elements in the system. The shear strength of the member is defined using the height of the web in the cross-section (depth minus two flange thicknesses) and the web thickness. The shear capacity of the web is taken from the AISC *Specification* (AISC, 2005).

Time-histories of nondimensional axial load, shear, and bending moment demands along with DCRs for member 1,143 are given in Figure 17. The majority of the DCR is contributed by the bending moment demand and the axial load demand throughout the time-history is low (e.g., less than 10% of nominal capacity). The DCR for member 1,143 nears 1.25, which exceeds 1.00 by a significant margin. If the load and resistance factor design method were utilized to evaluate the capacity of this member, the nondimensional

Table 1. Peak Nondimensional Member Demands and Demand-to-Capacity Ratios for Inelastic Response to Ineffective Column at Location D-5

Member (1)		$\frac{P}{P_n}$ (2)	$\frac{V}{V_n}$		$\frac{M}{M_n}$		$DCR = \frac{P}{P_n} + \left[\left(\frac{V}{V_n}\right)^2 + \frac{M}{M_n}\right]$	
			Left/Bot. (3)	Right/Top (4)	Left/Bot. (5)	Right/Top (6)	Left/Bot. (7)	Right/Top (8)
BEAMS	268	0.018	0.255	0.126	1.014	0.950	1.095	0.967
	271	0.016	0.121	0.256	0.959	1.015	0.976	1.097
	269	0.019	0.244	0.082	0.997	0.990	1.071	1.012
	272	0.017	0.077	0.245	0.990	0.998	1.011	1.071
	270	0.037	0.231	0.080	0.796	0.994	0.882	1.037
	273	0.034	0.103	0.251	0.997	1.000	1.039	1.092
COLUMNS	1139	0.336	—	0.046	—	0.223	—	0.558
	1140	0.240	0.182	—	0.403	—	0.665	—
	1141	0.240	—	0.181	—	0.470	—	0.605
	1142	0.113	0.361	—	0.701	—	0.942	—
	1143	0.113	—	0.361	—	1.038	—	1.278
	1168	0.133	—	—	—	—	0.133	—
	1170	0.038	—	—	—	—	0.038	—
	1199	0.227	—	0.020	—	0.067	—	0.285
	1200	0.166	0.102	—	0.158	—	0.328	—
	1201	0.166	—	0.101	—	0.196	—	0.358
	1202	0.083	0.253	—	0.347	—	0.491	—
	1203	0.083	—	0.253	—	0.503	—	0.647

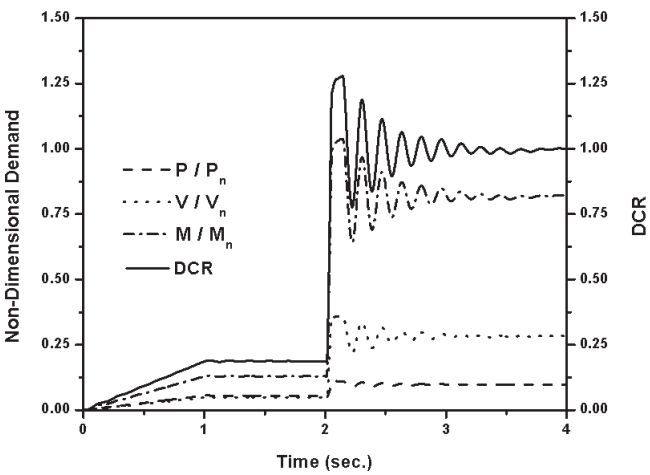

Fig. 17. Nondimensional force demands and demand-to-capacity ratio time-histories for element 1143 at the top (roof level).

axial demand component would be reduced by a factor of 2, and as a result, the DCR would migrate toward 1.00. Furthermore, the analytical model assumed that a friction-free pin connection exists at the left side of column 1,143 (see Figure 9). In all likelihood, this connection will not be a friction-free pin, but would have a moment capacity on the order of 10% of the plastic moment capacity of the connected beam. This would further reduce the demand on the column and the DCR would therefore reduce further.

The peak nondimensional demands and DCRs seen in the simulation conducted are given in Table 1. The peak axial load demands for the beam members are all low (e.g., less than 4% of the axial tension or compression capacity of the member's cross-section). The peak axial force demand for member 1,143 is seen to be 11%, and the bending moment demand is slightly greater than 1.00. The peak tension forces occur in the floor beams immediately above those adjacent to the compromised floor level. The maximum tension force is 17.5 kips, or approximately 2% of the tension capacity of the girder (Foley et al., 2007). It should be noted that

compression force will likely be carried by the floor slab and beam in a symbiotic manner.

One additional item of importance in the assessment of the frame's ability to compensate for an ineffective column and prevent disproportionate collapse is the plastic rotation demands that are placed on the connections at the ends of the beams. Plastic rotation was computed using the displacement results taken from the inelastic time-history analysis. The displacement and moment demand data indicated plastic rotation demands that were fairly consistent across all members. The plastic rotation demands were on the order of 0.022 rad in the girders. If the plastic rotation at the top of member 1,143 is assumed to provide all rotation at the joint facilitating vertical movement at column line D, then the plastic rotation in this member is on the order of 0.016 rad.

The plastic rotation demands encountered during the compromising event are significant. A recent compendium of connection testing information (FEMA, 2000c), indicated a wide variety of plastic rotation capacities for typical fully restrained moment-resisting connections with many exceeding the 0.022 rad demand predicted. Connections that give rise to concerns are welded-flange-bolted-web connections that utilize E70T-4 electrodes without minimum notch toughness and higher yield-to-tensile stress ratios and welded-flange-bolted-web connections utilizing E70T-4 electrodes with the backing bar removed. Welded-flange-bolted-web connections with improved access holes, free-flange connections, cover-plated connections, RBS connections, and welded flange plate connections all were shown to have expected (mean) plastic rotation capacities that exceed the peak demand computed. It is expected that a plastic hinge forming in the W14×74 member can sustain 0.016 rad of plastic rotation prior to significant moment capacity degradation. In many cases, the time-history analysis indicated that the plastic capacity of the cross-section was temporarily reached (refer to Figure 15) and inelastic reloading did not occur.

10-STORY BUILDING

A 10-story frame was also chosen for detailed structural analysis for compromising events. This frame was described earlier in Figure 3 and a column schedule describing the members was given in Figure 4. It is expected that the tension and compression demands on the connections in this framework will vary with the ability for deep-beam action to form within the structural system. Thus, the 10-story frame is considered to examine the variation in demand placed on the members and connections when additional framing is present above the compromised area. An overview of the analysis conducted on this frame is given in this paper, and details are given elsewhere (Foley et al., 2007).

Compromised interior and corner columns were not considered for the same reasons cited earlier with the 3-story frame. The three-story frame loading and combination given by Equation 1 was used. The framing plan suggested evaluation of the compromised column events shown in Figure 3. Slab membrane effects and the response characteristics for the connections at the ends of the orthogonal in-fill beams and the girders are likely to be very important but were not considered in the analysis. Zero-density X-bracing members were utilized to simulate the presence of a concrete and steel deck diaphragm system. The time-history function used to simulate column loss utilized a column turn off rate equal to 0.01 second.

The impact of geometric nonlinearity (P-δ or P-Δ effects) on the response was evaluated using a column turn off rate of 0.01 second. The peak vertical displacements in the floor immediately above the ineffective column were on the order of 2.5 in., indicating geometric stiffening (i.e., catenary action) is not present. Column ends did not tend to translate with respect to one another, and the axial loads in the columns were well below the Euler critical load; therefore, loss of stiffness due to geometric effects is negligible.

The peak strain rate caused by axial loading in the columns and beams was 5,650 με/s (0.0057 in./in./s). The largest strain rates caused by transverse shear occurred in the columns, and these rates were on the order of 105 με/s (0.00011 in./in./s). Bending strain rates in the columns were comparable to the strain rates caused by axial loading with a maximum of 2,000 με/s (0.002 in./in./s). As seen in the three-story building analysis, the strain rates seen in this structure are only slightly more than the intermediate loading rate and orders of magnitude lower than the dynamic loading rate (Barsom and Rolfe, 1999). The loading rates found in the elastic time-history analysis give no indication that fracture toughness of the constituent materials will be insufficient or that the elevated yield strength resulting from increased load rate should be considered. It should be emphasized again that stress raisers caused by connection geometry have been ignored.

The need to determine if inelastic time-history analysis was warranted was performed by evaluating demand-to-capacity ratios (DCRs) for the members in the framework as defined previously in Equation 2. The elastic time-history analysis indicated that the largest DCRs are found in the beams, which had a peak value of 0.68, and the columns on either side of the column rendered ineffective had DCRs less than 0.63 (Foley et al., 2007). Overall, the peak DCRs for the critical members in the vicinity of the ineffective column indicated that inelastic response is unlikely and no plastic hinges formed in the framing members in this framework. Peak elastic tie force demands in this system were determined to be $0.02P_n$, which is very similar to the demand seen in the three-story frame where the response was inelastic.

In the case of the W36×135 girders used in the present framework, this works out to be 0.02(50 ksi)(39.7 in.^{2}) = 40 kips.

As the number of stories above the compromised column increases, a deep-beam mechanism exhibited by beam tension and compression forces is activated. The axial load distribution seen in the beams above the compromised column is analogous to the normal stress (strain) distribution seen in beams with very deep cross-sections. The axial loads seen in the beam members include many levels of compression being equilibrated with a single relatively large tension force in the beams immediately above the compromised column. As a result, the axial tension loading is much greater in the beams/girders of this frame when compared to the three-story building (17.5 kips versus 40 kips). Furthermore, the peak tension forces in the three-story frame occurred simultaneously with the primary flexural hinging mechanism. Because the 10-story frame responds in an elastic manner, this flexural hinging is not present.

20-STORY FRAME

A 20-story structure based upon the SAC-FEMA project documents (Gupta and Krawinkler, 1999) was also analyzed. The pre-Northridge Boston design was used as the base topology, and the framing plan for this building and its column schedule were given in Figures 5 and 6. Load magnitudes were the same as those used for the three- and 10-story buildings. A slightly modified version of the X-bracing diaphragm modeling was used for this framework. Elastic critical load analysis of the framework demonstrated that the massless X-bracing members were sufficient to model diaphragm action (Foley, Barnes and Schneeman, 2008). Several minor changes were made to the frame found in the SAC document (Gupta and Krawinkler, 1999). These changes were focused on the sizes of the infill beams and several column members in the interior of the framework. The nodes in the analytical model for the building are restrained from lateral movement at the lowest two subterranean floor plates, but vertical movement and rotation was allowed. Translational restraints were provided at the bottom of each column. Details of the modeling and analysis completed for framework can be found elsewhere (Foley et al., 2008).

Elastic time-history analysis conducted for the 20-story frame considered a variety of column removal scenarios at the ground-floor level. Because the perimeter framing contained moment resisting frames where all girders and beams were rigidly connected to the columns (with the exception of the corner columns in the east and west frame elevations), six column-removal scenarios were identified for analysis (Figure 5). Each involved rendering one column at the ground floor level ineffective. The columns were chosen based on symmetry of the floor plan and their ability to represent generalized response.

Preliminary time-history analysis indicated that linear geometric analysis was sufficient to assess response of the frames if elastic material response occurred. The initial analyses conducted assumed linear material response and the validity of this assumption was subsequently evaluated through use of demand-to-capacity ratios for members. The removal of columns A3 and C1 were found to produce the most significant results and these scenarios were selected for detailed analysis. The framing plan used in this structural system results in very low levels of axial loading in the corner columns and therefore, loss of column A1 was not critical. Maximum vertical displacements at the floor level immediately above the ineffective column occurred between 0.0 and 0.25 second after the column was rendered ineffective. The peak vertical displacement for these two scenarios was 0.89 in. and 0.81 in. for removal of A3 and C1, respectively. As in the case of the previous frames, catenary action is not occurring in these scenarios.

Maximum overall strain rates when column A3 is compromised were also evaluated. The peak strain rate resulting from axial load was on the order of 190 με/s for the girders and 3,400 με/s for the columns. Peak strain rates resulting from transverse shear were 1,200 με/s and 2,400 με/s for the columns and beams, respectively. Peak strain rates that resulted from bending moments were on the order of 5,500 με/s for the beam members and 1,700 με/s for the columns. The strain rates seen in this structure are only slightly more than the intermediate loading rate and orders of magnitude lower than the dynamic loading rate (Barsom and Rolfe, 1999). The loading rates found in the elastic time-history analysis give no indication that fracture toughness of the constituent materials will be insufficient or that the elevated yield strength resulting from increased load rate should be considered. It should be emphasized again that stress raisers caused by connection geometry have been ignored.

One interesting item of note is that because the ground floor columns are rendered ineffective, there is an upward rebound of the floor immediately below the compromised column as its stored strain energy is released. This rebounding effect suggests that moment resisting connections at the ends of beams (be they infill or otherwise) should be designed for full reversal of moments.

The demand-to-capacity ratio (DCR) defined in Equation 2 was used to evaluate members in the 20-story frame. Peak DCR magnitude for columns was 0.82 and peak DCR magnitude for beams was 0.36, indicating elastic behavior. The peak tension forces in the girders immediately adjacent to the compromised column were approximately 40 kips, which is approximately 1.6% of the nominal tension capacity of the beam/girder member. It appears that expressing the tie force as a function of the nominal axial tension capacity of the beam/girder member is relatively consistent across all three frames: 1.9% for the three-story frame; 2.0% for the

10-story frame; and 1.6% for the 20-story frame. It should be emphasized that the three-story frame responded in an inelastic manner to the compromising event whereas the 10- and 20-story frames responded in an elastic manner.

CONCLUDING REMARKS AND RECOMMENDATIONS

Three structural steel frames were chosen for detailed evaluation of system response during compromising events. The event selected was interior column removal at the perimeter of the first floor level. Three-dimensional structural analysis models were developed and the presence of the concrete-steel composite deck floor system was simulated using massless X-bracing members within the plane of the floor plate. Column removal scenarios were modeled using time-history functions. Inelastic and elastic time-history analysis of the 3D systems was used as required by a series of analyses with systematically increasing complexity.

The inelastic analysis results for the three-story frame indicated that the floor system becomes an active participant in load transfer in the response of the system to a compromising event. The diagonal X-bracing members simulating shear racking stiffness of the floor plate were able to preserve the dominate aspects of frame response while preventing undesired removal of axial forces in the main tie members that would result with rigid diaphragm modeling. It also suggests that further study regarding the participation of the concrete-steel composite floor system typically present in the building is warranted and that compartmentalization of damage is likely most effective accomplished within the influence area of the compromised column. Damage compartmentalization may involve one or more floors. As the number of stories decreases, the number of sacrificed floors may need to increase.

It is recommended that all moment-resisting connections be designed for equal moment magnitudes in positive and negative bending. The structural analysis also suggested that full moment reversal at plastic moment capacity magnitudes is likely in the beam and girders in a framework in the event a column is compromised. Therefore, it is recommended that all moment-resisting connections be designed for fully plastic moment capacity in both loading directions.

Strain rates seen in the frames studied were of intermediate magnitude. Therefore, it is expected that elevated levels of yield stress and reduced fracture toughness may not need to be considered in the analysis. However, it should be emphasized that geometric effects that will be present in the connections of the system were not considered. It is recommended that the demand-to-capacity ratios computed in the present study be used to further examine detailed connection response.

If the members in the framework respond in a predominantly elastic manner, it is likely a result of a significant number of floor levels above the compromised area acting as a deep beam. This will be exhibited by beams at several levels above the compromised column being subjected to compression forces and the girders immediately adjacent to the compromised column being subjected to a relatively large tension force. When few floors are present above the compromised column (e.g., the three-story building) an inelastic flexural mechanism is likely to form. The axial tension forces in the girders appear to be independent of the presence of inelastic behavior. The inelastic response of the three-story frame indicated that the girder tension forces were approximately 1.9% of the nominal tension capacity of the girder. The elastic response of the 10-story and 20-story frame suggested a tension tie force of 2.0% and 1.6%, respectively. Therefore, if one tie force magnitude were to be specified as a minimum general structural integrity criterion, it is best to have this as a percentage of the tension capacity of the beams or girders. Two percent of the axial tension capacity (yield) appears reasonable.

The axial, transverse shear, and bending moment demands and application rates for these forces taken from the time-history response traces can be used as the formulation bases for analytical and experimental testing efforts to evaluate detailed connection response. The rotational demands seen in the inelastic analysis of the three-story frame can also be used as initial demand targets for this experimental and analytical work. For example, if one were to consider the DCRs in Table 1, a testing protocol for fully restrained moment connections could be developed as follows: Apply 2% of the tension (yield) capacity of the beam member simultaneously with the fully plastic moment capacity of the connection, and impart rotational demand of 0.022 rad in both positive and negative directions. The present analysis effort can serve as the basis for establishing experimental demand expectations and experimental protocols to be used to study a wide variety of connections in the structural steel framing system and conduct detailed evaluation of the connection response.

Finally, 3D response simulation should be carried out in order to evaluate the inherent structural integrity or robustness present in the structural steel framing system. This 3D response should consider connection characteristics and modeling of the concrete-steel floor slab system. It is very important that studies be undertaken to evaluate other column loss scenarios within this 3D environment to fully assess the tendency for initiation of progressive collapse and the formulation of general structural integrity provisions. Furthermore, situations where there are no floors above the compromised column should be studied as these may be one of the more critical compromising scenarios. This aspect is one focus of the companion paper (Foley et al., 2008).

It should be emphasized that this paper considered a single damage scenario (loss of exterior column). This scenario is but one of many that should be used to assess the inherent structural integrity in the steel framing system.

Part 2 of the two-part article considers additional damage scenarios occurring within the floor framing system. Taken together, these constitute a systematic effort to assess the inherent structural integrity in steel framing systems. It should be noted, however, that additional damage scenarios (e.g., loss of corner column) and the residual capacity of members likely to be present after localized damage occurs should be considered before the book is closed. The current article provides a first-draft roadmap for this activity.

ACKNOWLEDGMENTS

The authors would like to thank Thomas Schlafly of the American Institute of Steel Construction, the AISC Committee on Research, and Kurt Gustafson of AISC for their very helpful recommendations. Special thanks are due to Brian Crowder of Naval Facilities Engineering Command–Atlantic and David Stevens of Protection Engineering Consultants. Their extraordinarily diligent review of the report on which this manuscript is based with subsequent detailed and insightful comments is greatly appreciated. The authors would also like to thank Professor Sherif El-Tawil of the University of Michigan for his review of the report on which the manuscript is based and recommended corrections in the literature review.

REFERENCES

Abruzzo, J., Matta, A. and Panariello, G. (2006), "Study of Mitigation Strategies for Progressive Collapse of a Reinforced Concrete Commercial Building," *Journal of Performance of Constructed Facilities*, ASCE, Vol. 20, No. 4, pp. 384–390.

ACI (2005), *Building Code Requirements for Structural Concrete (ACI 318-05) and Commentary (ACI 318R-05)*, American Concrete Institute, Farmington Hills, MI.

AISC (2005), *Specifications for Structural Steel Buildings*, ANSI/AISC 360-05, American Institute of Steel Construction, Chicago, IL.

ASTM (1997), *E 399—Standard Test Method for Plane-Strain Fracture Toughness of Metallic Materials*, ASTM, West Conshohocken, PA.

Barsom, J.M. and Rolfe, S.T. (1999), *Fracture and Fatigue Control in Structures: Applications of Fracture Mechanics*, ASTM, West Conshohocken, PA.

Breen, J.E. and Siess, C.P. (1979), "Progressive Collapase—Symposium Summary," *ACI Journal*, ACI, Vol. 76, No. 9, pp. 997–1004.

BSI (2003), *BS 5950—Structural use of Steelwork in Building. Part 1: Code of Practice for Design in Simple and Continuous Construction*, British Standards Institution, London, U.K.

Christiansson, P. (1982), *Steel Structures Subjected to Dynamic Loads in Connection with Progressive Collapse — Dynamic Buckling.* Report Number D7:1982 (ISBN 91-540-3681-X), Swedish Council for Building Research, Stockholm, Sweden, Vol. 118.

CISC (2004), *Handbook of Steel Construction—Eighth Edition*, Canadian Institute of Steel Construction, Willowdale, Ontario.

Corley, W.G. (2002), "Applicability of Seismic Design in Mitigating Progressive Collapse," *NIBS Workshop on Prevention of Progressive Collapse*, Rosemont, IL, National Institute of Building Sciences, www.nibs.org.

CSI (2004), *SAP2000 Version 9*, Computers & Structures, Inc., Berkeley, CA.

Culver, C.G. (1976), "Live Load Survey Results for Office Buildings," *Journal of the Structural Division*, ASCE, Vol. 102, No. ST12, pp. 2269–2284.

DOD (2005), *Unified Facilities Criteria (UFC)—Design of Buildings to Resist Progressive Collapse (UFC 4-023-03)*, http://www.wbdg.org/ccb/browse_cat.php?o=29&c=4.

Dusenberry, D.O. and Hamburger, R.O. (2005), "An Energy-Based Pushdown Analysis Procedure for Evaluating Progressive Collapse Resistance," *Proceedings of the North American Steel Construction Conference*, Montreal, Quebec, Canada, CD-ROM.

Dusenberry, D.O. and Hamburger, R.O. (2006), "Practical Means for Energy-Based Analysis of Disproportionate Collapse Potential," *Journal of Performance of Constructed Facilities*, ASCE, Vol. 20, No. 4, pp. 336–348.

Ellingwood, B. and Leyendecker, E.V. (1978), "Approaches for Design Against Progressive Collapse," *Journal of the Structural Division*, Vol. 104, No. ST3, pp. 413–423.

Ellingwood, B., Leyendecker, E.V. and Yao, J.T.P. (1983), "Probability of Failure from Abnormal Load," *Journal of Structural Engineering*, ASCE, Vol. 109, No. 4, pp. 875–890.

Ellingwood, B.R. (2002), "Load and Resistance Factor Criteria for Progressive Collapse Design," *National Workshop on Prevention of Progressive Collapse*, Rosemont, IL, Multihazard Mitigation Council, National Institute of Standards and Technology.

Ellingwood, B.R. (2005), "Strategies for Mitigating Risk of Progressive Collapse," *Proceedings of the 2005 Structures Congress and the 2005 Forensic Engineering Symposium*, New York, NY, ASCE, CD-ROM.

Ellingwood, B.R. (2006), "Mitigating Risk from Abnormal Loads and Progressive Collapse," *Journal of Performance of Constructed Facilities*, ASCE, Vol. 20, No. 4, pp. 315–323.

Ellingwood, B.R. and Culver, C. (1977), "Analysis of Live Loads in Office Buildings," *Journal of the Structural Division*, ASCE, Vol. 103, No. ST8, pp. 1551–1560.

Ellingwood, B.R. and Dusenberry, D.O. (2005), "Building Design for Abnormal Loads and Progressive Collapse," *Computer-Aided Civil and Infrastructure Engineering*, Blackwell Publishing, Vol. 20, pp. 194–205.

Ettouney, M., Smilowitz, R., Tang, M. and Hapij, A. (2006), "Global System Considerations for Progressive Collapse with Extensions to Other Natural Man-Made Hazards," *Journal of Performance of Constructed Facilities*, ASCE, Vol. 20, No. 4, pp. 403–417.

FEMA (2000a), *FEMA-355A: State of the Art Report on Base Metals and Fracture*, SAC Joint Venture and Federal Emergency Management Agency, Washington, DC.

FEMA (2000b), *FEMA 356—Prestandard and Commentary for the Seismic Rehabilitation of Buildings*, American Society of Civil Engineers and the Federal Emergency Management Agency, Washington, DC.

FEMA (2000c), *State of the Art Report on Connection Performance (FEMA-355D)*, SAC Joint Venture and Federal Emergency Management Agency, Washington, DC.

Fintel, M. and Schultz, D.M. (1979), "Structural Integrity of Large Panel Buildings," *ACI Journal*, ACI, Vol. 76, No. 5, pp. 583–620.

Foley, C.M., Martin, K. and Schneeman, C. (2007), *Robustness in Structural Steel Framing Systems*, Report No: MU-CEEN-SE-07-01, AISC, 253 p.

Foley, C.M., Barnes, K.M. and Schneeman, C.L. (2008), "Quantifying and Enhancing Robustness in Steel Structures: Part 2—Floor-Framing Systems," *Engineering Journal*, AISC, Vol. 45, No. 4, pp. 267–287.

Girhammar, U.A. (1980a), *Behavior of Bolted Beam-Column Connections Under Catenary Action in Damaged Steel Structures.* Report Number D12:1980 (ISBN 91-540-3213-X), Swedish Council for Building Research, Stockholm, Sweden, 144 p.

Girhammar, U.A. (1980b), *Dynamic Fall-Safe Behavior of Steel Skeleton Structures Having Bolted Connections,* Report Number D13:1980 (ISBN 91-540-3215-6), Swedish Council for Building Research, Stockholm, Sweden, 86 p.

Girhammar, U.A. (1980c), *Dynamic Response of Two-Span Steel Beams Subject to Removal of Interior Support.* Report Number D11:1980 (ISBN 91-540-3211-3), Swedish Council for Building Research, Stockholm, Sweden, 127 p.

Grierson, D.E., Safi, M., Xu, L. and Liu, Y. (2005a), "Simplified Methods for Progressive-Collapse Analysis of Buildings," *Proceedings of the 2005 Structures Congress and the 2005 Forensic Engineering Symposium*, New York, NY, American Society of Civil Engineers, CD-ROM.

Grierson, D.E., Xu, L. and Liu, Y. (2005b), "Progressive-Failure Analysis of Buildings Subjected to Abnormal Loading," *Computer-Aided Civil and Infrastructure Engineering*, Blackwell Publishing, Malden, MA, Vol. 20, pp. 155–171.

Griffiths, H., Pugsley, A. and Saunders, O. (1968), *Report of the Inquiry into the Collapse of Flats at Ronan Point, Canning Town*, Her Majesty's Stationary Office, London, U.K.

GSA (2003), *Progressive Collapse Analysis and Design Guidelines for New Federal Office Buildings and Major Modernization Projects*, www.oca.gsa.gov.

Gupta, A. and Krawinkler, H. (1999), *Prediction of Seismic Demands for SMRF's with Ductile Connections and Elements,* Report No: SAC/BD-99/06, SAC Joint Venture.

Guravich, S.J. and Dawe, J.L. (2006), "Simple Beam Connections in Combined Shear and Tension," *Canadian Journal of Civil Engineering*, National Research Council, Canada, Vol. 33, pp. 357–372.

Hamburger, R. and Whittaker, A. (2004), "Design of Steel Structures for Blast-Related Progressive Collapse Resistance," *North American Steel Construction Conference (NASCC)*, Long Beach, CA, American Institute of Steel Construction, CD-ROM.

Hawkins, N.M. and Mitchell, D. (1979), "Progressive Collapse of Flat Plate Structures," *ACI Journal*, ACI, Vol. 76, No. 8, pp. 775–808.

Hodge, P.G. (1959), *Plastic Analysis of Structures*, McGraw Hill, Inc., New York, NY.

ISE (1969), "The Implications of the Report of the Inquiry into the Collapse of Flats at Ronan Point, Canning Town," *The Structural Engineer*, The Institution of Structural Engineers, Vol. 47, No. 7, pp. 255–284.

ISE (1971), "The Resistance of Buildings to Accidental Damage," *The Structural Engineer*, The Institution of Structural Engineers, Vol. 49, No. 2, 102 p.

ISE (1972a), "Discussion—Stability of Modern Buildings," *The Structural Engineer*, Vol. 50, No. 7, The Institution of Structural Engineers, pp. 275–288.

ISE (1972b), "Stability of Modern Buildings," *The Structural Engineer*, Vol. 50, No. 1, The Institution of Structural Engineers, pp. 3–6.

Iwankiw, N. and Griffis, L.G. (2004), *Comparison of Structural Performance of Multi-Story Buildings Under Extreme Events*, American Institute of Steel Construction, Chicago, IL.

Khandelwal, K. and El-Tawil, S. (2005), "Progressive Collapse of Moment Resisting Steel Frame Buildings," *Proceedings of the 2005 Structures Congress and the 2005 Forensic Engineering Symposium*, New York, NY, American Society of Civil Engineers, CD-ROM.

Leyendecker, E.V., Breen, J.E., Somes, N.F. and Swatta, M. (1976), *Abnormal Loading on Buildings and Progressive Collapse: An Annotated Bibliography, Building Science Series 67*, U.S. Department of Commerce, National Bureau of Standards, Washington, DC.

Leyendecker, E.V. and Burnett, E.P. (1976), *The Incidence of Abnormal Loading in Residential Buildings—Building Science Series 89*, National Bureau of Standards, Washington, DC.

Leyendecker, E.V. and Ellingwood, B.R. (1977), *Design Methods for Reducing the Risk of Progressive Collapse in Buildings*, NBS Building Science Series 98, Center for Building Technology, Institute for Applied Technology, National Bureau of Standards, U.S. Department of Commerce, Washington, DC.

Lim, J. and Krauthammer, T. (2006), "Progressive Collapse Analysis of 2D Steel-Framed Structures with Different Connection Models," *Engineering Journal*, AISC, Vol. 43, No. 3, pp. 201–215.

Liu, R., Davison, B. and Tyas, A. (2005), "A Study of Progressive Collapse in Multi-Storey Steel Frames," *Proceedings of the 2005 Structures Congress and the 2005 Forensic Engineering Symposium*, New York, NY, American Society of Civil Engineers, CD-ROM.

Loizeaux, M. and Osborn, A.E.N. (2006), "Progressive Collapse—An Implosion Contractor's Stock in Trade," *Journal of Performance of Constructed Facilities*, ASCE, Vol. 20, No. 4, pp. 391–402.

Magnusson, J. (2004), "Learning from Structures Subjected to Loads Extremely Beyond Design." *North American Steel Construction Conference (NASCC)*, Long Beach, CA, American Institute of Steel Construction, CD-ROM.

Mahendran, M. and Moor, C. (1999), "Three-Dimensional Modeling of Steel Portal Frame Buildings." *Journal of Structural Engineering*, ASCE, Vol. 125, No. 8, pp. 870–878.

Majanishvili, S. and Agnew, E. (2006), "Comparison of Various Procedures for Progressive Collapse Analysis." *Journal of Performance of Constructed Facilities*, ASCE, Vol. 20, No. 4, pp. 365–374.

Marchand, K.A. and Alfawakhiri, F. (2004), *Blast and Progressive Collapse.* Facts for Steel Buildings Number 2, American Institute of Steel Construction, Chicago, IL.

McGuire, R.K. and Cornell, C.A. (1974), "Live Load Effects in Office Buildings." *Journal of the Structural Division*, ASCE, Vol. 100, No. ST7, pp. 1351–1378.

McNamara, R.J. (2003), "Conventionally Designed Buildings: Blast and Progressive Collapse." *AISC and Steel Institute of New York Symposium: Blast and Progressive Collapse*, New York, NY, American Institute of Steel Construction, Chicago, IL.

Mitchell, D. and Cook, W.D. (1984), "Preventing Progressive Collapse of Slab Structures." *Journal of Structural Engineering*, ASCE, Vol. 110, No. 7, pp. 1513–1532.

Mohamed, O. (2006), "Progressive Collapse of Structures: Annotated Bibliography and Comparison of Codes and Standards." *Journal of Performance of Constructed Facilities*, ASCE, Vol. 20, No. 4, pp. 418–425.

Munoz-Garcia, E., Davison, B. and Tyas, A. (2005) "Structural Integrity of Steel Connections Subjected to Rapid Rates of Loading." *Proceedings of the 2005 Structures Congress and the 2005 Forensic Engineering Symposium*, New York, NY, American Society of Civil Engineers, CD-ROM.

Nair, R.S. (2004), "Progressive Collapse Basics." *North American Steel Construction Conference (NASCC)*, Long Beach, CA, American Institute of Steel Construction, CD-ROM.

Nair, R.S. (2006), "Preventing Disproportionate Collapse." *Journal of Performance of Constructed Facilities*, ASCE, Vol. 20, No. 4, pp. 309–314.

NIST (2005), *Final Report on the Collapse of the World Trade Center Towers.* NIST NCSTAR 1—Federal Building and Fire Safety Investigation of the World Trade Center, National Institute of Standards and Technology, Technology Administration, U.S. Department of Commerce, Washington DC, 248.

ODPM (2005), *The Building Regulations 2000—Structure; Approved Document A*, Office of the Deputy Prime Minister, London, http://www.odpm.gov.uk/.

Owens, G.W. and Moore, D.B. (1992), "The Robustness of Simple Connections." *The Structural Engineer*, Institution of Structural Engineers, Vol. 70, No. 3, pp. 37–46.

Popoff, J. A. (1975), "Design Against Progressive Collapse." *PCI Journal*, March-April, Precast Prestressed Concrete Institute, pp. 44–57.

Powell, G.P. (2005), "Progressive Collapse: Case Studies Using Nonlinear Analysis." *Proceedings of the 2005 Structures Congress and the 2005 Forensic Engineering Symposium*, New York, NY, ASCE, CD-ROM.

Rahamian, A. and Moazami, K. (2003), "Non-Linear Structural Integrity Analysis." *AISC and Steel Institute of New York Symposium: Blast and Progressive Collapse*, New York, NY, American Institute of Steel Construction, Chicago, IL, www.aisc.org.

Ricles, J.M. and Popov, E.P. (1994), "Inelastic Link Element for EBF Seismic Analysis." *Journal of Structural Engineering*, ASCE, Vol. 120, No. 2, pp. 441–463.

Ruth, P., Marchand, K.A. and Williamson, E. (2006), "Static Equivalency in Progressive Collapse Alternate Path Analysis: Reducing Conservatism While Retaining Structural Integrity." *Journal of Performance of Constructed Facilities*, ASCE, Vol. 20, No. 4, pp. 349–364.

Shipe, J.A. and Carter, C.J. (2004), "Defensive Design: Blast and Progressive Collapse Resistance in Steel Buildings," *2004 AISC/SEI Structures Congress*, Nashville, TN, ASCE, CD-ROM.

Speyer, I.J. (1976), "Considerations for the Design of Precast Concrete Bearing Wall Buildings to Withstand Abnormal Loads." *PCI Journal*, March-April, Precast Prestressed Concrete Institute, pp. 18–51.

Quantifying and Enhancing Robustness in Steel Structures: Part 2—Floor Framing Systems

CHRISTOPHER M. FOLEY, KRISTINE BARNES and CARL SCHNEEMAN

Typical structural steel framing systems contain many attributes desired when seeking inherent structural integrity and robustness. The framing systems are most often orthogonal, alleviating the need to layout tying systems and contain many potential secondary load paths (e.g., membrane/catenary action in the steel-concrete composite slab and infill beams). If a better understanding of the demands placed on primary and secondary load paths in the structural steel framing system during abnormal loading events and their likely capacities existed, general structural integrity provisions for structural steel systems could be generated and the tendency for disproportionate collapse in these systems would be better understood.

A companion paper (Foley, Schneeman and Barnes, 2008) provides a detailed review and synthesis of the literature related to design and analysis for progressive collapse resistance and outlines the motivation for the present effort. It discusses the results of a three-dimensional (3D) simulation of 3-, 10- and 20-story buildings exposed to compromised column scenarios and provides insights into the inherent robustness and structural integrity of moment-resisting frames. However, the analyses carried out in this former effort did not consider what may happen at locations within the steel skeleton outside the perimeter at the ground floor level, and it did not attempt to quantify inherent structural integrity contributed by components other than the steel skeleton. Furthermore, the analytical models did not support response simulation considering ineffective interior columns, interior girders, exterior girders, or in-fill beams. If robustness in the structural steel framing system is to be quantified and mechanisms for enhancement identified, analysis must go beyond the simple removal of columns around the perimeter of the framework.

The objectives of the present manuscript are (1) provide a targeted review of literature pertaining to catenary and membrane action in the floor slab within the structural steel building system; (2) provide an overview of the methodologies that have been proposed and validated via experimental testing for quantifying the catenary and membrane mechanisms in concrete floor systems; and (3) outline a methodology for quantifying the membrane and catenary capacity in structural steel floor framing systems, and identify high-level provisions for ensuring structural integrity by enhancing the potential for successful activation of catenary and membrane action in the framing system. Through detailed evaluation of the response of the floor framing systems to compromising event scenarios, it is hoped that the present effort can further contribute to the understanding of the load transfer mechanisms inherent in the structural steel building, provide insights into developing analysis and design methodologies and systems to enhance this inherent structural integrity, and provide guidance for developing simple and effective general structural integrity provisions for specifications.

MEMBRANE AND CATENARY ACTION IN SLAB SYSTEMS

Researchers in the field of reinforced concrete design have had a long history of attempting to understand the tensile behavior of structural concrete floor systems and proposing methodologies for quantifying the beneficial effects of catenary and membrane action. Much of the research conducted in this regard (Hawkins and Mitchell, 1979; Mitchell and Cook, 1984) has made its way into ACI 318 (ACI, 2005) provisions for general structural integrity. Investigators studying the response of structural steel systems to fire have also begun to understand and capitalize on the inherent robustness present in steel framing systems contributed by the reinforcement in the concrete floor slab (Allam, Burgess and Plank, 2000; Bailey, White and Moore, 2000; Huang, Burgess and Plank, 2003a, 2003b).

It has long been recognized that flat plate concrete floor systems have the potential to suffer from disproportionate collapse after a rather simplistic event—punching shear failure at interior and exterior columns (Hawkins and Mitchell, 1979; Mitchell and Cook, 1984). Hawkins and Mitchell (1979) provide a very nice description of the development of

Christopher M. Foley is associate professor, department of civil and environmental engineering, Marquette University, Milwaukee, WI.

Kristine Barnes is a structural engineer, AREVA NP, Inc., Naperville, IL.

Carl Schneeman is a structural engineer, Walker Parking Consultants, Minneapolis, MN.

membrane action in a concrete flat-plate floor system. When a concrete floor is loaded to the point of inelastic behavior, there is a tendency for the bottom fibers (assuming loading is from the top) to lengthen, and this fiber lengthening is restrained by the concrete slab at the perimeter of the panel being loaded. In a theoretical sense, the concrete slab will have a load versus vertical deflection response that exhibits snap-through prior to the formation of membrane tension in the system. The hanging net effect cannot take place without significant vertical deformation, and all sections through the floor plate can be subjected to large tensile strains.

The Hawkins and Mitchell (1979) expressions for computing the membrane capacity of concrete floor panels are simple and include a significant amount of engineering feel. More complicated methods for computing membrane capacity of slab systems are available (Park, 1964; Regan, 1975; Park and Gamble, 1980). The fundamental assumption of the proposed methodology is that the deformed membrane between supports follows a circular shape. This makes the mathematics tractable, and errors are relatively small when compared to the more correct catenary parabola. The basic slab system and membrane forces considered are schematically shown in Figure 1. Two slab span directions are assumed: a short direction, l_1, and a long direction, l_2. The reinforcement area on a per unit length basis in the short and long directions are A_{s1} and A_{s2}, respectively. The normal strains in the fibers of the membrane are assumed to be uniform over the membrane thickness and are functions of the curvature. Uniformly distributed loading over the surface of the membrane is assumed, and positive loading is taken to be downward. Membrane tension forces (edge tensions) per unit length parallel to the short and long directions and tangent to the deformed membrane's mid-surface are T_1 and T_2, respectively.

The free-body diagram for catenary behavior is shown in Figure 2. The tension force in the membrane follows a tangent to the deformed shape at any point along the catenary. There is a tension force resultant at the edge, T_{max}, and the centerline, T, when the uniformly distributed loading, w_o, is applied. A major structural engineering-related issue that needs to be considered when examining catenary and membrane behavior in floor systems is the trade-off between allowing significant catenary deflection, h, and the peak tension force. The catenary forces will significantly increase if the shape of the catenary is held close to the horizontal plane (e.g., a tight-rope). If one does not allow significant deflection in the catenary to occur, tension forces can become very large, thus rendering catenary action infeasible. If one allows significant deflection in the catenary and the strains in any deflected shape assumed will not exceed those corresponding to rupture, these tensile forces can be reduced.

Attention can now be turned to membrane action in the concrete slab portion of the system illustrated in Figure 1. A typical structural mechanics solution procedure (e.g., imposition of vertical equilibrium, ensuring compatibility of deformations, and adherence to constitutive laws for the material) is employed to develop a relationship for the capacity of the tensile membrane that is a function of the edge tension, strain in the membrane (and therefore, vertical deflection), and the panel dimensions. When the panel dimensions differ (e.g., rectangular panel) the membrane capacity of the panel based upon the tensile reinforcement capacity at the edges can be written as (Hawkins and Mitchell, 1979),

$$w_{mem} = \frac{2T_1 \sin\left(\sqrt{6\varepsilon_1}\right)}{l_1} + \frac{2T_2 \sin\left(\frac{l_1}{l_2}\sqrt{6\varepsilon_1}\right)}{l_2} \qquad (1)$$

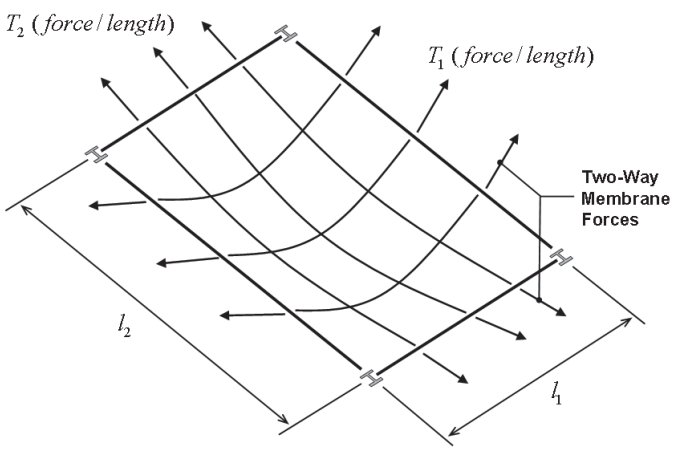

Fig. 1. Two-way membrane action in reinforced concrete slab.

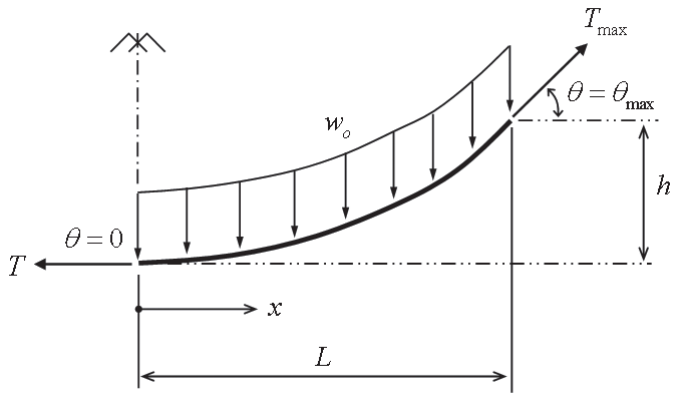

Fig. 2. Fundamental representation of catenary action.

where

ε_1 = tensile strain in the membrane fibers parallel to the short (dominant) direction

As l_2/l_1 increases, the slab panel begins to behave as a single direction membrane. In the present case, welded wire mesh and steel deck are the primary reinforcement components.

The strains in the direction parallel to the short and long dimensions are related to one another as a result of the assumed circular shape of the membrane. The strain in the direction parallel to the short dimension is computed using (Hawkins and Mitchell, 1979),

$$\varepsilon_1 = \varepsilon_2 \left(\frac{l_2}{l_1} \right)^2 \tag{2}$$

Therefore, once the strains in the two directions are computed (long direction assumed, then short direction computed), the constitutive laws for the reinforcement can be used to determine the state of stress and then the tensile membrane forces. The maximum deflection within the panel can be estimated using (Mitchell and Cook, 1984),

$$\delta = \frac{3 l_1 \varepsilon_1}{2 \sin\left(\sqrt{6 \varepsilon_1} \right)} \tag{3}$$

The vertical deflection is important when assessing the capacity of the membrane. Assuming end anchorage is present, the membrane is capable of carrying more loading in a highly deflected configuration for a fixed tensile force capacity. Therefore, if a large amount of loading is present and there is a fixed tensile capacity for the reinforcement in the membrane (assuming no rupturing of the reinforcement), then there is a tendency for the membrane to continue to deflect vertically to generate greater vertical components in the catenary forces.

The response of a slab structure as a membrane depends upon the steel reinforcement, the vertical support conditions, and the horizontal restraint conditions at the panel edges (Mitchell and Cook, 1984). When the slab panel has vertical support at its edges, the slab is capable of providing its own in-plane compression ring restraint conditions at the perimeter. This compression ring helps to resist the horizontal component of the maximum tensile forces (Figure 1). Edge or corner panels can develop the necessary compression ring behavior if the edges are supported by beams that have significant flexural stiffness when compared to the slab itself. Anchorage of the tension reinforcement at the panel edges is also very important to facilitate compression ring formation.

One-way catenary action may also arise in a floor system. A catenary subjected to uniformly distributed loading, w_o, shown in Figure 2, will be utilized as a basis for the following discussion. The uniformly distributed loading capacity of the catenary can be computed using (Hibbeler, 2006),

$$w_o = w_{cat} = \frac{T_{max}}{L} \left[1 + \left(\frac{L}{2h} \right)^2 \right]^{-0.50} \tag{4}$$

The catenary sag is denoted as h, one-half the catenary span is defined as L, and the tension force in the membrane is T at mid-span and T_{max} at the edge. The reinforcement at the central portion and edge of the catenary is assumed to be the same. As the sag increases, the length of the catenary relative to original horizontal span increases, and this can lead to significant strains.

The fundamental theory of the parabolic catenary can be used to develop a relationship for the length along the catenary parabola given by,

$$L' = \int_0^L \left[\sqrt{1 + \frac{4h^2}{L^4} x^2} \right] dx \tag{5}$$

Equation 5 can be used to compute the length of the components in the catenary in its deformed position, and this length can be used along with the initial length to estimate ductility demand in the catenary system.

MEMBRANE ACTION IN COMPOSITE DECK FLOOR SYSTEMS

Although structural steel floor framing systems are significantly different in many ways from that of a two-way flat plate or flat slab cast-in-place concrete system, there are enough similarities to justify using the existing theory and expressions (Hawkins and Mitchell, 1979; Mitchell and Cook, 1984) to assess the inherent integrity and robustness of structural steel floor framing systems.

It is felt that membrane and catenary action are indeed possible within the structural steel framing systems commonly found in buildings, and fire researchers have long recognized the importance of this load transfer mechanism (Wang and Kodur, 2000). Tension reinforcement present in these systems will need to be quantified and their anchorage discussed prior to detailed examination of ineffective supporting member scenarios. In composite steel-concrete floor systems, there is typically welded-wire mesh and light gage steel deck that can be utilized as tension reinforcement within the slab system should membrane and/or catenary action be needed. However, one must understand the usefulness of these components as reinforcing mechanisms in the slab system before it can be relied upon as sources of membrane and catenary reinforcement.

The light gage steel deck is essentially a unidirectional spanning entity. In the direction parallel to the flutes in the

deck, it is likely to be a very useful form of tension reinforcement for facilitating catenary action. However, in the direction orthogonal to the flutes, the steel deck likely has puddle welds or TEK screws that are unlikely to preserve tensile forces within the deck in this direction. Furthermore, the fluted nature of the deck results in a tension force that has two distinct elevations at the floor deck soffit, making it questionable to rely on the steel deck providing tensile membrane or catenary reinforcement in two directions. The present analysis assumes that the steel deck provides one-way reinforcement within the floor framing system. It should be noted that if the steel deck panels are not continuous over the supporting beam, a supplemental force-transfer mechanism must exist.

The welded-wire fabric present in the floor system is also a source of potential membrane and catenary tension reinforcement. This steel fabric generally has a slightly elevated yield stress when compared to the usual mild-steel reinforcement. Furthermore, the spacing of the wires in the mesh can change with direction. This reinforcement is considered continuous through the panel perimeter with sufficient lap splicing throughout. A typical lap splice requirement for 6×6-W1.4×1.4 plain welded wire fabric in tension is 10 in. for concrete with 4,000 psi, 28-day unconfined compression strength (ACI, 2005).

In the steel building system considered in this study, a panel is defined as having infill beams and/or girders bounding a panel of concrete slab. In most cases, the perimeter of the slab panel will have puddle welds or even steel studs connecting the steel deck to the perimeter beams/girders. Furthermore, these perimeter members will have significantly greater flexural stiffness when compared to that of the slab. The present analysis assumes the slab system can develop compression ring anchorage.

The basic process used to assess and quantify the membrane and catenary action present in the structural steel floor framing system is to use Equations 1 through 3 to describe two-way membrane behavior in the floor framing system and Equations 4 and 5 to describe one-way catenary behavior. The strain demands must be compared to rupture strains. This is done using Equation 2 in the case of two-way behavior and Equation 5 in conjunction with the initial horizontal length for one-way behavior. The following sections proceed with evaluating several ineffective element scenarios and make recommendations regarding the levels of inherent robustness in the floor system, or make recommendations regarding simple measures that can be taken to enhance structural integrity in these systems.

INEFFECTIVE ELEMENT SCENARIOS

The present study considered the following main structural components being rendered ineffective: an interior column, an interior infill beam, a spandrel beam, two adjacent infill beams, and spandrel girder. The 30-ft framing bays of the 3-story and 10-story frameworks considered in the companion effort (Foley, Schneeman and Barnes, 2008) are used as base topologies for this study. Exhaustive detail of the computations outlined in this manuscript can be found in Foley, Martin and Schneeman (2007).

Ineffective Infill Beam(s)

The first scenario considered is shown in Figure 3, and it results in two-way membrane action with panel dimensions equal to 20 ft by 30 ft. A 2VLI22 steel deck provides formwork and tension reinforcement for the concrete slab (5 in. total height composite slab) and 6×6-W1.4×W1.4 shrinkage and temperature reinforcement is present. The steel deck is assumed to provide membrane tension reinforcement parallel to the short direction, and the welded wire fabric is assumed to provide reinforcement in both directions. The reinforcement is assumed to have elastic-perfectly-plastic stress-strain behavior. The yield stress of the welded wire mesh is taken as 65 ksi, and the tension area provided on a unit length basis is 0.00233 in.^{2}/in. (ACI, 1997). The steel deck is assumed to have yield stress equal to 40 ksi, and the cross-sectional area on a unit length basis is 0.03542 in.^{2}/in. (Vulcraft, 2005).

If the full cross-sectional area of the steel deck is at yield, the tension force that can be developed is 1.42 kips/in. If the steel deck panel terminates at a beam or girder, the horizontal component of this potential membrane/catenary force will require anchorage. If anchorage mechanisms (e.g., puddle welds, shear studs) are located at 6 in. on center, an estimate

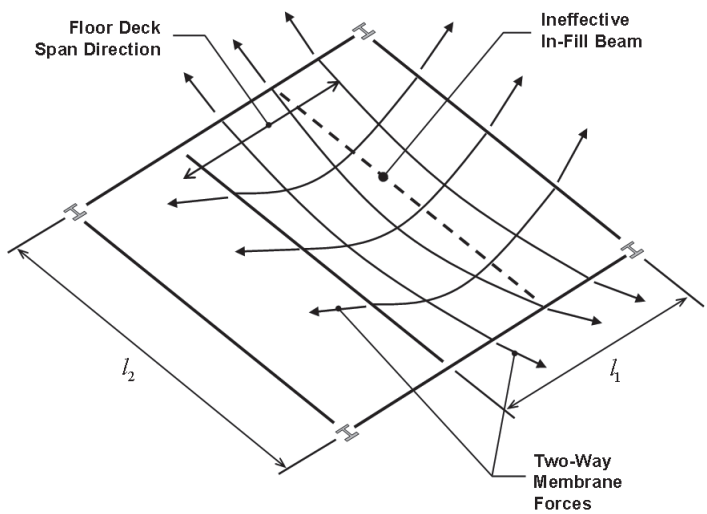

Fig. 3. Schematic of two-way membrane action in composite steel-concrete floor system when one in-fill beam is rendered ineffective.

for the anchorage force is 8,500 lb. The nominal strength of a ⅝-in. arc spot weld to structural steel substrate through 2VLI22 steel deck is 1.64 kips (AISI, 2001). Therefore, ⅝-in. puddle welds at 3 in. on center would yield 550 lb/in. capacity. Therefore, 40% of the steel deck cross-sectional area was assumed to be effective in the analysis. The membrane force in the short direction is composed of a percentage of the total steel deck cross-sectional area at yield and the welded wire mesh (WWM) cross-sectional area at yield. In the long direction, the membrane force is exclusively provided by the cross-sectional area of the WWM at yield.

An analysis of the two-way membrane capacity of the floor slab indicated that the force at the perimeter of the panel in the steel deck was 566 lb/in. and that the force parallel to the long direction was 152 lb/in. The uniformly distributed load-carrying capacity of the panel was estimated to be 110 psf with nearly 7 in. of vertical deflection (Foley et al., 2007). The strain in the reinforcement spanning in the short direction is 0.00225 in./in., which is approximately two times the yield strain for the deck and much less than the yield strain for the WWM. Keeping the yield strain in the steel deck equal to or less than $2\varepsilon_y$ was considered to be sufficient to prevent rupture.

The total loading present on the panel at the instant the infill beam is rendered ineffective is 93 psf (50 psf, concrete steel composite deck; 3 psf, ceiling/floor/fireproofing; 7 psf, m.e.p; 20 psf, partitions; 12.5 psf, live loading). If current progressive collapse mitigation guidelines are employed (GSA, 2003; DOD, 2005), this would require that the two-way membrane be capable of supporting,

$$\beta_{dynam}\left(1.0D + 0.25L\right) = 2\left(93\right) = 186 \text{ psf} > 110 \text{ psf}$$

The membrane is not capable of carrying this loading magnitude; therefore, the system would require additional structural engineering to prevent slab system collapse. If the 2VLI22 gauge deck remains, but mild-steel reinforcement of #3 at 12-in. spacing (60-ksi yield strength) is used, the two-way membrane capacity increases to 189 psf, and a dynamic load factor of 2.0 may be accommodated (Foley et al., 2007). All previous scenarios resulted in membrane deflections of approximately 7 in. and strains in the deck and reinforcement equal to or less than $2\varepsilon_y$.

A second scenario involving two ineffective infill beams is shown in Figure 4. This scenario is interesting because the membrane is square, but the tensile reinforcement is orthotropic. The loading capacity of the 30-ft by 30-ft membrane utilizing 6×6-W1.4×W1.4 welded wire mesh with 2VLI22 steel deck is lower than the previous scenario. The two-way membrane capacity is approximately 93 psf with 12 in. of membrane deflection (Foley et al., 2007). The strain present in the steel deck is approximately $2.2\varepsilon_y$. The benefit of two-way action should be apparent as the capacity of the membrane was reduced 15% from the previous scenario. The typical panel found in structural steel floor systems appears incapable of supporting the required 2.0 multiplier for dynamic effects required by current guidelines (GSA, 2003; DOD, 2005), but is capable of supporting its self-weight and expected point-in-time sustained live loading.

Alternate reinforcement schemes using mild-steel reinforcing bars were also studied (Foley et al., 2007). The yield stress for the mild-steel bars was assumed to be 60 ksi without strain hardening. This study yielded the following reinforcement alternatives:

#3 at 24 in. on center; 0.00458 in.^{2}/in. . . .
119 psf at 12-in. deflection $\left(\beta_{dynam} \simeq 1.3\right)$

#3 at 18 in. on center; 0.00611 in.^{2}/in. . . .
140 psf at 12-in. deflection $\left(\beta_{dynam} \simeq 1.5\right)$

#3 at 12 in. on center; 0.0092 in.^{2}/in. . . . .
178 psf at 12-in. deflection $\left(\beta_{dynam} \simeq 1.9\right)$

Ineffective Spandrel Beam

A scenario involving a spandrel beam being rendered ineffective was also studied (Figure 5). The steel deck flutes run perpendicular to the direction of assumed catenary action. Exterior cladding being supported by the spandrel element is assumed to fall off with the spandrel beam. Welded wire fabric/mesh was found to be incapable of facilitating catenary action in the floor slab (Foley et al., 2007). There are two possibilities for creating structural integrity and robustness in this scenario. The first involves lumping catenary

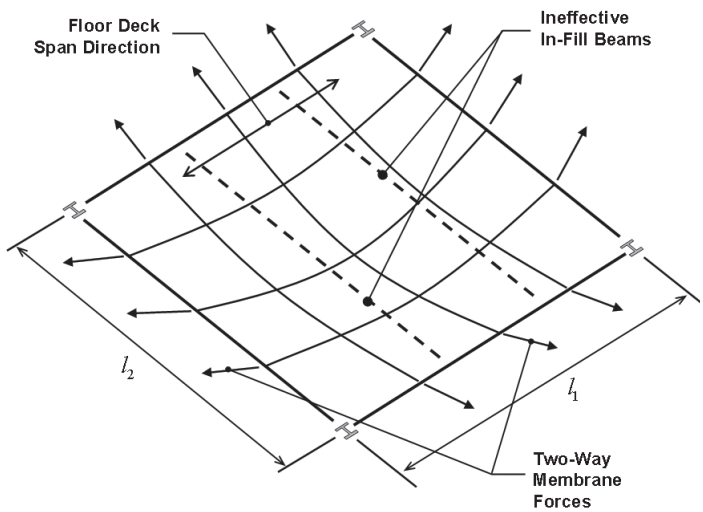

Fig. 4. Schematic of two-way membrane action in composite steel-concrete floor system when two in-fill beams are rendered ineffective.

Table 1. One-Way Catenary Reinforcement Capacities with Variation in Distributed Slab Reinforcement					
Reinforcement Scenario (1)	h, in. (5)	A_s, in.²/ft (2)	q_u, lb/ft ² (3)	β_{dynam} (4)	$\mu = \frac{\varepsilon_s}{\varepsilon_y}$ (6)
6×6-W1.4×W1.4	16.2	0.028	21.5	0.23	2.4
#3 at 24-in. o.c.	16.2	0.055	39	0.42	2.6
#4 at 18-in. o.c.	16.2	0.133	94	1.01	2.6
#4 at 14-in. o.c.	16.2	0.1714	122	1.31	2.6
#4 at 9-in. o.c.	16.2	0.2667	189	2.03	2.6
#4 at 14-in. o.c.	18.0	0.1714	135	1.45	3.2
#4 at 12-in. o.c.	18.0	0.20	157	1.68	3.2

tensile reinforcement at the perimeter of the slab system (i.e., immediately above the ineffective spandrel in-board of the columns); and the second involves distributing catenary tensile reinforcement. Equations 1 and 4 are used to evaluate the load carrying capacity of the catenary if the yield stress in the reinforcement is attained.

The first scenario considered is lumped mild-steel catenary reinforcement—four #4 Gr. 60 reinforcing bars continuous at the perimeter. The catenary span is 360 in. (30 ft), and the tributary width of deck perpendicular to the catenary is 5 ft. The loading capacity for this scenario was found to be 100 psf (Foley et al., 2007). The strains present in the reinforcement with the assumed catenary sag of 14 in. is approximately $2\varepsilon_y$. One could argue that the 5-ft tributary width is conservative because it is likely that the steel deck could be a very effective cantilever. If the tributary width of slab carried by the catenary drops to 3 ft (assuming that the steel deck and WWM acting together transmit more loading to the first interior in-fill beam), four #4 bars are capable of supporting 168-psf loading, allowing for a dynamic multiplier of 1.8.

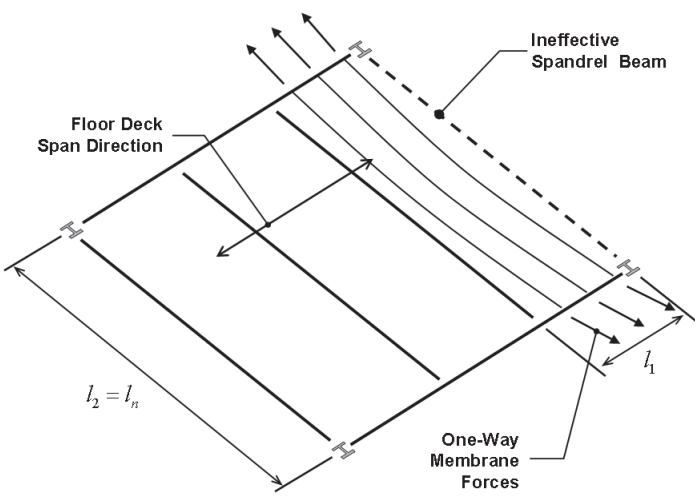

Fig. 5. Schematic illustrating ineffective spandrel beam scenario.

A second mild-steel reinforcement scenario considered reinforcement distributed throughout the slab, thus creating one-way membrane action wherever needed. This creates a tributary width to the catenary of 1 ft. A variety of reinforcement scenarios were considered, and they are shown in Table 1 (Foley et al., 2007). The magnitude of point-in-time static loading present at the time the system is compromised is 93 psf. The reinforcement scenarios and load-carrying capacities indicate that the typical WWM in a steel-concrete composite floor system is not capable of carrying the expected 93-psf loading. It should be noted that more capacity is gained as the catenary is allowed to sag, but one should recognize that with sag comes strain, and the rupture strain may be exceeded.

A second ineffective spandrel beam scenario considered assumes the spandrel beam is lost as well as the first interior infill beam (Figure 6). Two-way action is not considered. Catenary action at the edge of the panel considered in the previous scenario has been deemed ineffective without additional slab reinforcement. The results in Table 1 indicate that if #4 bars are provided at 9 in. on center throughout this bay, a significant level of general structural integrity and enhanced robustness can be gained if the spacing is 18 in. The floor slab with this reinforcement will likely be capable of supporting the expected loading.

Ineffective Spandrel Girder

The final floor member scenario considered is shown in Figure 7. It is assumed that when the spandrel girder is rendered ineffective, exterior cladding attached to this member falls off the structure. This situation benefits from the presence of composite steel deck in the direction of the one-way membrane action. Therefore, this reinforcement is considered in the membrane analysis. It should be noted that because the vertical supporting element at the edge of the panel is lost, two-way action is not considered. It should be emphasized that there is an assumption that the connections at the ends of the beams framing into the exterior columns are capable of supporting the additional loading. The 75% reduction in applied live loading from that used for the original design of the connections makes this assumption palatable.

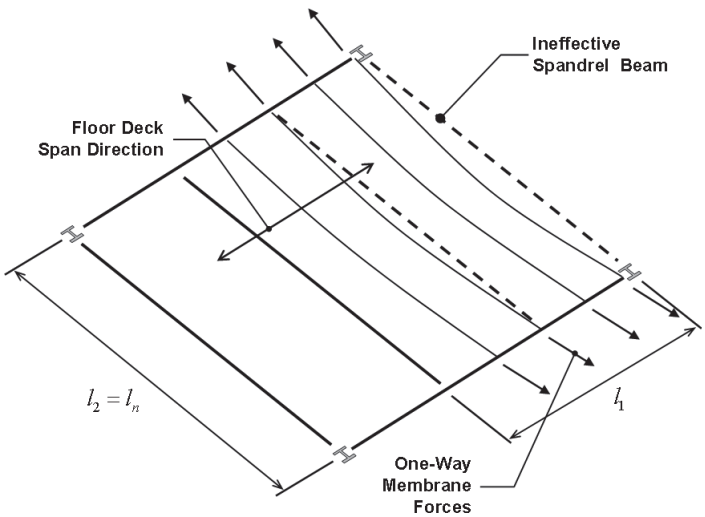

Fig. 6. Schematic illustrating ineffective spandrel and immediately adjacent beam scenario.

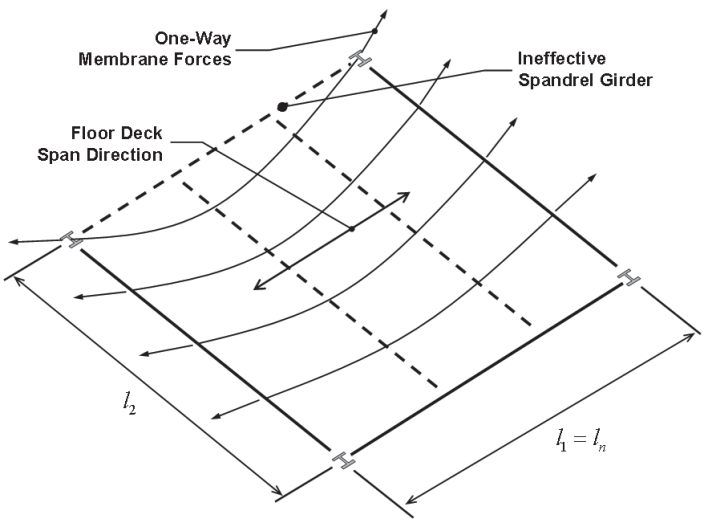

Fig. 7. Schematic illustrating ineffective spandrel girder scenario.

If one assumes that 50% of the steel deck is considered anchored at the end of the catenary and that 2VLI22 composite steel deck is used along with the typical shrinkage and temperature reinforcement (6×6-W1.4×W1.4); the one-way membrane capacity of the system is approximately 102 psf with 13.5 in. of sag and strains in the WWM and steel deck are equal to or less than $2.7\varepsilon_y$ (Foley et al., 2007). Assuming one or both of the panel edges are exterior, the connections at the ends of the catenary must support a tensile force equal to

$$T_{end} = A_{deck} f_{dy} = [0.50(0.03542 \text{ in.}^2/\text{in.})(12 \text{ in./ft})](40 \text{ ksi}) = 8.5 \text{ kip/ft}$$

Steel studs at 1-ft spacing may be able to develop this force, but it is unknown if the deck is capable of channeling this force to discrete connection points. In the case of continuous panel edges and continuous deck panels over the support, this connection is of moderate concern. The capability of the steel deck and its attachment to the structural steel beam substrate in meeting this demand is worthy of further study.

Ineffective Interior Column

The 3-, 10-, and 20-story building analyses considered in the companion paper (Foley et al., 2008) indicated that as one rises through a steel building framework and loses the beneficial effects of deep beam action in the stories above an ineffective column and the flexural mechanisms provided by several girder lines above the compromised column, the floor system may be required to develop catenary and/or membrane action in addition to flexural capacity in order to resist disproportionate collapse.

The robustness inherent in structural steel simply connected framing systems was evaluated through consideration of the typical interior framing bays present in the 3-story and 10-story buildings previously considered (Foley et al., 2008) and the assumption that an interior column would become ineffective. In this situation, the ineffective column facilitates activation of two-way membrane action in the concrete floor framing system and two-way flexure/catenary action in the structural steel framing. A critical assumption is that each floor carries its own expected point-in-time superimposed loading and self weight. As a result, each floor can be treated as an independent entity within the multistory system. A second important assumption is that the columns at the corners of the panel are not overloaded as the interior column loses its axial capacity. As discussed earlier, the 75%

reduction in live loading from that used in design makes this reasonable.

There is a synergy between the slab and steel grillage that has recently been studied in relation to fire (Allam et al., 2000; Bailey, et al, 2000; Huang, Burgess and Plank, 2000a, 2000b; Burgess, Huang and Plank, 2001; Cai, Burgess and Plank, 2002; Huang, Burgess and Plank, 2003a, 2003b). In the present analysis, a deformation compatibility approach is used in conjunction with two separate static analyses: the first considers two-way membrane action in the slab, and the second considers two-way-grillage catenary/flexure action in the steel framing. These two analysis components are illustrated in Figures 8 and 9. As the interior column is rendered ineffective, the slab and grillage of steel members is forced to deform in a compatible manner, and they both resist vertical deformation to the extent that their strength and stiffness allow. The two-way membrane behavior in the slab is assumed to follow the theory described and used previously. Two way grillage (catenary/flexure) behavior in the steel framing can be computed using nonlinear structural analysis theory. These can be used together to evaluate the robustness present in the typical 30-ft by 30-ft simple structural steel framing system.

The analysis undertaken implies superposition, which may appear to be an incorrect assumption. However, closer examination of system behavior coupled with the assumption that the floor slab is not composite with the steel framing at the strength limit state makes this assumption appropriate for the modeling conducted. As an example, consider two steel plates lying on top of one another. The top plate has a thickness of ½ in. and the bottom plate has a thickness of 1 in. The widths of the plates are identical, their materials have identical stress-strain behavior, and the plates are simply supported with concentrated loading applied at midspan. As the concentrated loading is applied, the plates will attract force according to their flexural stiffness. As expected, the thicker plate will carry a larger percentage of the loading prior to yield. As loading increases, the thicker plate will begin to yield, and its flexural strength will begin to reach a limit. The stiffness of this thicker plate also now reduces as a result of yielding. As yielding in the thicker plate occurs with the corresponding stiffness change, the thinner plate begins to pick up loading and tries its best to compensate for the limited capacity of the thicker plate. In the end, both plates will experience flexural mechanism, and the capacity of the two-plate system is the capacity of the two independent plates added together. Compatibility of deformation must be ensured.

The framing connection considered is a double-angle web connection (i.e., web cleats), and the moment, tension and shear capacities of this connection need to be determined. This process can be started by decomposing the web cleat connection into bolt elements (Figure 10). Researchers have been studying methodologies for determining moment and tension capacities of bolted angle connections for some time (Wales and Rossow, 1983; Astaneh-Asl, Call and McMullin, 1989a; Astaneh-Asl, Nader and Malik, 1989b; DeStefano and Astaneh-Asl, 1991; DeStefano, Astaneh-Asl, DeLuca and Ho, 1991; DeStefano, DeLuca and Astaneh-Asl, 1994; Shen and Astaneh-Asl, 1999; Liu and Astaneh-Asl, 2000a,

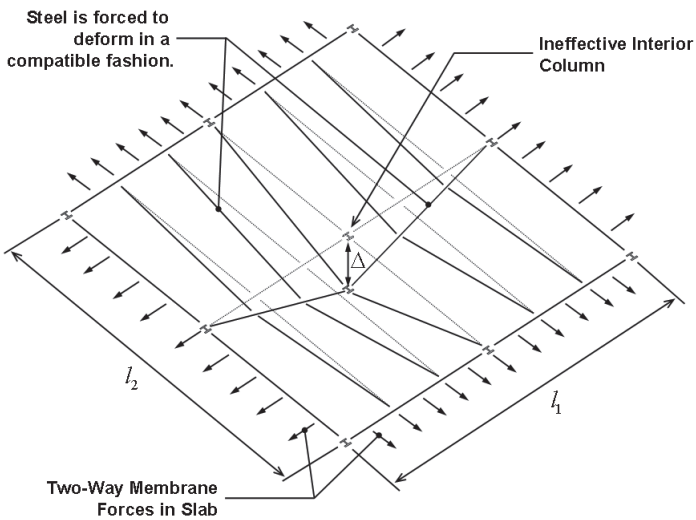

Fig. 8. Two-way membrane action resulting from ineffective interior column.

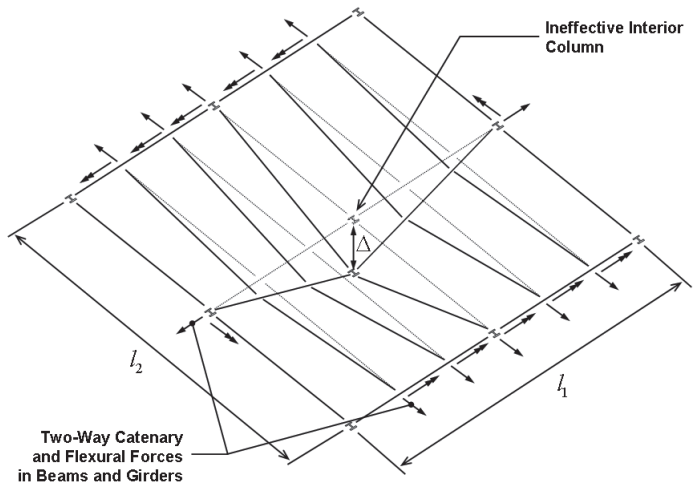

Fig. 9. Two-way catenary/flexure action resulting from ineffective interior column.

2000b; Shen and Astaneh-Asl, 2000; Astaneh-Asl, Liu and McMullin, 2002). The present study uses the approach of Shen and Astaneh-Asl (2000) and Liu and Astaneh-Asl (2000b) to develop nonlinear tension and compression behavior for bolt elements. These bolt elements can then be assembled to form web cleats whereupon moment-rotation behavior of the connections or tension/compression response of the connection can be approximated.

The process begins with developing tension-deflection and compression-deflection response of the double-angle bolt elements (Foley et al., 2007). A tri-linear tension-deformation response for the bolt element is derived using established procedures (Shen and Astaneh-Asl, 1999; Liu and Astaneh-Asl, 2000a, 2000b; Shen and Astaneh-Asl, 2000) with slight modification. The tri-linear bolt element response assumed is shown in Figure 11. Three characteristic points on the response are generated. Point (δ_{T1}, P_{T1}) is defined using the yield moment in the legs of the angle. The initial stiffness, K_{T1}, is the linear elastic stiffness of the bolt element considering bending of the legs perpendicular to the beam web and the axial extension of the leg parallel to the beam web. Point (δ_{T1}, P_{T1}) corresponds to the plastic mechanism capacity of the angle legs perpendicular to the beam web. The post-yield mechanism stiffness is defined as K_{T2}. The final point on the tension-deformation response is (δ_{TU}, P_{TU}), and it corresponds to the ultimate loading for the bolt element exclusive of bolt tension rupture or bolt shear rupture. It is defined through consideration of the angle legs perpendicular to the beam web forming catenary tension between the bolts and the legs parallel to the beam web. The tension in the angle-leg catenary at this ultimate loading is taken to be the loading corresponding to fracture on the net area through the angle leg perpendicular to the beam web. The final stiffness in the response is defined as K_{T3}.

The catenary tension force may or may not be able to form. For example, the bolts may fracture in tension prior to attaining the catenary tension limit state. Therefore, a third point (δ_{T3}, P_{T3}) is used, where P_{T3} is defined through consideration of the following bolt-element limit states (Foley et al., 2007):

- catenary tension fracture in the angle legs perpendicular to the beam web
- tear-out bearing failure of the bolts in the beam web
- tear-out bearing failure of the bolts in the angles
- tension fracture of the bolts including prying action (Thornton, 1985)
- tension fracture of the bolts excluding prying (superfluous)
- shear fracture of the bolts

The third and final point is located along the response defined using K_{T3}. This stiffness, along with P_{T3} defines the deformation capacity of the bolt element, δ_{T3}.

The bolt element compression-deformation response is assumed to be bilinear as indicated in Figure 12. The yield point (δ_{C1}, P_{C1}) is defined by considering three strength limit states (Foley et al., 2007):

- yield in the angle legs parallel to the beam web
- yielding in the beam web
- shear fracture of the bolts

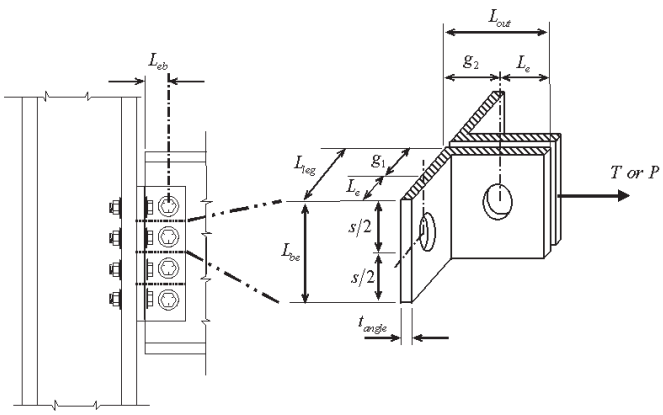

Fig. 10. Web-cleat to bolt element transformation.

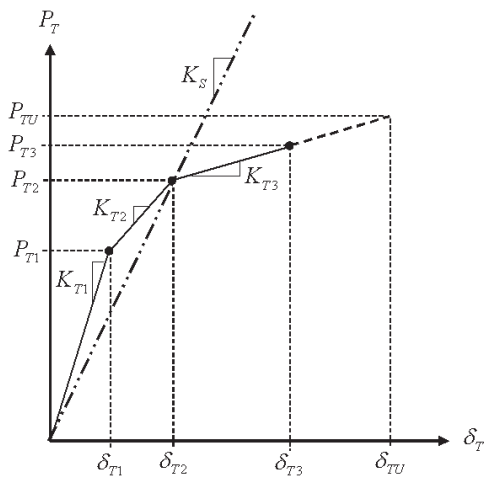

Fig. 11. Double-angle bolt element tension-deformation response.

The ultimate loading capacity of the bolt element in compression is defined through consideration of the following strength limit states (Foley et al., 2007):

- crushing in the angle legs denoted by the ultimate stress being reached in the angle legs parallel to the beam web (conservative)
- crushing in the beam web denoted by the ultimate stress in the beam web being reached (conservative)
- 20% increase above the ultimate bolt shear stress magnitude

The initial stiffness, K_{C1}, is defined using the smaller of two stiffness magnitudes. If beam web yielding controls, the stiffness is defined as,

$$K_{C1} = \frac{A_{web}E}{L_c} \tag{6}$$

and if angle leg yielding controls, the stiffness is defined by,

$$K_{C1} = \frac{A_{angles}E}{L_c} \tag{7}$$

The areas are defined on the basis of the bolt element dimension, L_{be}. The compression length in the angle (or length over which strain accumulates in the beam web) is defined as,

$$L_c = g_2 - \frac{d_h}{2} \tag{8}$$

The post-yield stiffness is defined rather arbitrarily using a 0.5% multiplier to account for moderate strain hardening in the material on the way to crushing. It should be noted that the behavior of the supporting element (e.g., a column flange, a column web, and girder web) is omitted. This is likely very important, but the complexity incurred through consideration of this behavior would render the analysis proposed intractable. Obviously, this requires further evaluation.

Nonlinear tension and compression response for a bolt element consisting of A325-N bolts in 2L4×3.5 were computed (Foley et al., 2007). Expected yield and ultimate tensile stresses for the materials were used. The tension- and compression-deformation response parameters for bolt elements consisting of various angle leg thicknesses are given in Table 2. These parameters depend upon the limits states discussed previously; therefore, the beam web thickness will affect the parameter magnitudes. The W-shapes assumed are consistent with those in the buildings analyzed previously. The tension and compression response for the bolt elements are shown in Figures 13 and 14. The tension-deformation response varies considerably with beam shape and angle thickness. When thin angles are considered, the catenary tension action is allowed to form and rupture of the angle legs is the controlling limit state. However, as the angles get thicker, other limit states control the behavior. This is indicated by the "capping" of the tension forces in the 5/16-, 3/8- and 1/2-in. angle thickness in the W18×35 beam shape and the 3/8- and 1/2-in. angle thickness with the W21×68 girder shape. The compression-deformation response indicates that the limit states controlling the strength are consistent.

The bolt element ultimate strengths can be used to contribute to the determination of the tension capacity of the double-angle connections through simple summation of

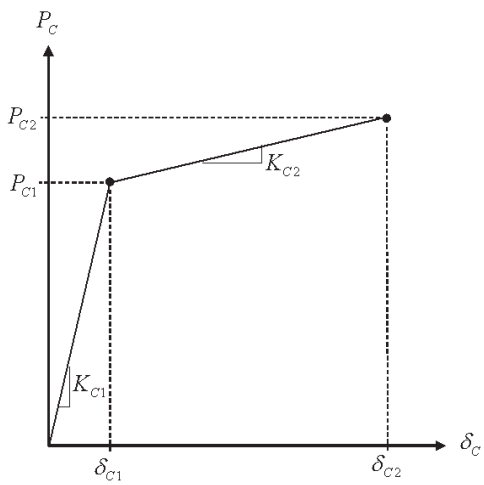

Fig. 12. Double-angle bolt element compression-deformation response.

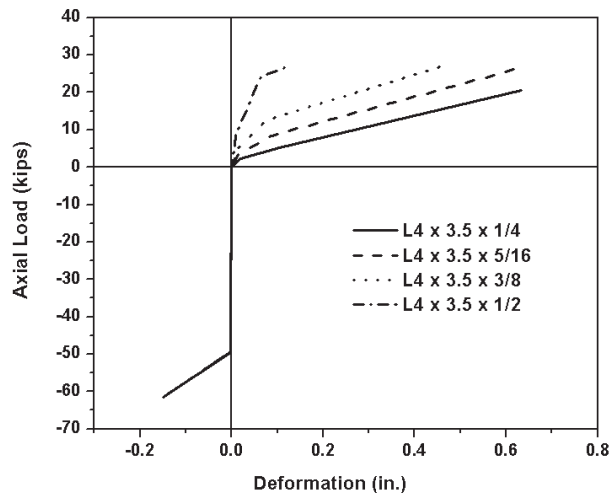

Fig. 13. Bolt element tension and compression response for L4×3.5 double angles and W18×35.

Table 2. Bolt-Element Tension and Compression Response Parameters for Varying Angle Thickness									
Response Direction (1)	Parameter (2)	W18×35				W21×68			
		L4×3½ Angles				L4×3½ Angles			
		¼ (3)	5/16 (4)	3/8 (5)	½ (6)	¼ (7)	5/16 (8)	3/8 (9)	½ (10)
Tension	δ_{T1}, in.	0.019	0.015	0.013	0.0095	0.019	0.015	0.013	0.0095
	δ_{T2}, in.	0.105	0.088	0.077	0.064	0.105	0.088	0.077	0.064
	δ_{T3}, in.	0.632	0.640	0.457	0.124	0.632	0.697	0.752	0.386
	P_{T1}, kips	2.205	3.445	4.961	8.820	2.205	3.445	4.961	8.820
	P_{T2}, kips	5.232	8.462	12.629	24.212	5.232	8.462	12.629	24.212
	P_{T3}, kips	20.491	26.873	26.873	26.873	20.491	28.745	37.93	38.519
	K_{T1}, kips/in.	116.00	226.56	391.50	928.00	116.00	226.56	391.50	928.00
	K_{T2}, kips/in.	35.344	69.031	119.28	282.75	35.344	69.031	119.28	282.75
	K_{T3}, kips/in.	28.947	33.326	37.480	44.489	28.947	33.326	37.480	44.489
Compression	δ_{C1}, in.	0.0030	0.0030	0.0030	0.0030	0.0022	0.0022	0.0022	0.0022
	δ_{C2}, in.	0.1490	0.149	0.149	0.149	0.092	0.092	0.092	0.092
	P_{C1}, kips	49.500	49.500	49.500	49.500	52.590	52.590	52.590	52.590
	P_{C2}, kips	61.425	61.425	61.425	61.425	63.108	63.108	63.108	63.108
	K_{C1}, kips/in.	16380	16380	16380	16380	23470	23470	23470	23470
	K_{C2}, kips/in.	81.882	81.882	81.882	81.882	117.36	117.36	117.36	117.36

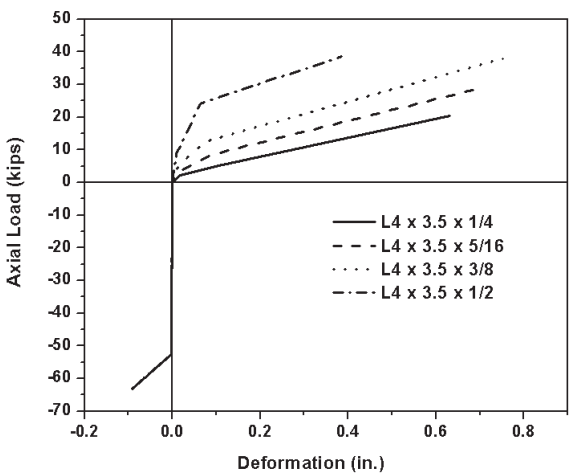

Fig. 14. Bolt element tension and compression response for L4×3.5 double angles and W21×68.

the bolt element tension strengths. However, two additional strength limits states must be considered beyond those considered in the bolt element strength determination. Therefore, the tensile capacity of the double-angle connection is determined through consideration of the following limit states (Foley et al., 2007):

- shear rupture of the bolts
- tension fracture of the bolts, including prying
- block shear rupture in the angle legs parallel to the beam web
- block shear rupture in the beam web
- bearing tear out failure in the angle legs parallel to the beam web
- bearing tear out failure in the beam web
- catenary tension-rupture in the angle legs perpendicular to the beam web

The pure moment capacity of the double-angle web connection is determined using the bolt element tension- and compression-deformation response parameters described previously (Table 2). The pure moment condition is defined by the deformation and force states shown in Figure 15. The process for determining the pure moment capacity of the connection begins with defining the tension and compression response for each bolt element in the connection (Foley et al., 2007). A controlling state of deformation in the extreme tension angle, δ_4, or extreme compression angle, δ_1, is assumed. These deformations are taken from the curves corresponding to the angles in the bolt element. The connection rotation angle, θ, is then varied until the summation of all forces determined using the bolt element response curves is zero. This corresponds to the pure moment capacity of the double-angle connection. It should be noted that this process is iterative and the compression or tension deformation limit states control the behavior.

The shear strength of the double-angle connection given the beam shape chosen can be determined using the AISC *Load and Resistance Factor Design Manual of Steel Construction* (AISC, 2001), hereafter referred to as the AISC *Manual*. It should be noted that allowable stress design load combinations were utilized and therefore, all manual-obtained strengths were divided by 0.75. The shear strengths for the double angles and beam shapes considered assume L_{ev} = 1.5 in., L_{eh} = 1.5 in., ϕ = 1.0, and ¾-in. A325-N bolts in standard holes.

The beams in the grillage are assumed to be W18×35, and the girders are W21×68. The W18 sections can support three to five bolt rows, while the W21 sections can support four to six bolt rows with traditional spacing and end distances (AISC, 2001). Therefore, only these numbers of bolt rows were considered. Table 3 illustrates the pure tension, pure shear, and pure moment capacities of the double angle connections considered (Foley et al., 2007). All shear strengths are controlled by the strength of the beam or girder web (with yield stress of 50 ksi). A † symbol denotes exceptions where the shear strength is limited by the connection angle and/or bolt strength.

Table 3 indicates that the double-angle connection alone has a tensile capacity that ranges from 0.08 to 0.26 of the yield load of the beam cross-section. These are fairly significant tensile capacities (if taken as cumulative over all beam and girder members within the 3D system). The loading capacities are consistent with those found through testing (Owens and Moore, 1992). The moment capacities are very low, however. The bending moment capacities range from 0.05 to 0.18 of the plastic moment capacity of the beam cross-section. This is consistent with the strength portion of the definition of flexible connections (AISC, 2005).

Bilinear moment-rotation response and axial load-extension response curves can be generated for the double-angle connections using the bolt element models. The connections in the grillage are not expected to go into compression in the ineffective column scenario considered. The tension secant stiffness for the bolt element can be defined as shown in Figure 11 (Foley et al., 2007);

$$k_{BE} = K_s = \frac{P_{T2}}{\delta_{T2}} \tag{9}$$

The tensile capacity of each bolt element in the double-angle connection contributes to the tensile and moment capacity of the connection. The bilinear tension-deformation response of each bolt element is characterized by the secant stiffness, k_{BE}, and the bolt element tensile capacity, P_{T3}.

The rotational and axial stiffness of the web-cleat connections are estimated using the magnitudes of the bolt element secant stiffness. The axial stiffness of the double angle connection is the sum of the stiffness of each bolt element in the web cleat,

$$K_\delta = \sum_{i=1}^{n_b} k_{BE,i} \tag{10}$$

The rotational stiffness of the web-cleat connection varies with the number of bolts and a schematic illustration of its computation is shown in Figure 15. If the bolt element stiffness, k_{BE}, is known and there is n_b bolt elements in the web cleat connection, the rotational stiffness can be computed as (Foley et al., 2007),

$$K_\theta = \sum_{i=1}^{n_b-1} i^2 \left(k_{BE} s^2\right) \tag{11}$$

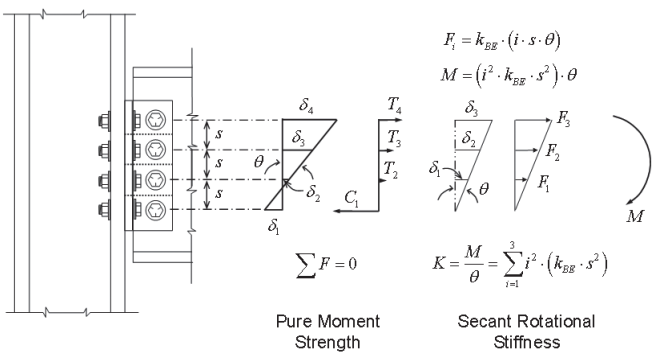

Fig. 15. Schematic illustrating procedure used to compute web-cleat connection flexural strength and stiffness.

Table 3. Pure Tensile, Pure Shear and Pure Moment Capacities for Double Angle Connections							
		W18×35			W21×68		
L4 × 3½ Thickness (1)	Bolt Rows (2)	Axial $\left(\frac{P}{P_y}\right)$ kips (3)	Shear $\left(\frac{V}{V_y}\right)$ kips (4)	Moment $\left(\frac{M}{M_p}\right)$ kip-ft (5)	Axial $\left(\frac{P}{P_y}\right)$ kips (6)	Shear $\left(\frac{V}{V_y}\right)$ kips (7)	Moment $\left(\frac{M}{M_p}\right)$ kip-ft (8)
¼ in.	3	61.5 (0.12)	78.0 (0.31)	13.07 (0.05)	—	—	—
	4	82.0 (0.16)	102.8 (0.41)	24.61 (0.09)	82.0 (0.08)	138.7 † (0.33)	24.61 (0.04)
	5	102.5 (0.20)	127.6 (0.50)	39.03 (0.14)	102.5 (0.10)	176.0 † (0.41)	39.54 (0.06)
	6	—	—	—	123.0 (0.12)	213.3 † (0.50)	56.28 (0.08)
5⁄16 in.	3	80.6 (0.16)	78.0 (0.31)	17.47 (0.06)	—	—	—
	4	107.5 (0.21)	102.8 (0.41)	32.21 (0.12)	115.0 (0.12)	147.3 (0.35)	34.60 (0.05)
	5	134.4 (0.26)	127.6 (0.50)	46.06 (0.17)	143.7 (0.14)	182.9 (0.43)	46.17 (0.07)
	6	—	—	—	172.5 (0.17)	218.4 (0.51)	57.98 (0.09)
⅜ in.	3	80.6 (0.16)	78.0 (0.31)	18.00 (0.06)	—	—	—
	4	107.5 (0.21)	102.8 (0.41)	33.07 (0.12)	151.7 (0.15)	147.3 (0.35)	35.28 (0.05)
	5	134.4 (0.26)	127.6 (0.50)	49.95 (0.18)	189.6 (0.19)	182.9 (0.43)	46.38 (0.07)
	6	—	—	—	227.6 (0.23)	218.4 (0.51)	65.00 (0.10)
½ in.	3	80.6 (0.16)	78.0 (0.31)	19.15 (0.07)	—	—	—
	4	107.5 (0.21)	102.8 (0.41)	32.95 (0.12)	154.1 (0.15)	147.3 (0.35)	37.68 (0.06)
	5	134.4 (0.26)	127.6 (0.50)	50.26 (0.18)	192.6 (0.19)	182.9 (0.43)	61.81 (0.09)
	6	—	—	—	231.1 (0.23)	218.4 (0.51)	93.34 (0.14)

where

s = pitch of the bolt elements (taken as a constant value of 3 in.)

The axial stiffness and flexural stiffness of the web cleat connections can be defined as a function of the axial rigidity and flexural rigidity of the connected member,

$$K_\delta = \alpha_\delta \frac{AE}{L} \quad (12)$$

$$K_\theta = \alpha_\theta \left(\frac{EI}{L}\right) \quad (13)$$

The stiffness characteristics of the steel grillage connections are summarized in Table 4. The rotational stiffness of the web-cleat connections are well below the stiffness limit corresponding to flexible connections (AISC, 2005) given by $\alpha_\theta = 2$. The majority of the rotational stiffness multipliers lie in the range $0.05 \le \alpha_\theta \le 1.50$. One exception is the five-bolt arrangement in the W18×35 beam member. The axial stiffness multiplier for the majority of the connection arrangements lies in the range $0.10 \le \alpha_\theta \le 1.8$ with an exception being the five-bolt connection in the W18×35 member with $\alpha_\delta = 2.3$.

The system analysis begins by computing the capacity of the concrete-steel composite slab system acting as a two-way membrane. The membrane capacity of the concrete slab-steel deck system is approximately 50 psf at 26.2 in. of vertical deflection at the center of the panel (Foley et al., 2007). This magnitude of vertical deflection corresponds to an approximate rotational demand of,

$$\theta = \tan^{-1}\frac{26.1 \text{ in.}}{30 \text{ ft}(12)} = 0.073 \text{ rad}$$

which is below a recommended limit of 0.21 rad (GSA, 2003). It should also be noted that the rotation computed here is total rotation (elastic plus plastic components). The tension force in the steel deck running perpendicular to the in-fill beams is approximately 566 lb/in. (Foley et al., 2007), which is consistent with all previous computations.

A structural analysis model for the steel floor framing system (shown in Figure 16) was developed for use in MASTAN2 (Ziemian and McGuire, 2000). The model contains

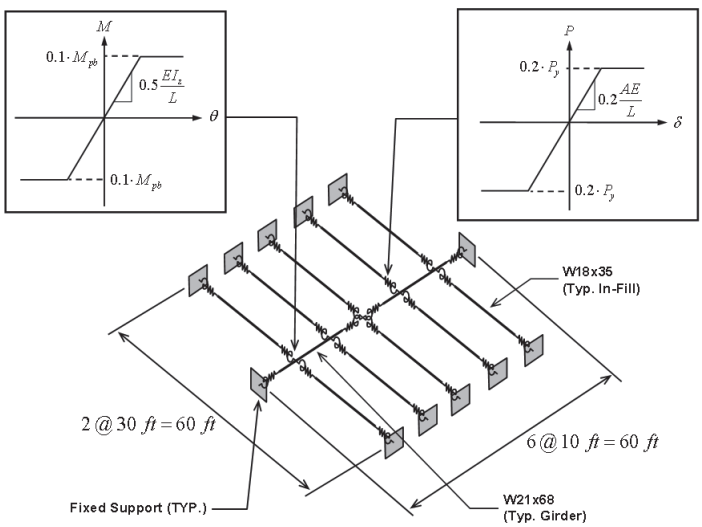

Fig. 16. Steel grillage model schematic (System 1) illustrating axial and moment connection modeling for MASTAN2 nonlinear analysis.

structural steel beam-column elements, bilinear partially restrained connections, and also axial-load-moment interaction diagrams that are used to define yielding at the ends of the beam-column elements. The basis for the analytical model is a structural steel grillage with fixed supports at all beams and columns located at the perimeter of the 60-ft by 60-ft panel. All members are modeled using multiple elements: ten for infill beams and nine for girders. The infill beams were modeled using four analytical segments. Two segments (half of the beam length) were centered on the beam midspan. The end one-quarter lengths of the beam were subdivided into four additional segments to facilitate connection modeling. Therefore, all infill beams contain end segments that are 1/16 of their span. The end segments in the girders (at column supports and interior column locations) were broken down into four segments resulting in end connection segments 1/12 of the girder span in length.

The connection characteristics typical of web-angle connections provided in Tables 3 and 4 were established in MASTAN2 in an indirect manner (Foley et al., 2007). Figure 16 illustrates the bilinear moment-rotation and load-extension behavior assumed in the connections. The axial tension and moment capacities chosen were consistent with those indicated in Table 3. Stiffness of the connections assumed were consistent with those found in Table 4. The bilinear connection characteristics are generated in MASTAN2 by using the built-in partial connection restraint capability for moment and then adjusting member cross-section properties to achieve moment capacities, axial stiffness characteristics, and axial capacity.

The end connections were modeled in the analytical segments of the beams and girders located immediately adjacent to the fixed supports, the supporting girders, and the interior column. The connection rotational stiffness was input using the built-in capabilities with the magnitude indicated in Figure 16 (for the first system considered—System 1). The connection moment capacity was input into the analysis by adjusting the beam or girder's plastic section modulus to $0.1Z_x$. This resulted in a plastic moment capacity in the end regions of the infill beams at the levels indicated in Figure 16. The axial loading characteristics were included in a slightly different manner (MASTAN2 does not allow axial hinges). The cross-sectional areas of the beam or girder in the end connection segments were defined to be 20% of the cross-sectional area of the members outside this hinge region. This reduction in cross-sectional area also created implied linear spring stiffness in this isolated region of the beam equal to 20% of the member's axial rigidity.

The method of modeling connections creates a "stub member" that has an axial capacity that is the same as the intended connection and a moment capacity that is the same as the connection intended. MASTAN2 then uses these pieces of information to create an interaction (yield) surface of

Table 4. Stiffness and Characteristics of Web Cleat Connections								
L4×3½ Thickness and Secant Stiffness Parameters (1)	k_{BE} (kip/in.) (2)	Bolt Rows (3)	K_δ (kip/in.) (4)	K_θ (kip-in./rad) (5)	W18×35 AE/L = 829.7 EI/L = 41,083		W21×68 AE/L = 1,611 EI/L = 119,222	
					α_δ (6)	α_θ (7)	α_δ (8)	α_θ (9)
¼ in. δ_{T2} = 0.105 in. P_{T2} = 5.23 kips	49.81	3	149.43	2,241.5	0.18	0.05	—	—
		4	199.24	6,276.1	0.24	0.15	0.12	0.05
		5	249.05	13,448.7	0.30	0.33	0.15	0.11
		6	298.86	24,656.0	—	—	0.19	0.21
5/16 in. δ_{T2} = 0.088 in. P_{T2} = 8.46 kips	96.14	3	288.42	4,326.3	0.35	0.11	—	—
		4	384.56	12,113.6	0.46	0.29	0.24	0.10
		5	480.70	25,957.8	0.58	0.63	0.30	0.22
		6	576.84	47,589.3	—	—	0.36	0.40
⅜ in. δ_{T2} = 0.077 in. P_{T2} = 12.63 kips	164.03	3	492.09	7,381.4	0.59	0.18	—	—
		4	656.12	20,667.8	0.79	0.50	0.41	0.17
		5	820.15	44,288.1	0.99	1.08	0.51	0.37
		6	984.18	81,194.9	—	—	0.61	0.68
½ in. δ_{T2} = 0.064 in. P_{T2} = 24.21 kips	378.28	3	1,134.8	17,022.6	1.37	0.41	—	—
		4	1,513.1	47,663.3	1.82	1.16	0.94	0.40
		5	1,891.4	102,136	2.28	2.49	1.17	0.86
		6	2,269.7	187,249	—	—	1.41	1.57

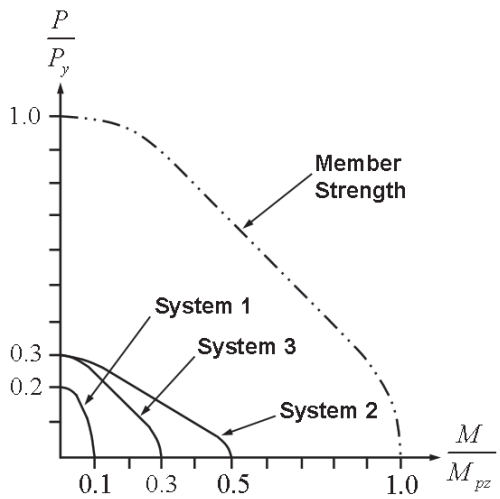

Fig. 17. Member and connection interaction surfaces for connected member and three grillage systems.

the form shown in Figure 17. It should be noted that minor-axis bending is assumed to have a connection capacity that is equal to the minor-axis plastic moment capacity of the members, and the connection stiffness in the minor-axis direction is assumed to be fully restrained. The validity of this interaction diagram for the end connections should be validated with experimental testing.

The beam members in the system were assumed to be composed of 50-ksi steel, and the expected yield stress of the material (55 ksi) was used. The strength ratios given in Table 3 are based upon 50 ksi. Uniformly distributed loading was applied to the in-fill beams in the system. The expected loading used previously was 93 psf. The floor slab system is capable of providing 50 psf toward this total with approximately 26 in. of deformation as discussed earlier. The steel grillage will then be required to carry the following superimposed loading (with a deformation that is assumed to be compatible),

$$q_{grillage} = \beta_{dynam}\left(1.0D + 0.25L\right) - 50$$
$$= \beta_{dynam}\left(93\,\text{psf}\right) - 50\,\text{psf}$$

At pseudo-dynamic loading levels ($\beta_{dynam} = 2.0$) prescribed in the GSA Guidelines (GSA, 2003), the grillage will need to support a uniformly distributed loading of 136 psf. Former studies (Marchand and Alfawakhiri, 2004; Liu, Davison and Tyas, 2005; Powell, 2005) and the companion effort (Foley et al., 2008) have shown that the multiplier commonly used to simulate dynamic loading can vary considerably. If the supporting column is simply compromised (i.e., it still has a fraction of its initial load capacity), then one might argue that the self-weight and mean point-in-time sustained live loading needs to be carried without dynamic amplification. In this case, the grillage must support 43-psf superimposed loading. A reference loading of 108 psf was assumed and this corresponds to $\beta_{dynam} = 1.7$.

Three systems were considered. Each had varying connection characteristics for the beam-to-girder and girder-to-column connections. System 1 contains the connection strength and stiffness characteristics shown in Figure 16. The load-deformation response is shown in Figure 18, and it indicates that there is a very early transition from flexural behavior to catenary behavior. The connection strengths and stiffness shown in Figure 16 reveal that the cross-sections at the ends of the members reach the yield surfaces very early in the response and the large displacements result in catenary tension in the grillage forming. The applied load ratio that results in deformations compatible with the membrane displacement computed earlier (26 in.) is 0.46, indicating that the capacity of the system (both slab and grillage) is,

$$q_{cap} = 0.46(108) + 50$$

$$\approx 100 \text{ psf}$$

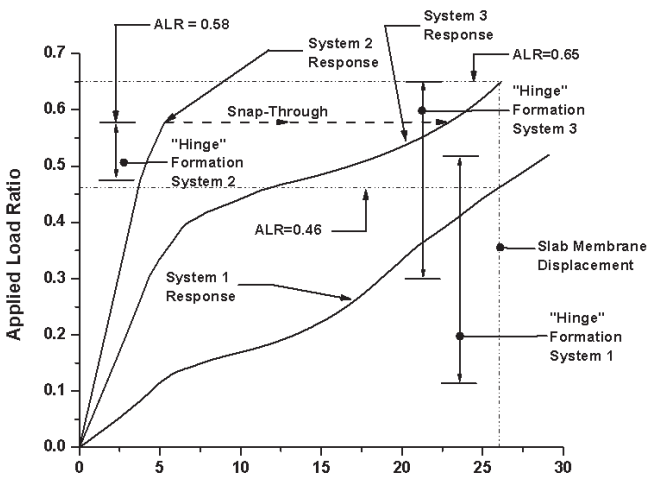

Fig. 18. Load deformation response of three grillage systems considered.

Therefore, the system appears to be capable of supporting its self-weight and the expected point in time sustained live loading with minor reserve for dynamic amplification, $\beta_{dynam} = 100/93 = 1.08$.

At 26 in. of vertical displacement, the total rotation over the beam and girder span of 30 ft was approximately 0.07 rad. This is very close to the plastic rotational limit of 0.06 rad recommended for web-angle connections (FEMA, 2000). However, the present rotational demand is "total," and the plastic demand will likely align itself closer to this limit. Therefore, the rotational demands at the level of loading considered are not likely to cause rupture of the connections, but should be further evaluated.

It should be noted that the response estimates were for a system without special modification or design considerations. Inspection of Tables 3 and 4 indicate the following connection configurations yield strength and stiffness characteristics consistent with the analytical assumptions,

W18×35	L4×3½×5⁄16, ⅜, ½ with 4 or 5 bolt rows
W21×68	L4×3½×⅜, ½ with 5 or 6 bolt rows

These angles will yield axial stiffness magnitudes that are a little bit stiffer than the analytical model and bending stiffness magnitudes that are slightly larger as well. The analysis results indicate that in order to enhance structural integrity in the steel system, one is better off choosing connection angles on the upper-end of those provided in the AISC *Manual* (AISC, 2001) and using the maximum number of bolt rows that the beam or girder web can support.

There are other connection types available for use in beam-to-girder and girder-to-column connections. For example, partially restrained beam-to-girder connections have been proposed (Rex and Easterling, 2002), and there is longstanding use of partially restrained girder-to-column connections. A second model was analyzed, and the connections chosen in this case were stronger and stiffer with respect to bending, but had slightly more strength and stiffness with respect to axial deformations. This simulates the concrete slab contributing to increased flexural stiffness and strength. This system (System 2) has the following connection characteristics,

$$P \approx 0.3P_y \text{ and } K_\delta \approx 0.3\frac{AE}{L} \qquad M \approx 0.3M_p \text{ and } K_\theta \approx 5\frac{EI}{L}$$

The connection rotational stiffness and strength are close to those previously reported for partially restrained beam-to-girder connections (Rex and Easterling, 2002). The axial strength and stiffness were increased slightly from that of System 1 to simulate the addition of a seat angle.

The same reference loading of 108 psf was applied to the steel grillage with the understanding that membrane

action in the slab would support 50 psf. The load deformation response of System 2 is shown in Figure 18. The vertical deformation corresponding to the steel grillage strength is insufficient to activate catenary action, and a conversion to catenary action will be needed once the flexural plastic hinge mechanism forms (e.g., snap-through type behavior). However, the structural analysis is not able to consider this transformation because the tangent stiffness matrix is singular at the instant these beam mechanisms form. There appears to be a better synergy in response between the slab system and the structural steel grillage in System 1. The benefits of this type of response remain to be fully quantified and understood.

The experimental rotations attained by Rex and Easterling (2002) for the partially restrained beam-to-girder connections were on the order of 0.05 rad. If one were to rely on catenary action after the flexural mechanisms occur, the vertical deformations in the system would likely rapidly increase to those found in the first system (approximately 26 in.). As a result, the rotational demands on these connections are likely to be on the order of 0.07 rad. It is unclear if the partially-restrained beam-to-girder connection can support this level of rotational demand without fracture, and additional study is recommended.

A third system evaluated had a better balance between axial capacity and moment capacity than System 2 and had the following connection characteristics;

$$P \approx 0.3P_y \text{ and } K_\delta \approx 0.3\frac{AE}{L} \qquad M \approx 0.3M_p \text{ and } K_\theta \approx 2\frac{EI}{L}$$

The load deformation response of this system is given in Figure 18, and it exhibits a smooth transition between flexural mechanism formation and catenary action. As in System 1, there is a significant range of loading over which the interaction surface at the member ends is reached. The increased flexural stiffness in the connections when compared to System 1 is the reason for the lessened vertical deformation prior to the formation of catenary tension behavior in the grillage.

The analysis outlined indicates that when connection moment capacity is low, there is a smooth transition between the initial formation of the flexural mechanism and the secondary catenary tension load transfer mechanism. If the moment capacity is too large, a significant magnitude of vertical displacement may rapidly take place prior to catenary formation. This appears undesirable, and further study is warranted. It is interesting to note that the desired behavior can likely be achieved in the structural steel framing systems considered; therefore, this study suggests the potential for limited special consideration of interior column ineffectiveness if the web angle bolt row recommendations previously described are followed.

CONCLUDING REMARKS

A variety of compromising scenarios in a typical steel floor framing system were considered in which interior infill beams, spandrel beams, and interior columns were rendered ineffective. The base system included 2VLI22 steel deck (5 in. total height composite slab) and 6×6-W1.4×W1.4 welded wire mesh reinforcement. Conclusions regarding behavior and strength of the typical slab system under a variety of compromising events follow.

The slab system typically present in a structural steel building appears capable of carrying point-in-time loading in the event infill beams are rendered ineffective. This statement quantifies one measure of the inherent structural integrity or robustness in the system. The membrane action in the slab system is most effectively enhanced by adding the mild steel reinforcement. The most effective method to enhance robustness and meet GSA-level dynamic multipliers in the event a spandrel beam is lost was determined to be providing a band of mild-steel reinforcement at the perimeter of the slab system. Distribution of mild-steel slab reinforcement throughout the exterior bays in the steel system appears to be an economical way to enhance inherent structural integrity in the case of spandrel beam loss coupled with the loss of adjacent infill beams. Another situation considered was the loss of a spandrel girder. The typical slab arrangement considered was shown to be capable of carrying point-in-time loading after such an event, thereby demonstrating the system has inherent robustness. Enhancing this is most economically attained through additional slab reinforcement.

A scenario whereby an interior column is rendered ineffective was also considered. A static nonlinear analysis of the typical 30-ft by 30-ft framing system that included nonlinear connection behavior consistent with that of web-cleat connections was conducted. The analysis indicated that the compromised system will likely be able to support the self-weight, partitions, and expected point-in-time sustained live loading of the floor system. It should be noted that dynamic response of the system needs to be evaluated in order to fully appreciate the demands that will be placed on puddle welds, shear studs, and internal slab reinforcement. The analysis results indicate that in order to improve the inherent structural integrity in the steel system, one should select connection angle thicknesses on the upper-end of those provided in the AISC *Manual* (AISC, 2001). It is also recommended to use the maximum number of bolt rows that the beam or girder web can support. Both of these rather simplistic measures will enhance the inherent robustness in the system.

The analysis conducted also indicated that it is likely more beneficial to have smaller moment capacity and flexural stiffness for connections distributed throughout the floor framing system (typically present in typical structural steel framing). When the moment capacity is low, there is the opportunity for smooth transition between the formation of the flexural

mechanism and the catenary tension behavior after the initial flexural mechanism forms. If the moment capacity is too large, there may be snap-through-type behavior, whereupon a significant magnitude of vertical displacement will rapidly take place prior to catenary mechanism formation. This appears undesirable, and further study is warranted.

In general, the analysis conducted indicates that balance between membrane action in the slab and catenary action in the steel grillage can be attained when the following axial and moment characteristics are met in regard to the connections at the ends of the beams and girders in the structural steel system:

$$M_{conn} \leq 0.30 M_{pb} \text{ and } K_{\theta} \leq 2\frac{EI}{L}$$

$$P_{conn} \leq 0.3 P_{y} \text{ and } K_{\delta} \leq 0.3\frac{AE}{L}$$

Therefore, this study suggests that there is opportunity to avoid special structural engineering consideration of interior column ineffectiveness scenarios if the web angle bolt row recommendations previously described are followed and larger connection angle thicknesses are implemented.

It is recommended that the response of the entire 3D steel building with the connection characteristics outlined in this section be conducted. This will likely lead to some very interesting results with regard to the true robustness inherent in steel building systems. This paper and the companion paper (Foley et al., 2008) simply summarize the observations made during the analyses conducted. One major item of note, however, is that better information regarding the catenary anchoring demands and capacities is needed. This information can serve as the basis for slab membrane strength computations and better estimates for the contribution of the composite steel-concrete floor deck system to the integrity of the building framing system. Finally, the capacity of steel studs as an anchoring mechanism should be assessed further.

ACKNOWLEDGMENTS

The authors would like to thank Thomas Schlafly of the American Institute of Steel Construction for his support and understanding in completing this work. The authors would also like to thank the AISC Committee on Research members for their input and comments as well as Kurt Gustafson of AISC for his very helpful recommendations. Special thanks are due to Brian Crowder of Naval Facilities Engineering Command–Atlantic and David Stevens of Protection Engineering Consultants. Their extraordinarily diligent review of the report on which this paper is based with subsequent detailed and insightful comments is greatly appreciated. The authors would also like to thank Professor Sherif El-Tawil of the University of Michigan for his review of the report on which the paper is based and recommended corrections in the literature review.

REFERENCES

ACI (1997), *ACI Design Handbook; SP-17(97)*, American Concrete Institute, Farmington Hills, MI.

ACI (2005), *Building Code Requirements for Structural Concrete (ACI 318-05) and Commentary (ACI 318R-05)*, American Concrete Institute, Farmington Hills, MI.

AISC (2001), *Load and Resistance Factor Design Manual of Steel Construction*, 3rd ed., American Institute of Steel Construction, Chicago, IL.

AISC (2005), *Specification for Structural Steel Buildings*, ANSI/AISC 360-05, American Institute of Steel Construction, Chicago, IL.

AISI (2001), *North American Specification for the Design of Cold-Form Steel Structural Members*, AISI/COS/NASPEC 2001, American Iron and Steel Institute, Washington, DC.

Allam, A., Burgess, I. and Plank, R. (2000), "Simple Investigations of Tensile Membrane Action in Composite Slabs in Fire," *International Conference on Steel Structures of the 2000's*, Istanbul, Turkey, pp. 327–332, www.shef.ac.uk/fire-research/publications.html.

Astaneh-Asl, A., Call, S.M. and McMullin, K.M. (1989a), "Design of Single Plate Shear Connections," *Engineering Journal*, AISC, Vol. 26, No. 1, pp. 21–31.

Astaneh-Asl, A., Liu, J. and McMullin, K.M. (2002), "Behavior and Design of Single Plate Shear Connections," *Journal of Constructional Steel Research*, Vol. 58, pp. 1121–1141.

Astaneh-Asl, A., Nader, M.N. and Malik, L. (1989b), "Cyclic Behavior of Double Angle Connections," *Journal of Structural Engineering*, ASCE, Vol. 115, No. 5, pp. 1101–1118.

Bailey, C.G., White, D.S. and Moore, D.B. (2000), "The Tensile Membrane Action of Unrestrained Composite Slabs Simulated Under Fire Conditions," *Engineering Structures*, Vol. 22, pp. 1583–1595.

Burgess, I.W., Huang, Z. and Plank, R.J. (2001), "Non-Linear Modeling of Steel and Composite Structures in Fire," *International Seminar on Steel Structures in Fire*, Shanghai, China, pp. 1–15, www.shef.ac.uk/fire-research/publications.html.

Cai, J., Burgess, I.W. and Plank, R.J. (2002), *A Generalized Steel/Reinforced Concrete Beam-Column Element Model for Fire Conditions*, University of Sheffield, Department of Civil and Structural Engineering, Sheffield, U.K., 40 p.

DeStefano, M. and Astaneh-Asl, A. (1991), "Axial Force-Displacement Behavior of Steel Double Angles," *Journal of Constructional Steel Research*, Vol. 20, pp. 161–181.

DeStefano, M., Astaneh-Asl, A., DeLuca, A. and Ho, I. (1991), "Behavior and Modeling of Double Angle Connections Subjected to Axial Loads," *1991 Annual Technical Session—Inelastic Behavior and Design of Frames*, Chicago, IL, Structural Stability Research Council, pp. 323–334,

DeStefano, M., DeLuca, A. and Astaneh-Asl, A. (1994), "Modeling of Cyclic Moment-Rotation Response of Double-Angle Connections," *Journal of Structural Engineering*, ASCE, Vol. 120, No. 1, pp. 212–229.

DOD (2005), *Unified Facilities Criteria (UFC)—Design of Buildings to Resist Progressive Collapse (UFC 4-023-03)*, www.wbdg.org/ccb/browse_cat.php?o=29&c=4.

FEMA (2000), *State of the Art Report on Connection Performance (FEMA-355D)*, SAC Joint Venture and Federal Emergency Management Agency, Washington, DC.

Foley, C.M., Martin, K. and Schneeman, C. (2007), *Robustness in Structural Steel Framing Systems,* Report No: MU-CEEN-SE-07-01, American Institute of Steel Construction, Chicago, IL, p. 253.

Foley, C.M., Schneeman, C.L. and Barnes, K.M. (2008), "Quantifying and Enhancing Robustness in Steel Structures: Part 1—Moment-Resisting Frames," *Engineering Journal*, AISC, Vol. 45, No. 4, pp. 247–266.

GSA (2003), *Progressive Collapse Analysis and Design Guidelines for New Federal Office Buildings and Major Modernization Projects,* www.oca.gsa.gov.

Hawkins, N.M. and Mitchell, D. (1979), "Progressive Collapse of Flat Plate Structures," *ACI Journal*, ACI, Vol. 76, No. 8, pp. 775–808.

Hibbeler, R.C. (2006), *Structural Analysis,* 6th ed., Pearson Prentice-Hall, Upper-Saddle River, NJ.

Huang, Z., Burgess, I.W. and Plank, R.J. (2000a), "Effective Stiffness Modelling of Composite Concrete Slabs in Fire," *Engineering Structures*, Vol. 22, pp. 1133–1144.

Huang, Z., Burgess, I.W. and Plank, R.J. (2000b), "Three-Dimensional Analysis of Composite Steel-Framed Buildings in Fire," *Journal of Structural Engineering*, ASCE, Vol. 126, No. 3, pp. 389–397.

Huang, Z., Burgess, I.W. and Plank, R.J. (2003a), "Modeling Membrane Action of Concrete Slabs in Composite Buildings in Fire. I: Theoretical Development," *Journal of Structural Engineering*, ASCE, Vol. 129, No. 8, pp. 1093–1102.

Huang, Z., Burgess, I.W. and Plank, R.J. (2003b), "Modeling Membrane Action of Concrete Slabs in Composite Buildings in Fire. II: Validations," *Journal of Structural Engineering*, ASCE, Vol. 129, No. 8, pp. 1103–1112.

Liu, J. and Astaneh-Asl, A. (2000a), "Cyclic Testing of Simple Connections Including Effects of Slab," *Journal of Structural Engineering*, ASCE, Vol. 126, No. 1, pp. 32–39.

Liu, J. and Astaneh-Asl, A. (2000b), *Cyclic Tests on Simple Connections Including the Effects of the Slab*, Report No. SAC/BD-00/03, SAC Joint Venture, p. 186.

Liu, R., Davison, B. and Tyas, A. (2005), "A Study of Progressive Collapse in Multi-Storey Steel Frames," *Proceedings of the 2005 Structures Congress and the 2005 Forensic Engineering Symposium*, New York, NY, American Society of Civil Engineers, CD-ROM.

Marchand, K.A. and Alfawakhiri, F. (2004), *Blast and Progressive Collapse*, Facts for Steel Buildings Number 2, American Institute of Steel Construction, Chicago, IL.

Mitchell, D. and Cook, W.D. (1984), "Preventing Progressive Collapse of Slab Structures," *Journal of Structural Engineering*, ASCE, Vol. 110, No. 7, pp. 1513–1532.

Owens, G.W. and Moore, D.B. (1992), "The Robustness of Simple Connections," *The Structural Engineer*, Vol. 70, No. 3, Institution of Structural Engineers, pp. 37–46.

Park, R. (1964), "Tensile Membrane Behaviour of Uniformly Loaded Rectangular Reinforced Concrete Slabs with Fully Restrained Edges," *Magazine of Concrete Research*, Vol. 16, No. 46, pp. 39–44.

Park, R., and Gamble, W.R. (1980), "Chapter 12—Membrane Action in Slabs," *Reinforced Concrete Slabs*, R. Park, ed., John Wiley & Sons, Inc., New York, NY, pp. 562–612.

Powell, G.P. (2005), "Progressive Collapse: Case Studies Using Nonlinear Analysis," *Proceedings of the 2005 Structures Congress and the 2005 Forensic Engineering Symposium*, New York, NY, American Society of Civil Engineers, CD-ROM.

Regan, P.E. (1975), "Catenary Action in Damaged Concrete Structures," *ACI Publication SP-48: Industrialization in Concrete Building Construction*, American Concrete Institute, Detroit, MI, pp. 191–224.

Rex, C.O. and Easterling, W.S. (2002), "Partially Restrained Composite Beam-Girder Connections," *Journal of Constructional Steel Research*, Vol. 58, pp. 1033–1060.

Shen, J. and Astaneh-Asl, A. (1999), "Hysteretic Behavior of Bolted-Angle Connections," *Journal of Constructional Steel Research*, Vol. 51, pp. 201–218.

Shen, J. and Astaneh-Asl, A. (2000), "Hysteresis Model of Bolted Angle Connections," *Journal of Constructional Steel Research*, Vol. 54, pp. 317–343.

Thornton, W.A. (1985), "Prying Action—A General Treatment," *Engineering Journal*, AISC, Vol. 22, No. 2, pp. 67–75.

Vulcraft (2005), *Vulcraft Steel Roof and Floor Deck Catalog*, Vulcraft—A Division of Nucor Corportation, www.vulcraft.com.

Wales, M.W. and Rossow, E.C. (1983), "Coupled Moment-Axial Force Behavior in Bolted Joints," *Journal of the Structural Division*, ASCE, Vol. 109, No. 5, pp. 1250–1266.

Wang, Y.C. and Kodur, V.K.R. (2000), "Research Toward Use of Unprotected Steel in Structures," *Journal of Structural Engineering*, ASCE, Vol. 126, No. 12, pp. 1442–1450.

Ziemian, R.D. and McGuire, W. (2000), *MASTAN2 Ver. 1.1*, John Wiley & Sons, New York, NY.

Current Steel Structures Research

REIDAR BJORHOVDE

Behavior, strength and design of all types of connections were addressed at the Sixth International Workshop on Connections in Steel Structures, which was held in Chicago, June 23–25, 2008. More than 60 international experts provided three days of paper presentations and extensive technical discussions of a variety of subjects. These workshops are a continuing and cooperative effort primarily between North America and Europe, with AISC and ECCS, the European Convention for Constructional Steelwork, serving as the hosts for the event. Some of the research efforts that are presented in this paper reflect studies of the workshop participants, and all of the papers are presented in a book that will be published by AISC later this year or early in 2009.

The research efforts discussed in this paper examine the behavior and strength of various forms of braced frames under seismic conditions, focusing on connection details for improved energy absorption as well as frame behavior. A novel connector in cast steel offers significant potential for braced frames using tubular members, and the development of a unique structural fuse system for bracing members is examined through an actual construction project. Further, block shear continues to be the subject of ongoing projects, and the most recent effort focuses on the limit states that govern connections with unusual failure paths. Punching shear failures in connections with high-strength bolts in tension is examined in a recent Hungarian study, and researchers in Chile are looking at improved response characteristics of certain types of shear lugs for column bases. Analytical models are critical for evaluation of frames with partially-restrained (PR) connections, and an American researcher has focused on a novel type of hybrid element. An unusual study of the performance of crane girders in actual structures offers novel and interesting findings regarding typical response accelerations of such girders. Finally, stainless steel continues to attract attention for several applications, and work in Hong Kong examines web crippling phenomena for thin-walled hollow structural sections

Reidar Bjorhovde is the Research Editor of the AISC *Engineering Journal*.

References are provided throughout the paper, whenever such are available in the public domain. However, much of the work is still in progress, and reports or publications have not yet been prepared for public dissemination.

STRUCTURAL BEHAVIOR AND STRENGTH UNDER SEISMIC LOADS

Behavior and Strength of Link-to-Column Connections in Eccentrically Braced Frames: This project has been conducted at the University of Texas in Austin, with Professor Michael D. Engelhardt as the director. Funded by the National Science Foundation and AISC, the study formed the basis for the doctoral dissertation of Taichiro Okazaki, who is now a professor at the University of Minnesota (Okazaki and Engelhardt, 2007; Okazaki, Engelhardt, Drolias, Schell, Hone and Uang, 2008).

Eccentrically braced frames have been used extensively as an efficient and stable seismic load-resisting structural system. The original usage focused on the shear links being used within the beams of a chevron-type frame, for example. However, the links certainly would appear to serve very well at the beam ends, connecting directly to the columns, and the performance of such elements was the focus of the University of Texas project. The work was in part prompted by the fact that the AISC seismic design specification (AISC, 2005b) contains detailed test performance criteria for link-to-column connections, and such test data were very scarce at the time the project was undertaken.

Using ASTM A992 steel and a range of different sizes of members and connection details, 24 full-scale tests were performed. It was initially found that the link-to-column connections tended to fail prematurely in the weld between the link and the column flange, unable to provide adequate inelastic rotation capacity. Figure 1 shows one such example. Modifying the welding details to have an all-around fillet weld between the link and the column flange proved successful, providing adequate inelastic rotation capacity. Another test used stiffeners parallel to the link web in the section of the link that was closest to the column; this was also found to supply adequate rotation capacity. Figure 2 shows this test specimen near the end of the loading regime. Additional work is now being done, focusing on the need for improved design criteria.

Use of Cast Steel Connectors for Bracing Connections in Special Concentrically Braced Frames: This project has been conducted at the University of Toronto, Ontario, Canada, with Professors Jeffrey Packer and Constantin Christopoulos as the directors. The study was undertaken specifically to examine the potential use of a cast element connecting the gusset plate and a circular hollow section (CHS) as the bracing member, to take advantage of the favorable buckling characteristics of the CHS. In addition to improved gusset plate geometries and overall connection performance criteria, it was felt that the fabrication of such framing systems would exhibit significant advantages. Figure 3 shows the details of a typical connection.

The initial part of the study used a single type of connector that was bolted to the gusset plate and shop welded to the ASTM A500 steel tubular member, using complete joint penetration welds (de Oliveira, Packer and Christopoulos, 2008). Subsequent developments provided additional sizes of connectors and tubular members, to arrive at more practical bracing member sizes that did not impose such large axial forces on the connection region. Figure 4 shows the range of connectors that were developed by the Cast ConneX Corporation.

Each of the connectors shown in Figure 4 were used together with the heaviest tubular shapes that fit the connector dimensions, and the connection assemblies were then tested cyclically in accordance with the criteria of the AISC *Seismic Provisions for Structural Steel Buildings* (AISC, 2005b). All of the tests satisfied the AISC criteria, and the failures of the

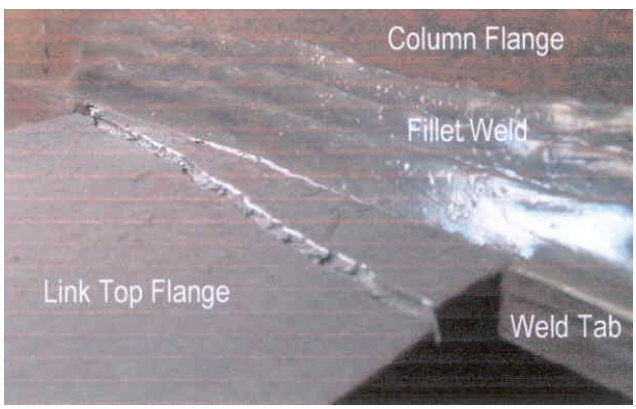

Fig. 1. Fracture of link-to-column flange connection (courtesy of Professor T. Okazaki).

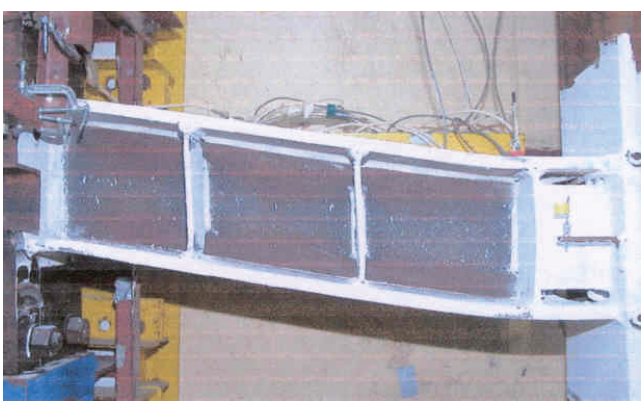

Fig. 2. Satisfactory performance of connection with stiffened link next to column (courtesy of Professor T. Okazaki).

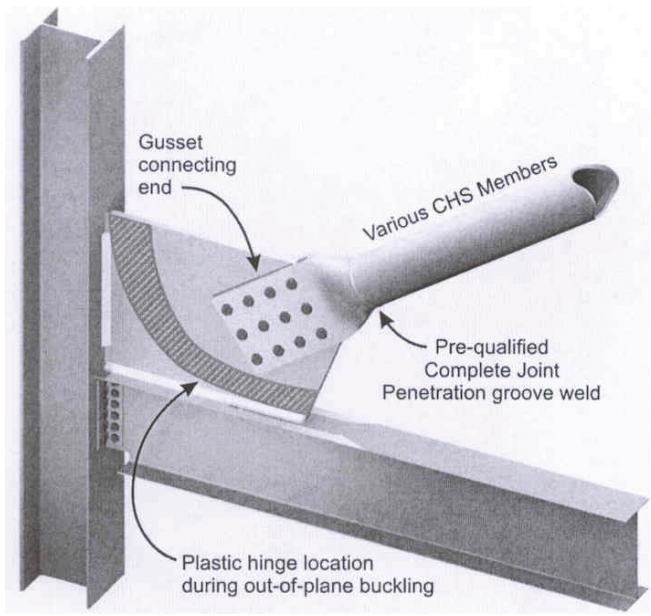

Fig. 3. Bracing connection with cast steel connecting element between gusset plate and tubular bracing member (courtesy of Professor J.A. Packer).

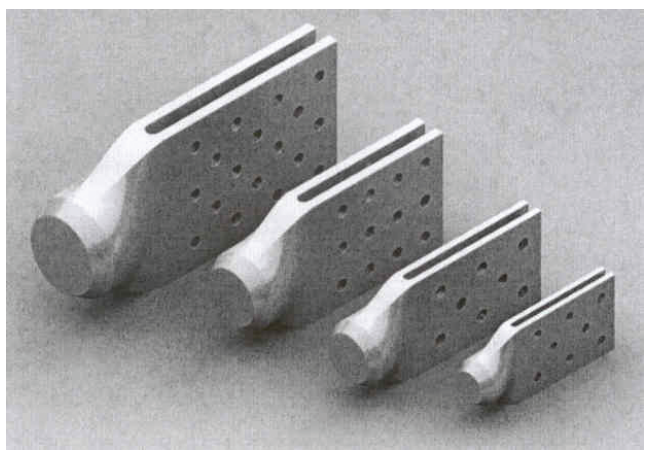

Fig. 4. Range of sizes of cast steel connecting elements (courtesy of Cast ConneX Corporation).

brace assembly occurred as flexural buckling of the tubular member with a plastic hinge forming at mid-length. Figure 5 shows one of the specimens after buckling. These tests were conducted at École Polytechnique in Montreal with Professor Robert Tremblay as the director, and further work will be done jointly by the two universities.

Full-scale tests of a complete connection region, as shown in Figure 3, with realistic member sizes, will subsequently be tested for inelastic cyclic performance assessment.

Minimizing the Strength of Bracing Connections: This is a study that was conducted by Canam Corporation in connection with the fabrication of structures for four major stadium projects in the New York City area. Richard Vincent, Vice President for Research and Development, was in charge of the study.

Recognizing that bracing member connections are designed to allow the member to yield in tension, and also that the size of such members may be governed by the compressive member capacity, the result is usually that the member size and its connections become large, complex and costly. This approach may also prompt increases in the column sizes for the structure, further increasing the project costs (Vincent, 2008).

The aim of this study was to arrive at members with smaller net areas for the tensile load demands, allowing the requisite yielding in tension and at the same time preventing local and overall buckling during the compressive load cycle. The size of the connection could therefore be reduced, while satisfying all performance requirements. The reduction of the net area of the member would effectively provide a structural fuse detail, with adequate inelastic deformation capacity in tension and satisfactory compression response. An example of a suitable fuse detail with a wide-flange bracing member is shown in Figure 6.

Additional evaluations will eventually be performed, including testing of the bracing members with the fuse detail, to establish ranges of member sizes and fuse details for various performance criteria.

OTHER CONNECTION PERFORMANCE ISSUES

Block Shear Evaluation for Members with Uncommon Failure Paths: This project has been conducted at the University of Alberta in Edmonton, Alberta, Canada, with Professor Robert Driver as the director. The work was supported by the Natural Sciences and Engineering Research Council (NSERC) of Canada, as well as the Steel Structures Education Foundation of Canada.

A number of research projects have addressed the many issues associated with block shear since the phenomenon was first identified (Birkemoe and Gilmor, 1978). Design standards in North America and elsewhere have undergone numerous revisions as additional findings were reported, although the subject now appears to have reached its final form and practical solution procedures (Driver, Grondin and Kulak, 2006; Cai and Driver, 2008).

In addition to analyzing all relevant tests that have been reported in research literature, an additional 12 tests were performed to assess limit states and failure paths of atypical connection geometries. Using wide-flange shape elements with ¾-in.-diameter ASTM A490 bolts, various gage sizes,

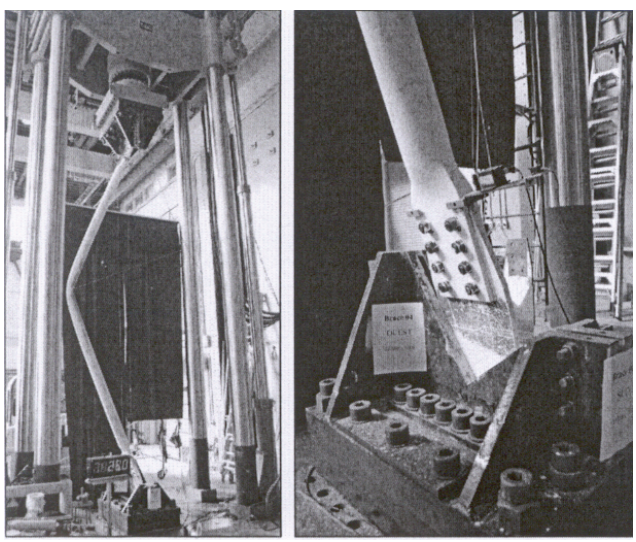

Fig. 5. Testing of tubular brace with cast steel connectors (courtesy of Professor J.A. Packer).

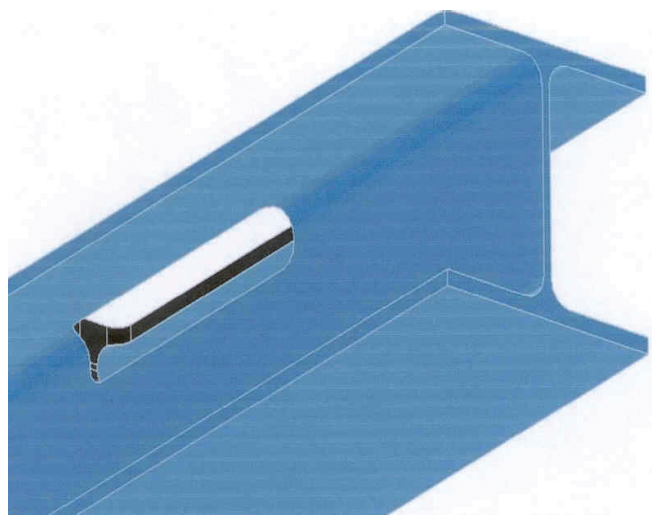

Fig. 6. Wide-flange bracing member with material removed to create structural fuse (courtesy of Richard Vincent).

and end distances, as well as the number of rows of bolts, the connections were made to the web of the shapes. The tests demonstrated failures through bolt tear-out along the shear planes on both sides of the bolt, as shown in Figure 7a. A splitting crack as shown in Figure 7b developed after the bolt tear-out limit state had reached is maximum load. Figure 7c shows the failure that developed in some cases, where fracture did not occur and the ductility of the steel allowed large hole deformations to take place. This is a phenomenon that also has been observed in other block shear tests.

Analyzing all of the previous and current test results, the researchers report excellent and consistent agreement with the so-called unified block shear equation. The requirements of the current AISC *Specification for Structural Steel Buildings* are found to be very conservative (AISC, 2005a). The authors note that the new equation has been adopted for the draft of the 2009 Canadian steel design standard, CSA-S16.

Testing of Shear Lugs for Column Bases: This is a recently started research project at the Technical University Federico Santa Maria in Valparaíso, Chile. Professor Carlos Aguirre is the director of the study.

Chile sometimes experiences very severe earthquakes, and for column base plates, shear lugs are therefore often used in combination with anchor rods. The study aims at determining the strength and deformation characteristics of different types of shear lugs, two examples of which are shown in Figure 8. The initial results show that the anchor rods yield prior to reaching the shear lug capacity, and the deformation capacity is substantial. Following a drop in load-carrying capacity, the anchor rods eventually fracture and the shear lug buckles locally along with weld fractures. The study will continue with additional tests; eventually the AISC-based design procedure will be reassessed and revised as necessary.

Punching Shear Resistance of Tension Bolts: This project is a joint effort between the University of Thessaloniki in Greece (Professor P. Baniotopoulos) and the University of Pécs in Hungary (Professor P. Ivanyi). The testing is done at the Budapest University of Technology and Economics in Hungary.

Individual bolts are loaded in tension perpendicularly to plates of thicknesses from 1 to 6 mm (0.04 to 0.25 in.); the bolts are used with and without washers. As an example of the results from this ongoing study, Figure 9 shows the punching shear failures with bolt pull-through of a 1-mm plate and a 5-mm-plate. In the case of the thinner plate (Figure 9a) the bolt and the nut simply pull directly through the plate, with fractures radiating from the corners of the nut. For the thicker plate (Figure 9b), the nut shears off a portion of the plate that reflects the shape of the nut. These and other punching shear failures will be modeled by finite element analyses, and additional static and dynamic tests will also be conducted.

METHODS OF FRAME ANALYSIS

Three-Dimensional Web-Based Semi-Rigid Steel Frame Analysis with Graphical Interface: This is an NSF-funded research project at the University of Texas at Arlington, with Professor Ali Abolmaali as the director.

A novel type of hybrid element has been developed for the analysis, utilizing pseudo spring elements to represent the full inelastic behavior of the connections. Thus, the changing stiffness of the connections as well as the local yielding within the beam ends are reflected in the representative terms in the structural stiffness matrix. One of the advantages of the approach is that the number of degrees of freedom can be reduced, because individual connection elements do not need to be modeled. The hybrid element is illustrated in Figure 10.

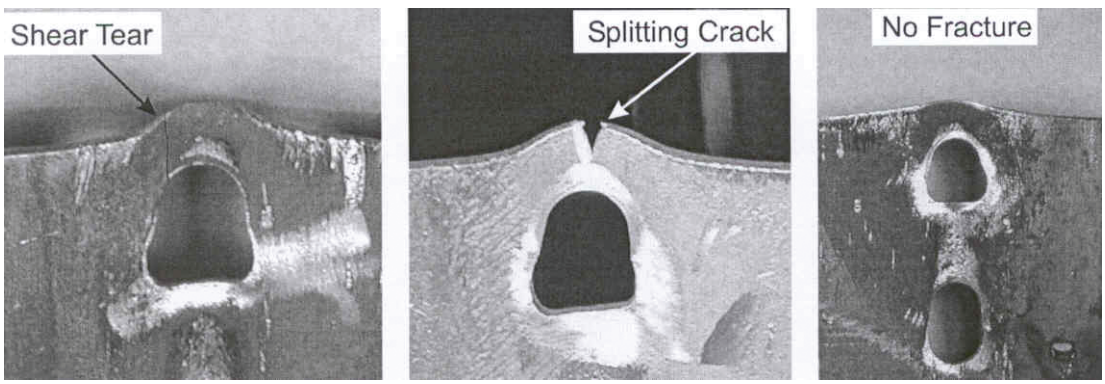

(a) (b) (c)

Fig. 7. Various failure modes in block shear tests (courtesy of Professor R.G. Driver).

INDUSTRIAL STRUCTURES

Monitoring of Crane Girders in Actual Structures: This is an ongoing project at the University of the Witwatersrand in Johannesburg, South Africa, with Professor A. Elvin as the director. The study is sponsored by the Southern African Institute of Steel Construction (SAISC).

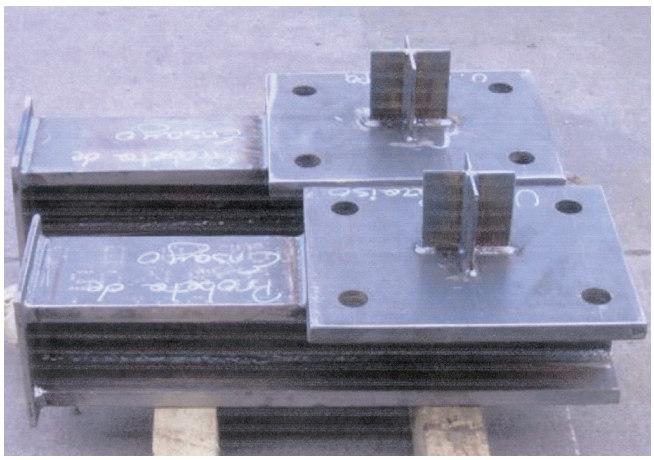

Fig. 8. Test specimens for column base plates with cruciform shear lugs (courtesy of Professor Carlos Aguirre).

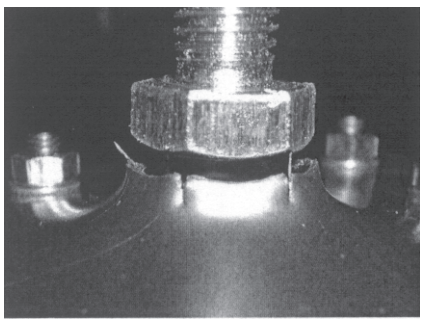

(a)

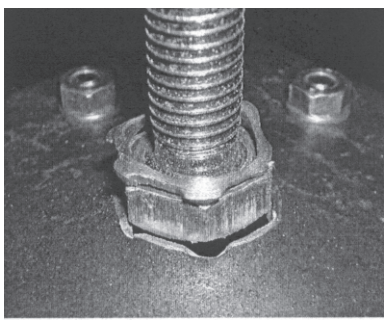

(b)

Fig. 9. Punching shear failures with bolts in 1-mm and 5-mm plates (courtesy of Professor Miklos Ivanyi).

Although cranes and crane girders have been examined for individual response characteristics, *in situ* data on their behavior as well as the structures they serve are very limited. The project aims at establishing deflections and accelerations for 30 to 50 cranes of a variety of classes and load capacities. Wireless sensors with a three-dimensional accelerometer are installed on the crane girders as shown in Figure 11, and data logging monitors the performance of the girders.

Because the project is currently under way, the final results are not yet available. However, the researchers note that "surprising results" have been found. Specifically, vertical as well as longitudinal and transverse accelerations larger than 1.0 g have been measured. This may entail additional design considerations for certain types and uses of crane girders.

STAINLESS STEEL APPLICATIONS

Cold-Formed Stainless Steel Hollow Structural Sections: This study has been conducted at the University of Hong Kong in China, with Professor Ben Young as the director.

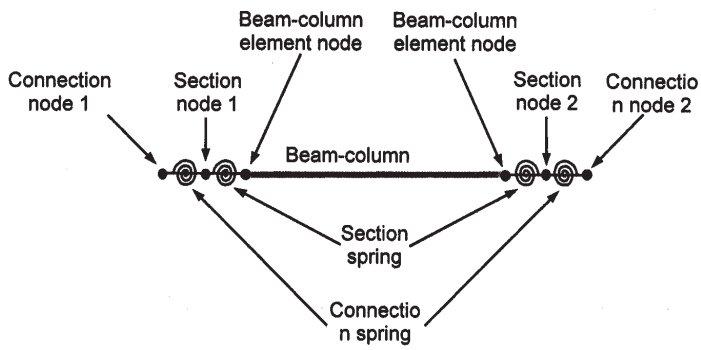

Fig. 10. Hybrid element for incorporation of connection and beam response characteristics (courtesy of Professor Ali Abolmaali).

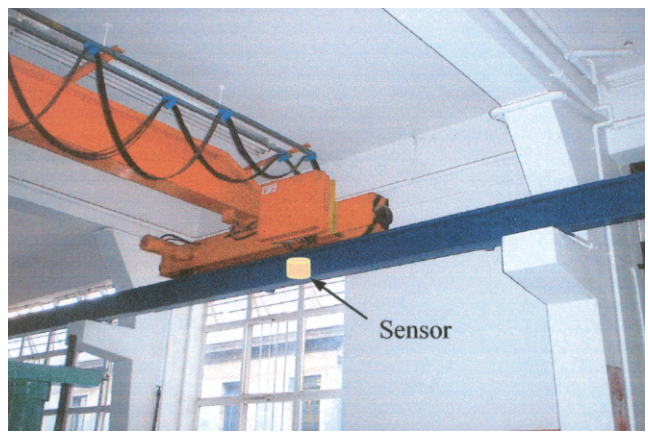

Fig. 11. Monitoring the dynamic response characteristics of crane girders (courtesy of Professor A. Elvin).

A very large program of physical testing was established for the project, using 155 pure web crippling tests, 15 pure bending tests, and 21 combined web crippling and bending tests. Figure 12 shows the test setup for a square hollow structural section (HSS) member. Finite element analyses were also performed, to assess current international design criteria, looking at American, Australian and European codes for stainless steel structures.

The results have shown that all current criteria for high strength stainless steel are either unconservative or very conservative. The researchers attribute this to the fact that the web crippling rules are generally based on tests alone and therefore empirical, and even more importantly that the tests have utilized cold-formed carbon steel instead of stainless steel. The project data have now been used to develop a unified web crippling equation for various types of stainless steel (Zhou and Young, 2007).

ACKNOWLEDGMENTS

Special thanks are due the following members of the International Structural Steel Research Advisors (ISSRA) who provided input to this paper:

Carlos Aguirre, Technical University Federico Santa Maria, Valparaíso, Chile

Hennie de Clercq, SAISC, Johannesburg, South Africa

Michael Gilmor, CISC, Toronto, Ontario, Canada

Miklos Ivanyi, Budapest University of Technology and Economics, Budapest, Hungary

Additional assistance has been provided by Ali Abolmaali, University of Texas at Arlington, Arlington, TX; Robert Driver, University of Alberta, Edmonton, Alberta, Canada; A. Elvin, University of the Witwatersrand, Johannesburg, South Africa; Taichiro Okazaki, University of Minnesota, Minneapolis, MN; Jeffrey Packer, University of Toronto, Toronto, Ontario, Canada; Richard Vincent, Canam Corporation, Boucherville, Quebec, Canada; and Ben Young, University of Hong Kong, Hong Kong, China.

As always, the assistance of Thomas Schlafly, AISC Director of Research, has been invaluable.

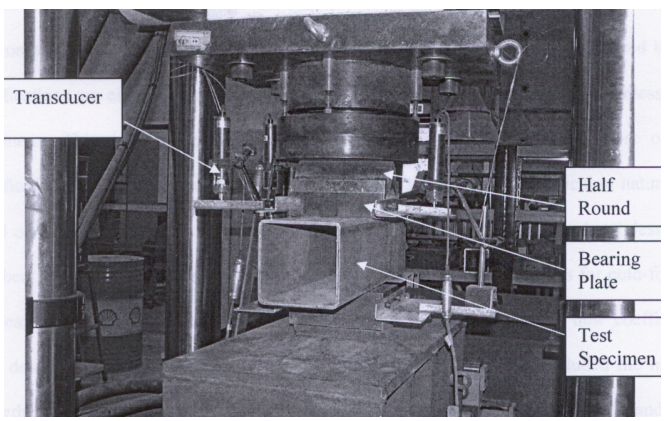

Fig. 12. Web crippling test of a stainless steel HSS (courtesy of Professor Ben Young).

REFERENCES

AISC (2005a), *Specification for Structural Steel Buildings,* ANSI/AISC 360-05, American Institute of Steel Construction, Chicago, IL.

AISC (2005b), *Seismic Provisions for Structural Steel Buildings,* ANSI/AISC 341-05, American Institute of Steel Construction, Chicago, IL.

Birkemoe, P.C. and Gilmor, M.I. (1978), "Behavior of Bearing-Critical Double-Angle Beam Connections," *Engineering Journal*, AISC, Vol. 15, No. 4, pp. 109–115.

Cai, Q. and Driver, R.G. (2008), "Performance of the Unified Block Shear Equation for Atypical Failure Paths," *Proceedings*, Sixth International Workshop on Connections in Steel Structures, AISC, Chicago, IL, June 23–25.

Driver, R.G., Grondin, G.Y. and Kulak, G.L. (2006), "Unified Block Shear Equation for Achieving Consistent Reliability," *Journal of Constructional Steel Research*, Vol. 62, No. 3, pp. 210–222.

Okazaki, T. and Engelhardt, M.D. (2007), "Cyclic Loading Behavior of EBF Links Constructed of ASTM A992 Steel," *Journal of Constructional Steel Research*, Vol. 63, No. 8, pp. 751–765.

Okazaki, T., Engelhardt, M.D., Drolias, A., Schell, E., Hong, J.-K. and Uang, C.-M. (2008), "Experimental Behavior of Link-to-Column Connections in Eccentrically Braced Frames," *Proceedings*, Sixth International Workshop on Connections in Steel Structures, AISC, Chicago, IL, June 23–25.

de Oliveira, J.C., Packer, J.A. and Christopoulos, C. (2008), "Cast Steel Connectors for Circular Hollow Section Braces under Inelastic Cyclic Loading," *Journal of Structural Engineering*, ASCE, Vol. 134, No. 3 pp. 374–383.

Vincent, Richard (2008), "Minimizing the Strength of Bracing Connections," *Proceedings*, Sixth International Workshop on Connections in Steel Structures, AISC, Chicago, IL, June 23–25.

Zhou, F. and Young, B. (2007), "Experimental Investigation of Cold-Formed High-Strength Steel Tubular Members Subjected to Combined Bending and Web Crippling," *Journal of Structural Engineering*, ASCE, Vol. 133, No. 7, pp. 1027–1034.

Suggested Reading from Other Publishers

The following abstracts summarize papers published by others on the subject of steel design and construction that may be of interest to *Engineering Journal* readers.

Reidar Bjorhovde, Research Editor of the AISC *Engineering Journal,* prepared the following abstracts from the *Journal of Constructional Steel Research*.

From Volume 64, Number 1, 2008 of the *Journal of Constructional Steel Research* (JCSR) published by Elsevier, Ltd.:

Sources of Elastic Deformation in Steel Frame and Framed Tube Structures
Part 1: Simplified Subassemblage Models
Part 2: Detailed Subassemblage Models
Finley A. Charney and Rakesh Pathak

The authors evaluate three analytical models that aim to determine the effects of the deformation of the beam-to-column joint. The models are referred to as the Fictitious Joint Model, the Krawinkler Joint Model, and the Scissors Joint Model. The models give the same expressions for the deflections that are caused by the shear displacement within the connection panel zone. The Fictitious Joint Model accounts for the flexural deformations within the connection; the other two models do not. The authors observe that although the flexural deformations are not the dominant component, they should not be ignored.

The displacements given by the three simplified models correlate closely with those obtained from a three-dimensional finite element analysis of the same subassemblage. However, the finite element analysis by itself cannot provide the breakdown of the individual components of the deformations in the joint. The second of the two papers provides a practicable approach to this problem.

From Volume 64, Number 2, 2008 of the *Journal of Constructional Steel Research* (JCSR) published by Elsevier, Ltd.:

A Practical Design Method for Semi-Rigid Composite Frames Under Vertical Loads
Jing-Feng Wang and Guo-Qiang Li

The analytical and design approach that is presented gives the solution for composite beams, columns and connections at the serviceability and ultimate limit states. Using a traditional approach to beam and column analysis, the technique determines the actual connection stiffness along with the column effective lengths. The theoretical solution is amplified by the results of two full-scale composite frame tests. The application of the approach is demonstrated by a design example, where it is shown that the actual behavior of connections and members can be taken into account by a practicable method.

From Volume 64, Number 3, 2008 of the *Journal of Constructional Steel Research* (JCSR) published by Elsevier, Ltd.:

Experiment on Restrained Steel Beam Subjected to Heating and Cooling
Guo-Qiang Li and Shi-Xiong Guo

Full-scale fire tests of restrained and unrestrained steel beams demonstrate the superior response of the restrained member. This well-known response characteristic of restrained beams is examined further, to the effect that the initial compressive force in the restrained beam is eventually reduced to zero. Subsequently, the catenary action of the beam develops the tensile force, which demonstrates the higher strength of the restrained member. The stiffness of the axial restraint is a major contributor to the higher strength of the restrained beam.

Location of Plastic Hinges in Axially Loaded Steel Members
Brian H.H. Peng, Gregory A. MacRae, Warren R. Walpole, Peter Moss, Rajesh P. Dhakal, Charles Clifton and Clark Hyland

Design codes usually prescribe that plastic hinges in axially loaded members should preferably develop at member ends as opposed to at locations within the length. This is achieved by limiting the axial force that can be applied to a yielding column, as a function of column slenderness and the end moment ratio. The study provides a procedure for determining the magnitude of the axial load as a function of plastic hinges forming at locations within the member length. The authors note that current code equations are conservative in the approach that is used to ensure that yielding will occur at member ends, and this will occur when the axial load ratio is larger than 0.15. The equations are unconservative for lower axial load ratios. Empirical equations are provided which will ensure that yielding will not occur away from member ends.

From Volume 64, Number 6, 2008 of the *Journal of Constructional Steel Research* (JCSR) published by Elsevier Ltd.:

Influence of Connection Design Parameters on the Seismic Performance of Braced Frames
Jung-Han Yoo, Dawn H. Lehman and Charles W. Roeder

As part of a major investigation of the response characteristics of special concentrically braced frames, full-scale tests and analyses have been conducted to determine the inelastic deformation capacity of such frames. The ability of gusset plates and other elements to provide the deformation sources for the frames without premature or otherwise undesirable responses is particularly important. A parametric study has been performed to assess the influence of the gusset plate and the frame members on the seismic response of the braced frame. The evaluations have considered all of the key details of the connections, including the gusset plates, the beam-to-column connections, the bracing members, and the overall inelastic deformation demands within the frame. The authors observe that proper detailing of the connections will produce significant improvement in the seismic response of such framing systems.

GUIDE FOR AUTHORS

SCOPE: The ENGINEERING JOURNAL is dedicated to the improvement and advancement of steel construction. Its pages are open to all who wish to report on new developments or techniques in steel design, research, the design and/or construction of new projects, steel fabrication methods, or new products of significance to the uses of steel in construction. Only original papers should be submitted.

GENERAL: Papers intended for publication must be submitted by mail to the Editor, Cynthia J. Duncan, ENGINEERING JOURNAL, AMERICAN INSTITUTE OF STEEL CONSTRUCTION, One East Wacker Drive, Suite 700, Chicago, IL, 60601-1802.

The articles published in the *Engineering Journal* undergo peer review before publication for (1) originality of contribution; (2) technical value to the steel construction community; (3) proper credit to others working in the same area; (4) prior publication of the material; and (5) justification of the conclusion based on the report.

All papers within the scope outlined above will be reviewed by engineers selected from among AISC, industry, design firms, and universities. The standard review process includes outside review by an average of three reviewers, who are experts in their respective technical area, and volunteers in the program. The maximum number of papers sent to a single reviewer is three per year, with a frequency of not more than one per quarter. Papers not accepted will be returned to the author. Published papers become the property of the American Institute of Steel Construction, Inc. and are protected by appropriate copyrights. No proofs will be sent to authors. Each author receives three copies of the issue in which his contribution appears.

MANUSCRIPT PREPARATION: Manuscripts must be provided on PC-formatted media, such as a CD-ROM, in Microsoft Word format. A laser-quality proof must accompany your submittal. Fonts and spacing must be suitable for easy reading and reproduction (for the peer-review process). Do not embed photographs, diagrams, illustrations, charts or graphs within the electronic manuscript files. Only equations may be embedded within the flow of the text. Specific requirements for electronic graphics are outlined below. *Engineering Journal* reserves the right not to publish a submittal if suitable graphics cannot be provided by the author.

Title and By-Line: Exact name, title and affiliation of the author or authors are required to appear on the first page of the manuscript.

Body Text: Please restrict font usage to Times, Helvetica, Times New Roman, Arial, and Symbol (for Greek and mathematical characters.)

Headings: All headings should be typed flush left, using upper and lower case, with two line spaces above.

Tables: Each table should appear on its own page. Footnotes to tables should appear below the table, identified by superscripted lower case letters (a, b, c, etc.).

Equations: Whenever possible, equations should be set using Microsoft Equation Editor or MathType (www.mathtype.com). Please set equations using Times New Roman, Times, and/or Symbol fonts.

Captions: Captions should be typed, double-spaced, and located at the end of the electronic manuscript. All photos and graphics must be clearly marked to indicate their corresponding caption.

References: Should be noted clearly in the text and listed, double-spaced, on a separate page in the following sample format.

In text: (Doe, 1992)

In Reference List:

Doe, J.H. (1992), "Structural Steel," *Engineering Journal*, AISC, Vol. 100, No. 1, 1st Quarter, pp. 2–10.

Footnotes: Footnotes should be noted clearly in the text with a superscript asterisk, and should appear at the bottom of the text page, in the following style:

*For a detailed discussion, see...

Graphics (other than photographs): Provide a clear $8\frac{1}{2}$ in. × 11 in. laser-quality proof of each graphic element. Graphics should reproduce cleanly in black-and-white format. Graphics may be submitted and reproduced in color at the Editor's discretion. Please restrict font usage to Helvetica, Arial or Symbol, in sizes suitable for at least 50% reduction (12 pt. minimum). Line weights must be suitable for 50% reduction. When possible, provide each graphic element in a separate electronic file. TIF or EPS file formats are preferred, with a minimum resolution of 300 dots per inch.

Photographs: Provide either original photographs or high-quality electronic files and laser-quality proofs. Electronic photographs may be submitted as grayscale TIF or JPG images, one photograph per file. Photographs may be submitted and reproduced in color at the Editor's discretion. Minimum image resolution is 300 dots per inch. Photographs should be a minimum of 4 in. wide, so the minimum image width is 1200 pixels. Detailed photographs may require resolutions up to 1200 dots per inch. Photos embedded in word-processing documents are not acceptable.

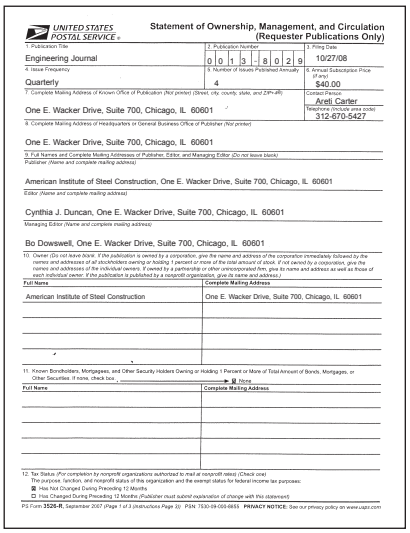

UNITED STATES POSTAL SERVICE

Statement of Ownership, Management, and Circulation (Requester Publications Only)

1. Publication Title: Engineering Journal
2. Publication Number: 0 0 1 3 - 8 0 2 9
3. Filing Date: 10/27/08
4. Issue Frequency: Quarterly
5. Number of Issues Published Annually: 4
6. Annual Subscription Price (If any): $40.00
7. Complete Mailing Address of Known Office of Publication (Not printer) (Street, city, county, state, and ZIP+4®): One E. Wacker Drive, Suite 700, Chicago, IL 60601
Contact Person: Areli Carter
Telephone (Include area code): 312-670-5427
8. Complete Mailing Address of Headquarters or General Business Office of Publisher (Not printer): One E. Wacker Drive, Suite 700, Chicago, IL 60601
9. Full Names and Complete Mailing Addresses of Publisher, Editor, and Managing Editor (Do not leave blank)
Publisher (Name and complete mailing address): American Institute of Steel Construction, One E. Wacker Drive, Suite 700, Chicago, IL 60601
Editor (Name and complete mailing address): Cynthia J. Duncan, One E. Wacker Drive, Suite 700, Chicago, IL 60601
Managing Editor (Name and complete mailing address): Bo Dowswell, One E. Wacker Drive, Suite 700, Chicago, IL 60601
10. Owner (Do not leave blank. If the publication is owned by a corporation, give the name and address of the corporation immediately followed by the names and addresses of all stockholders owning or holding 1 percent or more of the total amount of stock. If not owned by a corporation, give the names and addresses of the individual owners. If owned by a partnership or other unincorporated firm, give its name and address as well as those of each individual owner. If the publication is published by a nonprofit organization, give its name and address.)

Full Name	Complete Mailing Address
American Institute of Steel Construction	One E. Wacker Drive, Suite 700, Chicago, IL 60601

11. Known Bondholders, Mortgagees, and Other Security Holders Owning or Holding 1 Percent or More of Total Amount of Bonds, Mortgages, or Other Securities. If none, check box → ☒ None

Full Name	Complete Mailing Address

12. Tax Status (For completion by nonprofit organizations authorized to mail at nonprofit rates) (Check one)
The purpose, function, and nonprofit status of this organization and the exempt status for federal income tax purposes:
☒ Has Not Changed During Preceding 12 Months
☐ Has Changed During Preceding 12 Months (Publisher must submit explanation of change with this statement)

PS Form **3526-R**, September 2007 (Page 1 of 3 (Instructions Page 3)) PSN: 7530-09-000-8855 **PRIVACY NOTICE:** See our privacy policy on www.usps.com

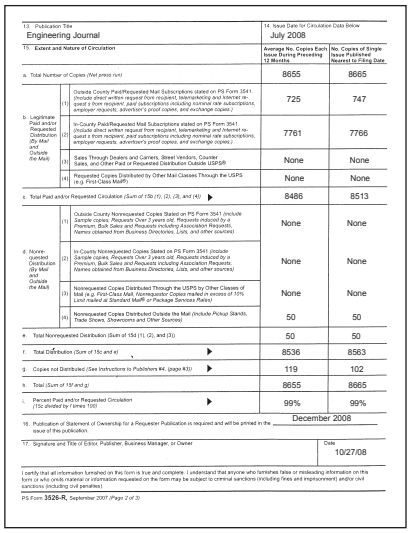

13. Publication Title: Engineering Journal
14. Issue Date for Circulation Data Below: July 2008

15. Extent and Nature of Circulation			Average No. Copies Each Issue During Preceding 12 Months	No. Copies of Single Issue Published Nearest to Filing Date
a. Total Number of Copies (Net press run)			8655	8665
b. Legitimate Paid and/or Requested Distribution (By Mail and Outside the Mail)	(1)	Outside County Paid/Requested Mail Subscriptions stated on PS Form 3541. (Include paid-in written request from recipient, telemarketing and Internet request from recipient, paid subscriptions including nominal rate subscriptions, employer requests, advertiser's proof copies, and exchange copies.)	725	747
	(2)	In-County Paid/Requested Mail Subscriptions stated on PS Form 3541. (Include direct written request from recipient, telemarketing and Internet request from recipient, paid subscriptions including nominal rate subscriptions, employer requests, advertiser's proof copies, and exchange copies.)	7761	7766
	(3)	Sales Through Dealers and Carriers, Street Vendors, Counter Sales, and Other Paid or Requested Distribution Outside USPS®	None	None
	(4)	Requested Copies Distributed by Other Mail Classes Through the USPS (e.g. First-Class Mail®)	None	None
c. Total Paid and/or Requested Circulation (Sum of 15b (1), (2), (3), and (4)) ▶			8486	8513
d. Nonrequested Distribution (By Mail and Outside the Mail)	(1)	Outside County Nonrequested Copies Stated on PS Form 3541 (Include Sample copies, Requests Over 3 years old, Requests induced by a Premium, Bulk Sales and Requests including Association Requests, Names obtained from Business Directories, Lists, and other sources)	None	None
	(2)	In-County Nonrequested Copies Stated on PS Form 3541 (Include Sample copies, Requests Over 3 years old, Requests induced by a Premium, Bulk Sales and Requests including Association Requests, Names obtained from Business Directories, Lists, and other sources)	None	None
	(3)	Nonrequested Copies Distributed Through the USPS by Other Classes of Mail (e.g. First-Class Mail, Nonequestor Copies mailed in excess of 10% Limit mailed at Standard Mail® or Package Services Rates)	None	None
	(4)	Nonrequested Copies Distributed Outside the Mail (Include Pickup Stands, Trade Shows, Showrooms and Other Sources)	50	50
e. Total Nonrequested Distribution (Sum of 15d (1), (2), and (3))			50	50
f. Total Distribution (Sum of 15c and e) ▶			8536	8563
g. Copies not Distributed (See Instructions to Publishers #4, (page #3)) ▶			119	102
h. Total (Sum of 15f and g)			8655	8665
i. Percent Paid and/or Requested Circulation (15c divided by 15f times 100) ▶			99%	99%

16. Publication of Statement of Ownership for a Requester Publication is required and will be printed in the December 2008 issue of this publication.

17. Signature and Title of Editor, Publisher, Business Manager, or Owner — Date: 10/27/08

I certify that all information furnished on this form is true and complete. I understand that anyone who furnishes false or misleading information on this form or who omits material or information requested on the form may be subject to criminal sanctions (including fines and imprisonment) and/or civil sanctions (including civil penalties).

PS Form **3526-R**, September 2007 (Page 2 of 3)

There's always a solution in steel.

ENGINEERING JOURNAL
American Institute of Steel Construction
One East Wacker Drive, Suite 700
Chicago, IL 60601